REPUBLIQUE DU CAMEROUN
Paix-Travail- Patrie
****
UNIVERSITE DE YAOUNDE I
****
FACULTES DES SCIENCES
****
CENTRE DE RECHERCHE ET DE FORMATION DOCTORALE EN SCIENCES, TECHNOLOGIES ET GEOSCIENCES
****
UNITE DE RECHERCHE ET DE FORMATION DOCTORALE EN PHYSIQUES ET APPLICATIONS
****
B.P 812 Yaoundé
Email: crfd_stg@uy1.uninet.cm

REPUBLIC OF CAMEROON
Peace-Work-Fatherland
****
THE UNIVERSITY OF YAOUNDE I
****
FACULTY OF SCIENCE
****
POSTGRADUATE SCHOOL OF SCIENCES, TECHNOLOGY AND GEOSCIENCES
****
RESEARCH AND POSTGRADUATE TRAINING UNIT FOR PHYSICS AND APPLICATIONS
****
P.O. Box 812 Yaoundé
Email: crfd_stg@uy1.uninet.cm

Department of Physics
Laboratory of Mechanics, Materials and Structures

PROBABILISTIC FLEXURAL ANALYSIS AND CHARACTERIZATION OF ENERGY HARVESTING SYSTEMS

Thesis

Submitted and defended in Fulfillment of the Requirements for the Degree of
Doctor of Philosophy/PhD in Physics

Option: **Mechanics, Materials and Structures**

By

FEZEU Georges Julius

Registration number: **03R145**

Master in Physics

Under the Supervisor of

TCHAWOUA Clément

Professor, University of Yaounde I

Under the direction of

SIEWE SIEWE Martin

Associate Professor, University of Yaounde I

Year 2021

UNIVERSITE DE YAOUNDE I
UNIVERSITY OF YAOUNDE I

FACULTE DES SCIENCES
FACULTY OF SCIENCE

DEPARTEMENT DE PHYSIQUE
DEPARTMENT OF PHYSICS

ATTESTATION DE CORRECTION DE LA THESE DE DOCTORAT/Ph.D

Nous, Professeur **NANA NBENDJO Blaise Roméo** et Professeur **ESSIMBI ZOBO Bernard**, respectivement Examinateur et Président du jury de la Thèse de Doctorat/Ph.D de Monsieur **FEZEU Georges Julius**, matricule 03R145, intitulée *"Probabilistic flexural analysis and characterization of energy harvesting systems"*, préparée sous la direction du Professeur **TCHAWOUA Clément** et du professeur **SIEWE SIEWE Martin**, soutenue le **mardi 14 Décembre 2021**, en vue de l'obtention du grade de Docteur/Ph.D en Physique, Spécialité **Mécanique**, **Matériaux et Structures** option **Mécanique Fondamentale et Systèmes Complexes,** attestons que toutes les corrections demandées par le jury de soutenance ont été effectuées.

En foi de quoi, la présente attestation lui est délivrée pour servir et valoir ce que de droit.

Fait à Yaoundé, le ..... 18 JAN 2022 .....

Examinateur

NANA NBENDJO Blaise Roméo
Professeur

Le Président du jury

ESSIMBI ZOBO Bernard
Professeur

Le Chef de Département de Physique

UNIVERSITE DE YAOUNDE I * FACULTE DES SCIENCES * DEPARTEMENT DE PHYSIQUE
Le Chef de Département

Ndjaka Jean-Marie Bienvenu
Professeur

Dedication

I dedicate this thesis to:

My mother TCHOUGUEU SUZANNE, my wife Wouadjie Diane Michelle, my brother NDOUBISSI Armand Marcel, all of my family through this thesis dissertation, find the fruit of the efforts made for my training.

Acknowledgements

We acquire perseverance and success very often with the support of people who are more or less close to us. So I want to express my deep gratitude to all who have contributed to the completion of this work and to those who have worked for my formation.

• I have furthermore to thank the Almighty God for the health, wisdom and comfort which he has always given me, and without whom nothing would have been possible.

•I thank the persons responsible of the Faculty of Sciences who gave and confirmed the permission and then encouraged me to go ahead with my thesis.

• I want to thank the Department of physics of the University of Yaoundé I, for giving me permission to commence this thesis in the first instance, and to do the necessary research work.

• I would like to express my sincere gratitude to my Director of thesis, **Professor SIEWE SIEWE Martin** who, despite his multiple academic and family occupations, accepted to guide this work. This thesis would not have been possible without his pernickety vision in nonlinear physics and the multitude seminars organized in the Laboratory. I want to thank him for the advices he has provided me and the expertise that he has enabled me to acquire.

• I express my deep gratitude and my thanks to my supervisor of thesis, **Professor TCHAWOUA Clément** who has accepted to lead this work. Professor, your advice and comments have always been of great benefit to me during my training since the undergraduate year. Find here the expression of my deep gratitude.

• I would like to especially thank the **members of the Jury**, for the honor they have done us by accepting to review this work.

• I would like to thank **Professor KOFANE Timoléon Crépin**, head of the Laboratory of Mechanics, Materials and Structures. I am very grateful for the quality of his teaching and for his constructive comments.

• I am grateful to **Professor WOAFO Paul**, Chairman of the Cameroon Physical Society for his teaching and his encouragements.

• I am grateful to **Professor** BEN-BOLIE Germain Hubert, for his teachings.

• I would like to thank **Professor NDJAKA Jean − Marie Bienvenu**, Head of the Department of Physics for his teaching.

• I address my sincere thanks to all the teachers of the Department of Physics of the Faculty of Sciences, for the teachings received.

• Special thanks to **Dr**. NONO Buckjohn , **Dr**. TOGUEU Alain, **Dr**. MOKEM Igor for their permanent support, for the interest and the contribution they brought to this work.

We will not fail to salute the multifaceted support we have received from:

•Mr. KWEKEM Vincent de Paul

• Mr. PIEUMI Henri

•Mr. BARRANO Fernando

•LEMOUPA Simon, ABESSOLO, NGUIMBOUS, CHEMBEU, KAPING

•All members of the DOMINICAL CHOIR, AMDI

My thanks to the members of my family:

•My mother Mme TCHOUGUEU Suzanne;

•My uncles Mr. SIPEHOU Guy Marcel, Late Mr. TEFANG Elie, NZALI Dieudonn;

•My brothers and sisters: NJEUGOUE Monique, KENMOGNE Roger, TEFANG Ludovic, KEWE Josiane, NDOUBISSI Armand, SIMEU Sandrine, MEWA France, TCHIDJE Elvis;

•My cousins: Roxette, Darius, Solange, Nadia, Marcel, Pastelie, Aureole

•To my tender and sweet wife WOUADJIE Diane Michelle;

• I express great gratitude to my friends from Mballa 2.

•Finally, i cannot forget the invaluable encouragement of my engineering friends. In particular: DOMBEU Dovani, YAKAM Loic, SOUFO Merime, YOGOUM Yannick, TEKENDO Rene. To all of those i left out, i want to say thank you.

• Thanks to all the unmentioned persons who have contributed even a little to this work. I did not forget you.

List of Abbreviations

FPK: **F**okker-**P**lanck **K**olmogorov
TMR : **M**ean **R**esident **T**ime
TR : **R**esident **T**ime
SDE : **S**tochastic **D**ifferential **E**quation
PZT : **L**ead **Z**irconate **T**itanate
PVDF : **P**olyvinylidene **F**luoride
WSN : **W**ireless **S**ensors **N**odes
DC : **D**irect **C**urrent
PVS : **P**hotovoltaic **S**olar **S**ystems
RFID : **R**adio **F**requency **I**dentification
MEMS : **M**icroelectromehanical **S**ystem
MIT : **M**assachusetts **I**nstitution **T**Technology
ICD : **I**mplantable **C**ardioverter **D**efibrillators

ECG : **E**lectrocardiogram

Contents

List of Figures

Abstract

Energy harvesting, known also as energy scavenging, covers a great body of technologies and devices that transform low grade energy sources such as solar energy, environmental vibrations, thermal energy, and human motion into usable electrical energy.

In this thesis, we proposed two physical models aiming to transduce the vibrations energy into electricity in order to energize the microelectronic devices. The first one is a hybrid model, using two mechanisms of transduction namely piezoelectric and electromagnetic transduction and subjected to the Gaussian white noise. The stochastic averaging method is used here in other to construct the $Fokker - Planck - Kolmogorov$ equation of the system whose the statistic response in the stationary state is the probability density. The mean square voltage and current are obtained for different value of white noise intensities as the output power generated by piezoelectric circuit and electromagnetic circuit. In addition, combining the Gaussian white noise and coherence excitation, the Ghost-Stochastic resonance is observed through the mean residence time and improve the amount of energy harvested by the scavenger. The agreement between the analytical method and those obtained numerically validates the effectiveness of analytical investigations. The second model proposed is also a hybrid model, built from the first model and subjected to the colored noise. Using the stochastic averaging method, the $Fokker - Planck - Kolmogorov$ equation of the system is constructed whose the statistic response in the stationary state is the probability density. The mean square voltage and current are obtained for different values of the linear and nonlinear resistance as the output power generated by piezoelectric circuit and electromagnetic circuit. The stability of the harvester is investigated by using probability approach. In addition, combining the colored noise and coherence excitation, the Ghost-Stochastic resonance is observed through the mean residence time and improve the amount of energy harvested by the scavenger. The agreements between the analytical method and those obtained numerically validate the effectiveness of analytical investigations. The results obtained in this thesis show the interest to use the load resistance exhibiting the nonlinearity in this research field and also, these results reveal that, while the natural frequency is absent in the coherent excitation, the system performance can be improved for a certain value of noise intensity.

Keywords: Stability; Stochastic p-bifurcation; Ghost Stochastic resonance; Probability; Nonlinear resistance; Energy harvesting.

Résumé

La récupération d'énergie, couvre un grand nombre de technologie et de dispositifs qui transforment des sources d'énergie de faible quantité telles que l'énergie solaire, l'énergie de vibrations, énergie thermique et mouvement humain en énergie électrique utilisable. Dans cette thèse, nous avons proposé deux modèles physiques visant à transformer les energies issues des vibrations mécaniques en électricité dans l'optique de rendre autonome les appareils microélectroniques. Le premier est un modèle hybride, combinant deux mécanismes de transduction à savoir la transduction piézoélectrique et transduction électromagnétique, et soumis à un bruit blanc Gaussien. Le deuxième modèle proposé est également un modèle hybride, construit à partir du premier modèle et soumis à un bruit coloré. Pour chacun des modèles, la méthode de la moyenne stochastique est utilisée afin de construire les équations de Fokker-Planck-Kolmogorov de chacun des systèmes dont la réponse statistique à l'état stationnaire est une densité de probabilité. Dans le premier dispositif, les carrés moyens de la tension et du courant sont obtenus pour des valeurs différentes du coefficient de couplage et de l'impedance électrique exprimant la puissance de sortie générée par les circuits piézoélectrique et électromagnétique. les carrés moyens de la tension et du courant du second modèle sont obtenus pour diverses valeurs du coefficient de la résistance linéaire et non linéaire. En combinant respectivement le bruit blanc Gaussien pour le premier modèle, le bruit coloré pour le second modèle avec une excitation cohérente, la résonance stochastique fantôme est observée à travers le temps moyen de résidence et améliore la quantité d'énergie récoltée par le système. La stabilité du système est étudiée en utilisant une approche probabiliste. Dans les deux modèles, La concordance entre la méthode analytique utilisée et celle obtenue numériquement valide l'efficacité des investigations analytiques. les résultats obtenus dans cette thèse montrent l'intérêt d'utiliser la résistance de charge exhibant des non-linarités dans ce domaine de recherche. En outre, ces résultats révèlent que, bien que la fréquence fondamentale soit absente dans la bande de fréquence de l'excitation cohérente, les performances du système peuvent être améliorées pour certaines valeurs de l'intensité du bruit.

Mots clés: Stabilité; Bifurcation phénoménologique; Résonance fantôme ; Probabilité; Résistance nonlinéaire; Récupération d'énergie.

General Introduction

A relatively recent area of research, dating from the $1990s$, is the ambient energy harvesting, especially that present in our environment. Thus, the energy harvesting, known also as energy scavenging, covers a great body of technologies and devices that transform low grade energy sources into usable electrical energy. The objective of this research area, which is the ambient energy harvesting, is to make portable or stationary microelectronic devices self-sufficient energicaly. Note that most of its microelectronic devices are powered by batteries. However, batteries have a low storage capacity of energy and therefore have a limited lifespan. The main problem with using these energy tank is the cost of maintenance associated with their periodic replacement and recharging. This periodic replacement and recharging not only decreases the lifespan of on-board systems, but can also pollute our environment. It is therefore wise to look for new sources of energy that can empower these electronic microsystems. It is in order to provide a solution to this problem posed by batteries that researchers have developed electromechanical systems that can transform ambient energy into electricity in order to directly power wireless devices or recharge batteries. It should be noted that the powers involved in this case are low, on the order of microwatt to watt. This self-supply is all the more conceivable as the new electronic technologies available are more and more energy-efficient as well as the technological progress made in the electronic field on storage devices which are also necessary to compensate for intermittences as well as the mismatch between production and consumption. In a context of battery or network power, the objective of ambient energy recovery is to be less restrictive and less expensive in terms of investment and operation.

Let's notice that, our environment is endowed with many forms of renewable energy. We can cite: mechanical energy from vibrations and mechanical stresses, thermal energy from heating devices, wind energy from the movement of air masses, solar

energy which is the first source of energy permanently received by the Earth. In this thesis, we are interested in mechanical energy. This interest in energy from mechanical vibrations is due to its ubiquity in the real environment. It is well known in the literature that, three transduction principles are commonly used to convert vibration energy into electricity: electrostatics, electromagnetic and piezoelectric[1, 2, 3]. The motivation behind this research is largely due to recent advancements in micro-electromechanical systems (MEMS) technology, specifically the construction of small low powered sensors which are low power, low weight, cheap to produce and, because of their small size, can be applied to a large variety of scenarios and capable of being placed in inaccessible or hostile environments [4, 5]. Using an assortment of different sensing techniques, MEMS technology can be used to develop sensors of millimeter-order. It is shown that MEMS sensors can also be used in the biomedical domain, in modern constructions such as pacemakers and electrical stimulation pain management devices, or being part of a wearable network of autonomous sensor systems which can monitor the health and/or comfort of an individual [6, 7, 8, 9].

Although one observes in the literature an exponential increase of the number of publications concerning the energy harvesting field, let us notice that, the most of these models suffer of the optimization problem because of their linear configuration. Indeed, the linear scavengers or resonance scavengers work efficiently with limited bandwidth near their resonant frequency [10, 11]. If the natural vibration frequency slightly shifts from the designed frequency, the performance of harvester can dramatically decrease. Thus resonance harvesters are therefore suited only for fixed narrow-band excitations. However, realistic environments vibration are likely composed of multi-frequency harmonics as well as broadband stochastic excitation [12], such linear vibration theory is inefficient for application. Thus, widening the bandwidth of the energy harvesting devices in the order to improve the harvested energy by the harvester is the main challenge of this research field.

Many optimization technique have been proposed by researchers in the literature. Nonlinear systems have proven to be capable of responding over a broad range of frequency [3]. In the energy harvesting systems, nonlinearities can appear in the spring

force in the mechanical subsystem or in electrical component such as the resistor. A number of recent contributions seek to use nonlinearity in a novel way to improve performance [13, 14, 15, 16]. Designers are exploring the use of nonlinearity to widen the bandwidth and reduce the ambient frequency sensitivity of such harvesters [17]. In addition, in the nonlinear systems, many phenomena can take place such as the stochastic bifurcation phenomenon.

The stochastic bifurcation contains the D-bifurcation and the P-bifurcation problems. It is worth noting that, the D-bifurcation focuses on the stochastic bifurcation point in the probability one sense which is measured by the maximal Lyapunov exponent [18]. The P-bifurcation studies the mode of the stationary probability density function or the invariant measure of the stochastic process. The stochastic P-bifurcation takes place when the mode of the stationary probability density function changes in nature. It indicates the jump of the distribution of the random variable in probability sense. The D-bifurcation and the P-bifurcation are independent. There is no direct relation between these two stochastic bifurcation phenomena [18].

An other optimization technique is to built the hybrid models [19, 20, 21]. The hybrid models combine many mechanisms of transduction such as piezoelectric with electromagnetic mechanism, electrostatic with electromagnetic mechanism or piezoelectric with electrostatic mechanism to scavenge energy from external vibration. These hybrid models have shown their capacity to improve the system performance. Some research group have shown that, by combining the coherent and random excitation, the stochastic resonance and ghost-stochastic resonance phenomenon can occur. These two phenomena are characterized by the large amplitude of vibration improving thus the amount of harvested energy. The stochastic resonance occurs when the frequency of system's vibration is present in the frequency bandwidth of the harmonic excitation. However, when the maximum amplitude of the system is reached for a frequency of vibration absent in the frequency bandwidth of the harmonic force, this phenomenon is called a ghost-stochastic resonance.

While one observes in the literature, a growing interest in the theoretical investigation of the ghost-stochastic resonance phenomenon in the nonlinear systems [22, 23, 24,

25, 26, 27, 28], the study of this phenomenon on the performance of energy harvesting devices according to our knowledge is not yet done. The main objective of this thesis is to investigated the performance of the hybrid system when the ghost-stochastic resonance occurs. It is around of the problematic of optimization of the output generated by the energy harvesting system that this research work has been organized.

•Chapter I is devoted to the presentation of the literature review on the energy harvesting system. This chapter also replaces the energy harvesting from the electrostatic, electromagnetic and piezoelectric in their context by insisting on the motivations what have leaded at the development of the energy scavengers.

•Chapter II is consecrated to the mathematical modeling of the dynamics of the proposed models in the framework of this thesis. We also present in this chapter, the analytical and numerical methods used.

•Chapter III is devoted to the presentation of the main results obtained in this thesis, followed by a conclusion with an outlook for future studies.

CHAPTER I

LITERATURE REVIEW ON THE ENERGY HARVESTING SYSTEM

I.1 Introduction

Energy harvesting covers a great body of technologies and devices that transform low grade energy sources such as solar energy, environmental vibrations, thermal energy, and human motion into usable electrical energy. Thanks to the recent technology progress recorded in the electronic domain, the electrical energy consumption by the electronics components has dramatically decreased, incited the proliferation of the wireless devices. Thus, the energy harvesting technology has become a very attractive solution for a wide variety of applications such as consumer electronics, outpatient medical electronics (hearing aids, pacemakers, smart implants) or imaging (camera inside the human body). This chapter aims to present the generality on some energies sources available in our real environment and their mechanism of transduction. Here, we insist on the micro energy source most particularly the mechanical vibrations and the motivations what have leaded at the development of the energy scavenging devices allowing thereby to power wearable appliances. First of all, the motivations of this thesis are presented followed the presentation of some potential energies sources in the real environment and their corresponding transduction mechanism and applications. A literature review on the energy scavenging devices is also made. The limits of applications of the models encountered in this research field are presented. From these limits, we give the contribution of this thesis.

I.2 Motivations

The decrease in energy consumption by electronic components has enabled the development of mobile applications, such as wireless sensors. Most of these sensors, or networks of sensors without such as those worn by the person (Body Sensor Area Network) are powered by batter-

ies. Wireless Radio frequency identification (RFID) sensors, which are the most commonly used, consume tens of microwatts in standby mode and several hundred microwatts in active mode. Although notable progress has been made in recent years, batteries still have a limited lifespan and their use can be problematic depending on their accessibility and volume constraints (especially for subcutaneous medical implants) . We are therefore seeking to explore other alternatives for supplying power to these sensors, for example by recovering the energy available in the ambient environment. Thus, thermal gradients, mechanical vibrations, light waves or radiofrequencies in particular, constitute potential sources of energy for supplying these sensors. Rabaey [29] and Starner [30] note that current progress on the energy consumption of on-board devices makes it possible to consider other power sources resulting from the exploitation of ambient energy, which makes it possible to get rid of the problem of batteries which are the main limit to the lifespan of wireless sensor networks. Indeed, in the case of networks made up of a very large number of nodes, it is difficult to envisage replacing all the batteries. Fig.1 shows the evolution of power density as a function of lifetime for batteries and for solar and vibration sources. Power densities are given in $\mu W/cm^3$, except in the case of energy solar where it is given in $\mu W/cm^2$. In this figure (fig.1), the densities of solar and vibratory energies are respectively represented by

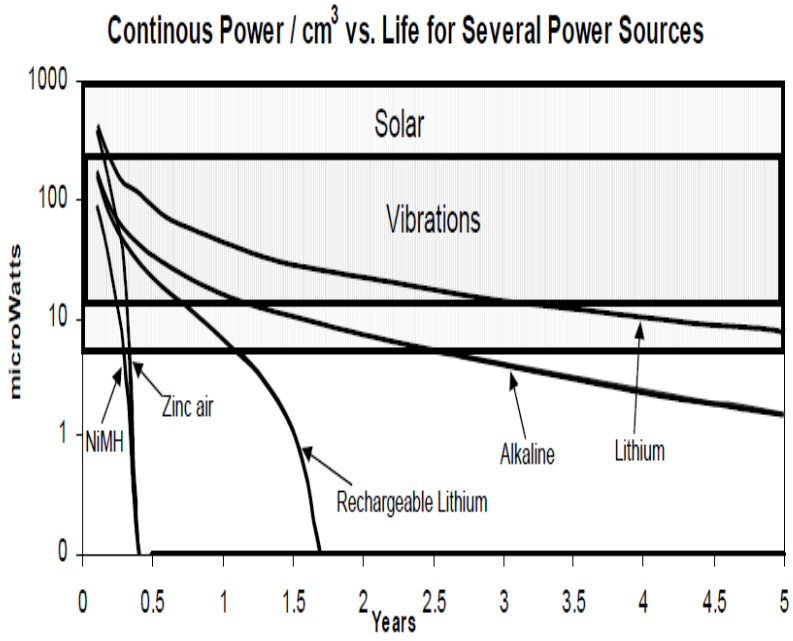

Figure 1: Power density versus lifetime for batteries, solar cells, and vibration generators. [29].

a light gray and dark gray rectangle. They are not function time, unlike the energy density of

batteries. In the case of solar energy, the bottom of the rectangle corresponds to the radiation in a lit room and the top to the direct sunlight. In the case of vibratory energy, the rectangle corresponds to common vibration levels, ranging from a human's walking to vibrations generated by a rotating machine for example. However, the use of batteries is still quite widespread, with research on hydrogen cells (which present miniaturization problems) or nuclear batteries , which includes energy densities thousands of times greater than Conventional Li-Ion batteries [31]. The work developed in this thesis is based on the optimization of electromechanical energy recovery systems using piezoelectric and magnetic elements in order to drastically increase the performance of this type of micro-generator, which allows for innovative applications. It is around these problematic that work of this thesis have been focused. Fig.2 shows the potential applications of MEMS vibration energy harvesters to power low-power devices such as sensor, calculator, watch.

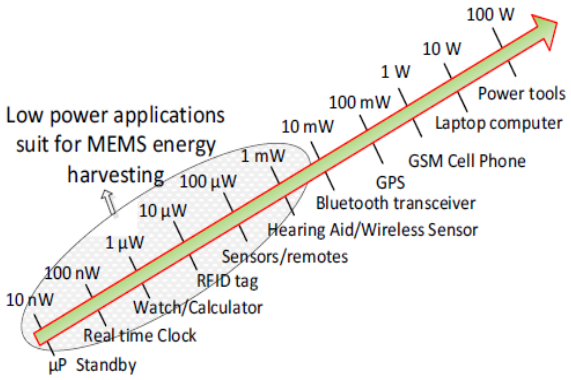

Figure 2: Power consumption of wireless sensor nodes [32].

I.3 Some potential sources of the ambient energy and theirs transduction mechanisms in another form of energy

Our environment is doted of a lot of energies sources. We can cite:

I.3.1 Radio frequency energy

Radio frequency energy (RF), also known as an "RF field", "RF wave" or "RF emission", is a form of electromagnetic energy that is part of the electromagnetic spectrum. It comes from

radiofrequency sources which can be of natural or human origin. Radiofrequency sources of natural origin have the advantage of being ubiquitous in our daily life. We can cite among others: the magnetic field of the Earth, which directs the compasses towards the North, visible light, lightning ... Regarding sources of human origin, they are ubiquitous much more in urban areas where we observe high density of electronic devices. These include: electrical devices such as microwave ovens, wireless devices (cell phones, Wi-Fi devices, Bluetooth devices), power lines, commercial radio and television broadcasting (radio stations, television). Note that these radiofrequency energies, transmitted continuously by telecommunication networks, are made available over a wide range of frequencies. The goal of radio frequency energy harvesting is to convert energy from ambient radio frequency sources into direct current and voltage. The conversion principle is based on an RF-DC converter, also called a rectifying antenna. Indeed, A rectifier antenna is a special class of antennas capable of converting radio frequency energy into direct current. They are used in systems that transmit electricity through radio waves. A simple rectifier unit consists of a dipole antenna with an RF diode linking the dipole elements. The diode rectifies the alternating current induced in the antenna by the microwaves, producing direct current which drives a load astride the diode. In general, rectifier antennas incorporate Schottky diodes thanks to their very low forward voltage threshold and very fast switching time. Fig.**??** thus shows a block diagram of the conversion of radiofrequency energy into electrical energy. According to this diagram, radiofrequency waves (1) are received by a receiving antenna (2), then converted into direct voltage and current by an RF-DC converter (3). The current thus generated can be used to supply a load, which represents for example a sensor to be supplied. More precisely, the RF-DC converter (3) comprises an input filter (5), also called a radiofrequency (RF) filter or high frequency (H F) filter, a rectifier (6) and an output filter (7), also called a DC filter. The input filter (5) is placed between the receiving antenna (2) and the rectifier (6). It is a low pass filter which is used to block unwanted harmonics.

Ekkaphol et al.[33] proposed a dual-band rectifier for RF energy harvesting systems that was designed to operate at 2.1 GHz and 2.45 GHz. In this work, the authors shown that, the first channel can provide the maximum efficiency of 24% with 1.9 V of the output voltage at 10 dBm of input power. On the other hand, a maximum efficiency of 18% and 1.7 V of the output voltage can be achieved by the second channel at 10 dBm of input power. Pavone et al.[34] shown the activities addressed to design a wideband system to recover wideband. energy from electromagnetic

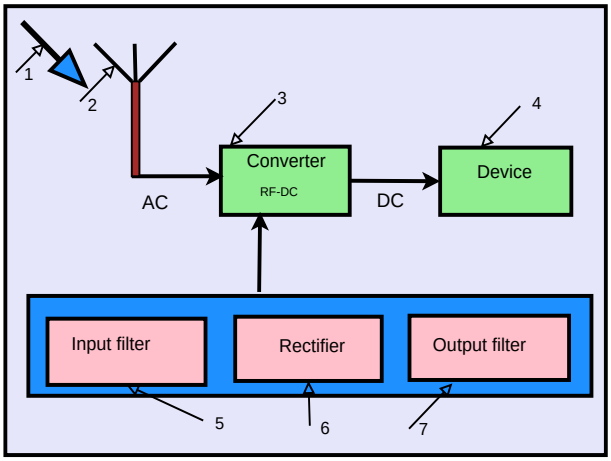

Figure 3: Schematic of the principle of conversion of radiofrequency energy into electrical energy.

sources present in the environment. The main idea of their work was to develop battery-free wireless sensors able to capture the available energy into the mentioned bandwidth. The authors also realized self-powered Wireless Networks based on Ultra Lower Power (ULP) sensors minimizing the need of dedicated batteries. Hemour and Wu [35] built the radio-frequency rectifier for electromagnetic energy harvesting. They examined and discussed the electromagnetic sources responsible for the presence of ambient radio-frequency (RF) energy. Mahima et al.[36] presented an experimental RF energy harvesting system to harvest energy from cell towers. In this work, an electromagnetically-coupled square microstrip antenna is designed and fabricated for deployment in the presented system. Antenna gain of 9.1dB and bandwidth from 877 MHz to 998 MHz is achieved. In addition, a Schottky diode-based single stage voltage doubler and six-stage voltage doubler has also been designed and fabricated for DC voltage generation. It emerges from the results obtained that a voltage of 2.78V is obtained at a distance of 10m from the cell tower and a voltage of 0.87V is obtained at a distance of 50m. Diego et al. [37] exploit genetic algorithms to design a rectenna required to harvest ambient radio-frequency (RF) energy from four different RF bands in critical (ultra-low power) conditions. For this purpose a set of multi-resonant annular-ring patch antennas are pixel-wise described inside an electromagnetic simulator to provide the population of individuals among which the genetic tool is able to select the most adapted one with respect to the design specifications. Danilo et al. [38] presented an UHF RFID(radio frequency identification) energy-harvesting system enhanced by a DC-DC charge pump in silicon-on-insulator technology. The authors demonstrate experimentally the capability of the system to autonomously perform temperature data logging up to a distance

of 5 m from a conventional UHF RFID (Radio Frequency Identification) reader used as an RF energy source. It is nothing that,although the electrical energy harvested by the radio-frequency energy harvesting devices is suitable for the embarked systems, these energy harvesters present some disadvantages. We can enumerate:

⋆ the cost of an energy harvester can be high when compared with the overall cost of a wireless sensor;

⋆ it is not easy to have a small converter;

⋆ low energy density compared to another form of energy existing in the environment. The table4 show the energy density for some energy source available in the real environment.

Table 1: Comparison of power density of energy harvesting methods [39]

Energy source	Power density
Acoustic noise	$0.96\mu W/cm^2$
Temperature variation	$10\mu W/cm^3$
Ambient radiofrequency	$1\mu W/cm^2$
Ambient light	$100mW/cm^2$(direct sun); $100\mu W/cm^2$(illuminated office)
Termoelectric	$6W/cm^2$
Vibration (micro-generator)	$4W/cm^3$(human motion); $800W/cm^3$(machines)
Vibration (piezoelectric)	$200\mu W/cm^3$
Airflow	$1\mu W/cm^2$
Shoes inserts	$330\mu W/cm^2$
Hand generator	$30W/kg$
Heel strike	$7W/cm^2$

These values should help you understand that the perfect energy harvester for your application depends on your application.

I.3.2 Thermal energy

Generation of electricity via thermal gradient is another form of regenerative power supply proposed for powering portable MEMS devices. Indeed, thermal energy is obtained from heat present in the ambience or from heat generated during some process. Thermoelectric power generators consist of three major components: thermoelectric materials characterized by a high electrical conductivity and low thermal conductivity, thermoelectric modules and thermoelectric systems that interface with the heat source. Thermoelectric materials the most used in the industrials applications are: alloys based on Bismuth (Bi) in combinations with Antimony (Sb), Tellurium (Te) or Selenium (Se); materials based on alloys of Lead (Pb); materials fabricated from

silicon germanium (SiGe) alloys; material semiconductor compound $\beta - Zn_4Sb_3$. A thermoelectric module is a circuit composing of thermoelectric materials that generate electricity from heat directly. It is consisted of two dissimilar thermoelectric materials joining in their ends: an n-type composed of a surplus electrons with respect to the holes and a p-type composed of a surplus of the holes with respect to the electrons semiconductors. A direct electric current will flow in the circuit when there is a temperature difference between the two materials. It is worth noting that, thermoelectric energy harvesters usually use two mechanisms to convert heat in useful electrical power namely thermoelectric effects like Peltier effect and Seeback effect [40]. Let us notice that, extraction of energy from a thermal source requires a thermal gradient and conversion efficiency mainly depends on the temperature difference between the heat source and the environment i.e. the cold and the hot side [41]. A greater temperature difference leads to a better output. However, Pyroelectric effect [41], based on the spontaneous polarization in certain anisotropic solids due to a time-dependent temperature variation can be used when there is a uniform temperature gradient in the ambience. The energy output from thermal variation is about $10\mu W/cm^2$ and can go up to $60W/cm^2$ in case of a thermoelectric source [39].

The advantages of thermoelectric generators are that they are reliable, solid state and have long operation times with little noise and emissions [42]. However, thermoelectric generators exhibit some drawbacks such as low efficiency and relatively high cost. Indeed, practical problems exist in using thermal energy harvester in certain types of applications resulting from a relatively high electrical output resistance, which increases self-heating, and a relatively low thermal conductivity, which makes them unsuitable for applications where heat removal is critical, as with heat removal from an electrical device such as microprocessors.

I.3.3 Solar energy

Solar energy is an energy source available on the earth surface. It can be converted in another form of energy according to the needs. Thus, we have:

• Solar thermal energy. Here, the solar energy is converted in calorific energy with the solar thermal installations (solar water-heater, solar conditioning). Indeed, the solar energy can be converted in heat thanks to the coolant that flows into the thermal module exposed at sun. One of the application of the solar thermal energy is the solar air-conditioning.

• Photovoltaic solar: Photovoltaic solar is the technology that generates direct current from

semiconductors when they are illuminated by photons. Contrary to the solar thermal energy that use the sun like heat source, the solar photovoltaic use the sun as light source by conversing the photons energy contained into the solar light in electricity via a semi-conductor material. Most of the semi-conductor material today are made of crystalline silicon (c-Si) [43]. The advantages of the photovoltaic solar systems (PVS) are their ease of integration, modularity, lack of emission or noise, lack of moving parts and use sunlight which is available in the real environment. The drawbacks of PVS are their low conversion efficiencies and high cost and the unequal repartition of the sunlight at the surface of the Earth.

• Solar at thermodynamic concentration: It is a technology that use the mirrors which concentrate the solar energy towards the tubes containing the coolant. The temperature of the tube can reach $500\mu C$. The heat obtained can be transferred to the water circuit, the steam generated by heating activate the turbine coupled to the alternator that produces the electricity.

I.3.4 Wind energy

Among the various forms of existing renewable energy sources, wind energy is one of the remarkable sources in the macro scale for generating electricity. A wind generator is a device that transforms the kinetic energy of the wind in electricity. Let us notice that, the wind generator generates the electricity from the wind motion in the macroscopic scale. A challenge here is to use small windmills on highways and other bridges nearby seas where the wind pressure is very large which in combination with speed induced by vehicular motion can be use to generate energy. This generated energy can be used to power lights and traffic signals on highways [44].

I.3.5 Vibrations energy and its transduction mechanism

a) Some potential sources of vibration energy

Multiple sources of induced vibration exist, characterized by different mechanisms of excitation and different effects. There are three of the most important sources of ground-induced vibration: piling, road traffic and railways. Indeed, the pile driving excitation at the head of the pile will generate stress waves inside the pile itself. Vibrations induced by road traffic are mainly generated by heavy vehicles [45]. According to Hunaidi [45] the predominant frequencies and amplitude of vibration from traffic sources depends on multiple factors including for instance the condition of the roads, the vehicle weight, the speed of the vehicle, the suspension

system, soil type and stratification. Railways are one of the most important sources of vibration, whether underground or surface railways. Trains generate vibration through mainly two excitation mechanisms: quasi static excitation and dynamic excitation. The quasi-static excitation, also called wheel-passing frequency, arises due to static train load generating deflection around the wheel. The effect of this excitation mechanism is dominant close to the track and generates excitation within a range of 0-20 Hz [46, 47]. Another potential source of vibration energy is Blood circulation in hearth. Indeed, At the onset of blood circulation, the heart is a tubular structure with a wall made up of three layers: an outer layer of contractile myocytes and an inner layer of endocardial cells in contact with the blood are separated by an elastic, cell-free layer known as the cardiac jelly [48]. The contraction wave squeezes different cross sections of the tube sequentially, pushing blood into the aortic arches and the dorsal aorta without significant backflow. This contraction is significantly shorter than the entire heart cycle [49], which is reflected by the generation of pulsatile flow [50], regardless of the contraction wave speed.

There are four types of flow in heart and circulatory sytem: laminar flow, turbulent flow, and vortex flow:

• Laminar flow refers to a predictable distribution of flow velocities in layers (lamina) that parallel the vessel wall. This form of flow is idealized but is nevertheless a fairly good approximation of the flow in medium and small sized blood vessels throughout the human circulatory system. In real vessels, however, the flow profile is usually more blunted because of elasticity and pulsatility effects, even though the general laminar pattern may be maintained. When the flow profile becomes flattened in this form with a nearly uniform distribution of velocities across the lumen, the term "plug flow" is sometimes applied

•Vortex flow refers to localized swirling or stagnant blood flow that has separated from the central streamlines within a vessel. Such vortices, also called flow eddies, frequently occur at vascular bifurcations and distal to areas of stenosis. Unlike turbulent regions, areas of vortex flow are composed of slowly moving currents and streamlines that are not random but are often countercurrent to the main flow direction.

•Turbulent flow is a noisy form of fluid transport in which velocity components randomly fluctuate. Turbulence takes place when blood velocities exceed a critical threshold or when vascular morphology creates conditions that disrupt the laminar flow state. In the human circulatory system, turbulent flow is seen in the heart aorta, in the region of vascular bifurcations,

and distal to areas of stenosis. In disturbed and turbulent blood flows, a fluctuating (random) velocity field is superimposed on the mean velocity field (which is often regular) [51].

Usually, a heart beats between 60 and 80 times per minute, but everyone has their own normal heartbeat rhythm. Some hearts beat faster or more slowly than others. The pumping action of the heart is triggered by electrical impulses that begin in your heart's natural pacemaker, called the sinus node (also called sinoatrial or SA node) [52]. A normal heartbeat makes two sounds like "lubb-dupp", which are the sounds of your heart valves closing but could sometimes been contaminated by heart murmurs. Heart murmurs are sounds during your heartbeat cycle such as whooshing or swishing made by turbulent blood in or near the heart. Doctors hear a heart murmur as a whooshing sound between heartbeats. The whoosh is just an extra noise that the blood makes as it flows through the heart [53]. These sounds can be heard with a stethoscope. Heart murmurs can be present at birth (congenital) [54, 55] or develop later in life. Often, heart murmurs are harmless (innocent) and don't need treatment. A heart murmur isn't a disease, but murmurs could indicate an underlying heart problem. Some heart murmurs may require follow-up tests to be sure the murmur isn't caused by a serious underlying heart condition. Treatment, if needed, is directed at the cause of your heart murmur [56].

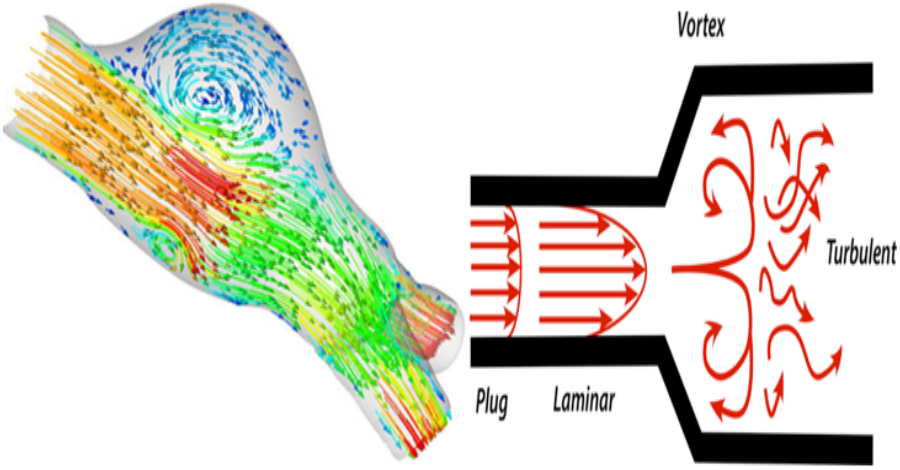

Figure 4: Schematic showing the types of flow in heart and circulatory system: laminar flow, turbulent flow, and vortex flow.

b) vibration powered generator

A vibration powered generator is a type of electric generator that converts the kinetic energy from vibration into electrical energy. The vibration may be from sound pressure waves or other ambient. Vibration powered generators usually consist of a resonator which is used to amplify the vibration source, and a transducer mechanism which converts the energy from the vibrations into electrical energy. As pointed out by Williams et al.[10], the vibration powered generator usually consists of a magnet and coil (electromagnetic transducer)[57], the capacitor (electrostatic transducer) [58] or a piezoelectric material (piezoelectric transducer) [59, 60]. Nowadays, vibration-based energy harvesting has received growing attention over the two last decade [61, 62, 63]. The research motivation in this field is due to the reduced power requirement of small electronic components, such as the wireless sensor networks used in structural health monitoring applications.

A) Electromagnetic generators and their applications

Electromagnetic based generators use Faraday's law of induction to convert the kinetic energy of the vibrations into electrical energy. They consist of magnets attached to a flexible membrane or cantilever beam and a coil. The vibrations cause the distance between the magnet and coil to change, causing a change in magnetic flux and resulting in an electromagnetic force being produced.

Generally the coil is made using a diamagnetic material as these materials have weaker interactions with the magnet that would dampen the vibration. It is well known in the literature that some pioneering studies on mini electromagnetic vibration-power generators were performed by researchers at the University of Sheffield [10] and MIT [64]. Their work indicated that a simple spring mass system can generate power at the $1\mu W$. Beeby et al.[65] designed an electromagnetic energy harvester by using four magnets arranged on an etched cantilever with a wound coil located within the moving magnetic field. This harvester successfully delivered 30% of the power supplied from an air compressor to useful electrical power in the load. Mann [66] designed a nonlinear electromagnetic energy harvester that uses magnetic interactions to create a bistable potential well and validated the potential well escape phenomenon can be used to broaden the frequency response by theory and experiments. Kulah et al.[67] proposed a different electromagnetic energy harvester structure with two resonators, the top of which is a plate sus-

pended with a soft spring to target the low resonance frequency, while the bottom resonator was a cantilever beam corresponding to higher resonance. Zhus research group designed a horizontal tunable electromagnetic vibration-based microgenerator, where an effective resonant frequency range from 67.6 to 98 Hz was obtained using variable axial loads from a horizontal magnetic force applied to the cantilever beam[68]. A detailed mathematical model for an electromagnetic energy harvesting architecture was proposed to estimate the energy generated by the architecture by computing the static and dynamic magnetic and electric fields in Ref.[69]. Following the same ideas, Marin et al.[70] improved the electromagnetic energy harvester by using an additional pair of magnets to create a secondary air gap, or cell, for a second coil to vibrate within, and observed a 23% enhancement in output with minor increase in volume. This double cell harvester was then further developed by using four double cells with varying resonance frequencies incorporated in the electromagnetic energy harvesting system [71]. It was found that the double cell array could generate a similar magnitude of power to a single cell but provided three times larger bandwidth. A multifrequency vibration-based micro-electromechanical system (MEMS) electromagnetic energy harvesting device was presented with a permanent magnet and a circular suspension structure on a MEMS EH chip[72]. This energy harvesting device can vibrate with three resonant frequency corresponding to 840, 1070, and 1490 Hz respectively. Oumbé et al.[73] analyzed an electromechanical energy harvester system with geometric and ferroresonant nonlinearities. Nowadays, a lot of electromagnetic generators have been fabricated, and details of these devices are provided in Ref.[74]. One of the most important advantages of these systems is that, they require no input voltage source to initiate power generation. The drawbacks of this transduction mechanism is that, an electromagnetic materials are bulky in size and are complicated to integrate with micro-electromechanical system. Electromagnetic generators could be used in the health area to power cardiac simulator so called peacemaker [74]. They can also used to power sensors.

B) Electrostatic generators and their applications

Electrostatic generators are mainly based on the variation of the gap between two electrodes of a capacitor. They need to be pre-charged before they can produce power [75]. The idea general is to place a certain amount of energy on the capacitor of the micro-generator and to use ambient vibratory energy to decrease the capacity of the micro-generator by increasing the gap between

the electrodes (which requires mechanical work). Two cases are possible:

• a decrease in capacity at constant voltage, in this case loads electric are generated,

• At constant load, and in this case, the voltage increases as well as the energy electrostatic on capacitance. In both cases, the mechanical work required for the separation of the electrodes is converted in electrical energy. Micro-electromechanical Systems (MEMS) based electrostatic harvesters were firstly reported by Chandrakasan group at Massachusetts Institution of Technology (MIT) [75, 76] and further developed by Roundy [77]. The reported electrostatic energy harvesters in the literature make use of changes in gap distances in multiple ways. Typical designs make use of comb drives and the changes in capacitance are driven by a vibration source [78]. The major drawback of electrostatic harvesters is the requirement of a bias for its operation. The bias can be provided by electrets [79], power management circuitry [80], by recharged floating electrodes [81] or by large re-charged capacitor [82]. Lin et al.[74] reviewing the state of the art on the electrostatic generators.

There are many potential applications of electrostatic energy harvesting devices. These generators can be used to power low-power Wireless sensors nodes (WSNs).

C) piezoelectric generators and their applications

• Generality on the piezoelectric materials

Piezoelectricity is a quality of material asymmetry that leads to the conversion of electric signals into physical deformation(indirect effect) and conversely physical deformation into electric signal (direct effect). Among these effect of the piezoelectric materials, alone the direct effect is useful in the energy harvesting field. In fact, an applied pressure in the piezoelectric materials causes movement of the dipole moment within these latter, and a flow of charges if crystals are aligned [83]. This makes piezoelectricity useful for a variety of industry purposes, particularly those related to vibrational generation and actuation. More work was done to explore and define the crystal structures that exhibited piezoelectricity. This culminated in 1910 with the publication of textbook on Crystal Physics [84], which described the 20 natural crystal classes capable of piezoelectricity, and rigorously defined the piezoelectric constants using tensor analysis. Piezoelectric materials can be broadly classified as crystalline, ceramic and polymeric piezoelectric materials [85]. The most commonly produced piezoelectric ceramics are lead zirconate titanate (PZT), barium titanate and lead titanate. Gallium nitride and zinc oxide can also be regarded

as a ceramic due to its relatively wide band gap, that can generate an instantaneous polarisation inside their lattice on application of a force. The semiconducting Piezoelectric material (PM) possesses unique advantage such as compatibility with the Integrated circuits and semiconductor devices. Further, inorganic ceramic piezoelectric materials have several advantages over single crystal, such as the ease of fabrication into a variety of shapes and sizes as single crystals requires cutting along the crystallographic directions, thus minimising the possibilities of cutting into different shapes. The next class of piezoelectric materials namely organic polymer such as PVDF, have low Young's modulus compared to the inorganic piezoelectric materials. Piezoelectric polymers (PVDF, 240 mV-m/N) possess higher piezoelectric stress constants (g_{33}), an important parameter in sensors, than ceramics (PZT, 11 mV-m/N)[85], which show that they can be better sensors than ceramics. Moreover, piezoelectric polymeric sensors and actuators, due to their processing flexibility, can be readily manufactured into large areas, and cut into a variety of shapes. In addition polymers also exhibit high strength, high impact resistance, low dielectric constant, low elastic stiffness, and low density, thereby a high voltage sensitivity which is a desirable characteristic along with low acoustic and mechanical impedance useful for medical and underwater applications. Among the PM, PZT ceramics are popular as they have a high sensitivity, a high g_{33} value. They are however brittle. Furthermore, they show low Curie temperature, leading to constraints in terms of applications in harsh environmental conditions. However, promising is the integration of ceramic disks into industrial appliances moulded from plastic. This resulted in the development of PZT-polymer composites, and the feasible integration of functional piezoelectric materials composites on large scale, by simple thermal welding or by conforming processes.

• Linear Theory of Piezoelectricity

Following Ref.[86], in linear piezoelectricity, the equations of linear elasticity are coupled to the charge equation of electrostatics by means of the piezoelectric constants. Let u_i, the Cartesian components of the infinitesimal mechanical displacement of a material point, S_{ij}, strain tensor. Thus, we can define the strain tensor as follow:

$$S_{ij} = \frac{1}{2}\left(u_{i,j} + u_{j,i}\right) \tag{1}$$

where a comma followed by an index denotes partial differentiation with respect to a space coor-

dinate ($\frac{\partial u_i}{\partial x_j}$). It is worth nothing that, the antisymmetric portion of the mechanical displacement gradient determines the infinitesimal local rigid rotation, which is allowed to take place without constraint in the continuum. The velocity of a point of the continuum is given by [86]:

$$w_i = \dot{u}_i = \frac{\partial u_i}{\partial t} \tag{2}$$

with t representing the time. Let T_i, the mechanical interaction force per unit area acting across a surface at a point and T_{ij}, the stress tensor. The traction vector T_i and the stress tensor can be related by the following formula:

$$T_j = n_i T_{ij} \tag{3}$$

where n_i denotes the components of the outwardly directed unit normal to the surface across which the traction vector acts. Let remind that, in electrical theory, the cartesian components of the electric field intensity and electric displacement are denoted, respectively by E_i and D_i. These two vectors can be related by the following relation [86]:

$$D_i = \varepsilon_0 E_i + P_i \tag{4}$$

with P_i, the components of the polarization vector, and ε_0, the permittivity of free space. Let φ a scalar electric potential whose the electric field vector E_i derive. The conservation of energy for the linear piezoelectric continuum results in the first law of thermodynamics [86]:

$$\dot{U} = T_{ij}\dot{S}_{ij} + E_i\dot{D}_i \tag{5}$$

where U is the stored energy density for the piezoelectric continuum. The electric enthalpy density H is defined by[86]:

$$H = U - E_i D_i \tag{6}$$

By combining Eq.(5)-6, we can write:

$$\dot{H} = T_{ij}\dot{S}_{ij} - D_i\dot{E}_i \tag{7}$$

Eq.(7) show that, the electrical enthalpy is a function of the strain tensor S_{kl} and the electric field E_k ($H = f(S_{kl}, E_k)$). Thus, we can write:

$$T_{ij} = \frac{\partial H}{\partial S_{ij}}; D_i = -\frac{\partial H}{\partial E_i} \tag{8}$$

In linear piezoelectric theory the form taken by H is [86]:

$$H = \frac{1}{2} C^E_{ijkl} S_{ij} S_{kl} - e_{iij} E_i S_{ij} - \frac{1}{2} \in^s_{ik} E_k E_i \tag{9}$$

where

C^E_{ijkl} is the modulus of elasticity expressed in P_a

e^E_{kij}, the piezoelectric modulus expressed in C/m^2

$\in^s_{ij}$, the permittivity expressed in F/m

These three constants verify the following equations:

$C_{ijkl} = C_{ijlk} = C_{jikl} = C_{klij}$; $e_{ijk} = e_{ikj}$; $\in_{ij} = \in_{ji}$. Substituting Eq.(9) into Eq.(45), we obtain the linear constitutive equations of the piezoelectric materials:

$$\begin{aligned} T_{ij} &= \frac{1}{2} C^E_{ijkl} S_{kl} - e_{kij} E_k \\ D_i &= e_{ikl} S_{kl} - \in^s_{ik} E_k \end{aligned} \tag{10}$$

Without loss the generality, we use the shorter matrix indices instead of the consistent tensor notation by tensor indices. The reason for this is the symmetry of the strain and stress tensor. Thus, the tensor double indices (ij) and (kl) can be replaced by the matrix indices. The table 2 shows the matrix index of the stress tensor.

Table 2: Matrix index

ij or kl	p or q
11	1
22	2
33	3
23 or 32	4
31 or 13	5
12 or 21	6

By using the table 2, the linear constitutive equations (Eq.(10)) and the electrical enthalpy(Eq.(9)) can be expressed in the following formula:

$$H = \frac{1}{2} C_{pq}^{E} S_p S_q - e_{ip} E_i S_p - \frac{1}{2} \in_{ik}^{s} E_k E_i \tag{11}$$

$$\begin{aligned} T_p &= \frac{1}{2} C_{pq}^{E} S_q - e_{pk} E_k \\ D_i &= e_{iq} S_q - \in_{ik}^{s} E_k \end{aligned} \tag{12}$$

• Literature review on the Piezoelectric Energy Harvesters and theirs applications

Piezoelectric based generators use thin membranes or cantilever beams made of piezoelectric crystals as a transducer mechanism. When the crystal is put under strain by the kinetic energy of the vibration a small amount of current is produced thanks to the direct effect of the piezoelectricity. These mechanisms are usually very simple with few moving parts, and they tend to have a very long service life. This makes them the most popular method of harvesting the energy from vibrations [87, 88]. The ability to make piezoelectric generators on such a small scale is the main advantage of this method over the electromagnetic generators, especially when the generator is being developed to power microelectronic devices. It is known in the literature that, a piezoelectric energy harvester was first described in 1969 in a patent awarded to Ko [89]. This energy harvesting system converts body motion into electrical energy to power Cardiac simulators. Spector et al.[90] proposed a theoretical model by using a beam element and performed experiment to harvest power from PZT material. They showed that a simple beam bending can provide the self-power source of the strain energy sensor. Kim et al.[91] reported that piezoelectric energy harvesting showed a promising results under pre-stress cyclic conditions and validated the experimental results with finite element analysis. S. Zhao et al. [92] studied the deterministic and band-limited stochastic energy harvesting from uniaxial excitation of a multilayer piezoelectric stack; they found that a quadratic relation between maximum power and pressure is observed for bandlimited stochastic excitation. M. Borowiec et al.[93], studied the effect of noise on energy harvesting in a beam with stopper. They showed how the noise component of the excitation influences the stability of the solution.

Although one observes in the literature an exponential increase of the number of publications concerning the energy harvesting field, let us notice that, the most of these models suffer of the optimization problem because of their linear configuration. Indeed, the linear scavengers or resonance scavengers work efficiently with limited bandwidth near their resonant frequency [11]. If the natural vibration frequency slightly shifts from the designed frequency, the perfor-

mance of harvester can dramatically decrease. Thus resonance harvesters are therefore suited only for fixed narrow-band excitations. However, realistic vibration environments are likely composed of multi-frequency harmonics as well as broadband stochastic excitation [12], such linear vibration theory is inefficient for application. Thus, widening the bandwidth of the energy harvesting devices in the order to improve the harvested energy by the harvester is the main challenge of this research field.

Many optimization technique have been proposed by researchers in the literature. Nonlinear systems have proven to be capable of responding over a broad range of frequency [3]. Jin et al. [19] found a Semi-analytical solution of random response for nonlinear vibration energy harvesters; the energy-dependent frequency have been obtained through an averaging process. Zhao et al. [20] studied the deterministic and band-limited stochastic energy harvesting from uniaxial excitation of a multilayer piezoelectric stack; they found that a quadratic relation between maximum power and pressure is observed for bandlimited stochastic excitation. Always in order to optimize the amount of energy harvested by the harvesters, the hybrid model is proposed. Di et al.[21] proposed a probabilistic response analysis of nonlinear vibration energy harvesting system driven by Gaussian colored noise[94]. Tao et al.[95] proposed a dynamics and energy generation of a hybrid energy harvester under colored noise excitations. They authors remarked that, noise-enhanced stability is very beneficial for energy harvesting. Vinicius et al.[96] investigated the nonlinear dynamics of a bistable energy harvesting system with colored noise disturbances. They authors studied the effects of the standard deviation on the system response. Yanxia et al.[97] studied the dynamics of a coupled nonlinear energy harvester under colored noise and periodic excitations. They showed that tri-stable vibration energy harvester can achieve better stochastic resonance effect and higher power conversion efficiency compared with bi-stable vibration energy harvester. Friswell et al.[98] proposed a hybrid cantilever beam harvester with piezoelectric and electrostatic transducers for narrow band base excitation; using an applied DC voltage as a control parameter to change the resonant frequency of the harvester to ensure resonance as the excitation frequency varies. Mokem et al.[99] proposed a hybrid device combining piezoelectric and electromagnetic transduction and subjected to the colored noise. The authors shows that, the system performance can be improve for the small value of the relaxation time. Foupouapouognigni et al.[100] built the hybrid model and studied the stochastic resonance phenomenon, which is characterized by the large amplitude of vibration and increase

the system performance. Zhenlong et al. [101] presented a novel tunable multi-frequency hybrid energy harvester. It comes from their study that the magnitude and direction of magnetic force have significant effects on the performance of the system. Bin et al. [102] built a hybrid energy harvester combined piezoelectric with electromagnetic mechanism to scavenge energy from external vibration. They studied the effect of the relative position of the coils and magnets on the PZT cantilever end and the poling direction of magnets on the output voltage of the harvested energy. Wang et al. [103] built a hybrid device for powering wireless sensor nodes in smart grid. It emerges from the results obtained that, from current-carrying conductor of 2.5 A at 50 Hz , the proposed harvester combining piezoelectric components and electromagnetic elements can generate up to 295.3 μW. Madinei et al. [104] developed a hybrid cantilever beam harvester and by using an applied DC voltage as a control parameter to change the resonant frequency of the harvester to ensure resonance as the excitation frequency varies. It is in this movement that a lot of scavengers have been built. Many authors namely Elvin et al.[105], Inman [106] and Lin et al.[74] reviewing the state of the art on the energy harvesting.

Piezoelectric generators have a lot of applications and most particularly in the civil engineering and health area. In the civil engineering, piezoelectric generators can be used to power the Wireless Sensors Nodes (WSN). In the health area, harvesting energy from biomechanical motions in the human body could directly power various wearable and implantable devices such as peacemaker and cochlear implant. The humans walking gait has been shown to produce a large enough force that multiple types of energy harvesters have been developed to translate its motions to useable energy. In Fig.5 shows a schematic representing many of these energy harvesting (EH) devices making use of various mechanical energy sources in the human body [107, 108, 109].

Others applications of the Piezoelectric generators can be found in the communication area for powering wireless communication devices such as portables devices. It is judicious to mention that, whatever the mechanisms of transduction of the mechanical vibration into electricity, these mechanisms present some limits. Table 3 show the comparison of Vibration Energy-Harvesting Techniques.

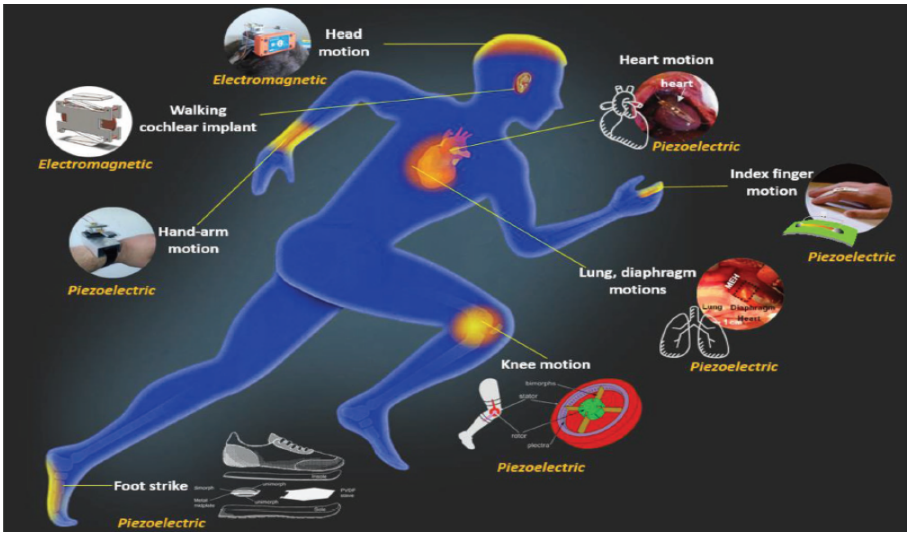

Figure 5: Schematic representing many of the energy harvesting devices making use of various mechanical energy sources in the human body [74]

Table 3: Comparison of Vibration Energy-Harvesting Techniques [39]

	Electrostatic	Electromagnetic	Piezoelectric
Complexity of process flow	Low	Very high	High
Energy density	$4mJ/cm^3$	$24.8mJ/cm^3$	$35.4mJ/cm^3$
Current size	Integrated	Macro	Macro
Problem	Very high voltage and need of adding charge source	Very low output voltages	Low output voltages

I.4 Utility of the proposed harvester studied in this thesis

I.4.1 Powering cardiac devices

Implantable bioelectronics represent an emerging technology that can be integrated into the human body for diagnostic and therapeutic functions [110]. Power supply devices are an essential component of bioelectronics to ensure their robust performance. Material strategies and architectural design of a broad array of power devices, include energy storage systems (batteries and supercapacitors), power devices which harvest sources from the human body (biofuel cells, devices utilizing biopotentials, piezoelectric harvesters, triboelectric devices, and thermoelectric devices), and energy transfer devices which utilize sources in the surrounding environment (ultrasonic energy harvesters, inductive coupling/radiofrequency energy harvesters, and others). These devices could operate inside or near the heart and have direct access to an immense collection of physiologic signals and therapy delivery methods. Classical cardiac devices

such as pacemakers and implantable cardioverter defibrillators (ICDs) measure fundamental diagnostic signals including electrocardiogram (ECG), heart rate, respiration rate, and thoracic impedance[111]. However, these devices require additional power budget to provide their wide functionality, and their continual energy expenditure for therapy delivery necessitates regular device explant and replacement. Therefore, efficient energy harvesting from the mechanical energy in cardiac motion is a highly desirable design feature that could eliminate the need for batteries in both sensing and therapy delivery devices. Cardiac motion, blood flow [112, 113], arterial deformation, and arterial pressure fluctuations hold the best promise in this purpose. Many reported results [114, 115, 116, 117] provide evidence that piezoelectric energy harvesters can yield significant electrical power from motions of internal organs, up to and exceeding levels relevant for practical use in implants. Theoretical models establish design rules and provide predictive capabilities for efficiencies associated with various single and multilayer layouts. In industry, there exist advanced materials and devices that enable high efficiency mechanical-to-electrical energy conversion from the natural contractile, blood pressure, and relaxation motions of the heart, lung, and diaphragm. A cointegrated collection of such energy-harvesting elements with rectifiers and microbatteries provides an entire flexible system, capable of viable integration with the beating heart via medical sutures and operation with efficiencies [118]. Innovative energy harvesting devices exploiting intra-cardiac regular blood pressure variation could then help to power the next generation of leadless pacemakers. The present devices could be used for harvesting energy from regular blood pressure variation in heart cavities. the proposed devices should provide the targeted electrical energy per heartbeat in real environment. As the major part of the heart consumed energy is used to expel blood to organs, many industrial projects have been lunched to exploit regular blood pressure variations in the heart to generate energy such as the one in [119].

In a original model used in this thesis, Lefeuvre et al.[121] have considered that, as the mechanical structure is vibrating with little displacements for which the motion remains linear, then the structure including the piezoelectric element can be simply modeled by the (mass + piezo + spring + damper) system. Although their schematic model was not rigouriosly based on the experimental structure, it gived a faithful description of the behavior of the vibration-powered electrical generator; precisely it gives a faithful description of the structure behavior near resonance, in the vicinity of its first bending mode, for instance. Moreover, only a few

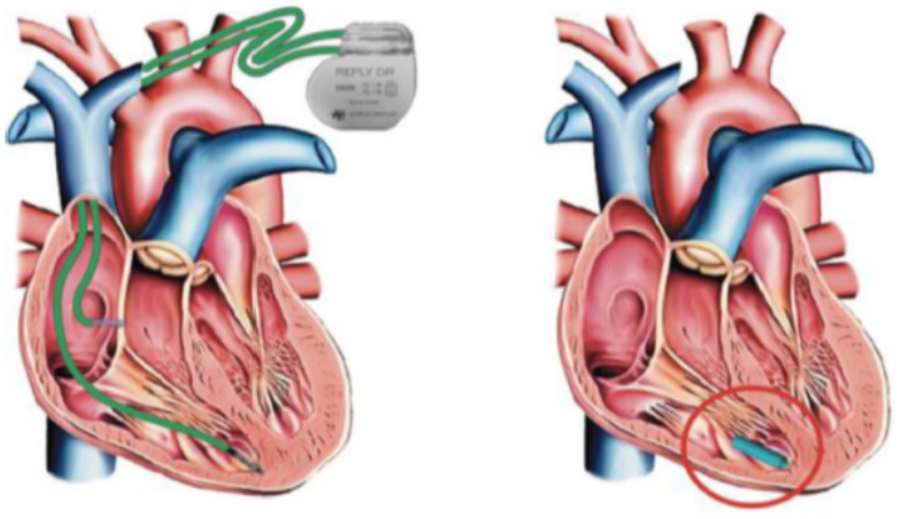

Figure 6: Schematic showing the peacemaker energized by a energy harvesting device [120].

measurements are needed to determine all the model parameters [121]. We made some new considerations to improve the model efficacity.

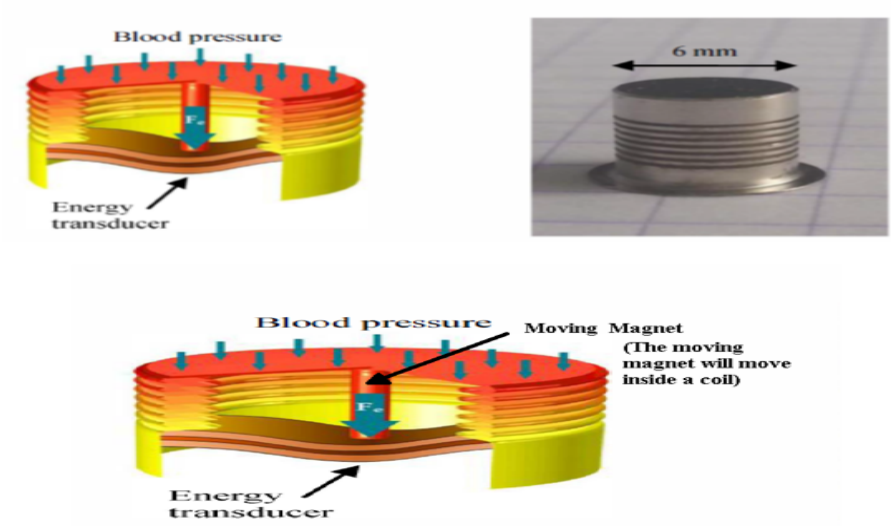

Figure 7: Schematic view of the micro-bellows-shaped deformable packaging (from [119]), that we modified.

Concerning pure piezoelectric harvesters, their cantilever beams suffer from material degradation including fatigue, depolarisation and micro-pressure, considerably reducing their longevity [122]. This degradation is accelerated when piezoelectric vibration harvesters are microscaled. To thus add a small electromagnetic element for harvesting energy can compensate for the deterioration of the device, and help to maintain the operationality of the harvester, before replacing

it. As mentioned before, the proposed mechanical model is based on a mass + piezo+spring + damper system having only one degree of freedom. This model simplicity allows the analytical calculation of the mechanical variables in the linearly elastic domain, as well as the electrical variables [123]. This is sufficient for the following developments as [124]:

- In the case of vibration control, only the forces that drive the system at one of its resonance frequencies lead to significant displacement.

- In the case of energy harvesting, the large majority of the energy that can be harvested is concentrated within the resonance frequency bands. However, it is proven that energy harvesters work better when it can collect energy on a broader waveband. The introduction of the cubic term of nonlinearity, which is inherent with the piezoelectric beam causes the broadening [125] of the frequency band. This is only possible by employing some sort of nonlinearity. For example, one can introduce mechanically induced nonlinearities to the resonator's springs [126]. In addition to proper placement, an energy harvesting device should be designed to match the frequency content of heart motion, which is particularly challenging given an excess of 200% variation in heart rate [127]. We then analysed the system when a noisy source term is added to the excitation and explored the concept of Ghost stochastic resonance phenomenon in this particular type of system, that could lead to the improvement of harvesting capability. By considering turbulent blood flow, effectively the wearable medical device corresponding to the system under study, could be subjected to noise. There are three main sources of noise generation regarding this type system: -Environmental noise, that could affect heart [128]. It have been experimental demonstrated that transportation noise could affects the heart rate during sleep and may be linked to cardiovascular disease [129, 130, 131]. -Pneumatic noise, which is emitted by blood flow. Heart sounds are created by blood flow and vibrations of tissues during the cardiac cycle and can be classified as transient (of short duration) and heart murmurs [132, 133] (abnormal, longer, occurring during normally silent part of the cycle). Innocent heart murmurs may disappear over time, or they may last the entire life without ever causing further health problems. Heart murmurs could be considered as noise, during the heartbeat cycle made by turbulent blood in or near the heart [134]. Common defects that cause heart murmurs are cardiac shunts that occur when there's an abnormal blood flow between the heart chambers or blood vessels, and Heart valve abnormalities. By exploiting the ghost stochastic resonance induced by this type of noise, major drawbacks inherent to inertial principle, such as matching of the resonance

frequency with the excitation, are thus nicely avoided. One can collect even more energy under these conditions.

I.4.2 Disease detection with a functioning pacemaker

In heart diseases detection, blood flow is generally measured with an electromagnetic flowmeter applied to the brachial artery prior to retrograde arterial catheterization of the left ventricle [135]. Pulsatile blood flow through the cavities of the heart and great vessels is time-varying. Derived flow parameters, generally needing further development or validation for clinical use, include measurements of wall shear stress, pressure difference, turbulent kinetic energy, and intracardiac flow components [136]. The devices could be used to detect some diseases such as atrial fibrillation and premature ventricular contractions. The first is a common form of tachycardia that occurs when the electrical activity in the atria is disorganized and very rapid. The pattern of electrical activity stimulates the atria randomly and at a high speed, which causes a series of very rapid and random contractions of the heart's upper chambers, preventing them from pumping effectively. Though not usually life-threatening, the rapid, irregular and uncoordinated beating of the ventricles may cause light-headedness or palpitations. If it goes on for several days or longer, it may increase the risk of stroke, because blood trapped in the atria can clot and travel from the heart to the brain, causing a stroke [137].

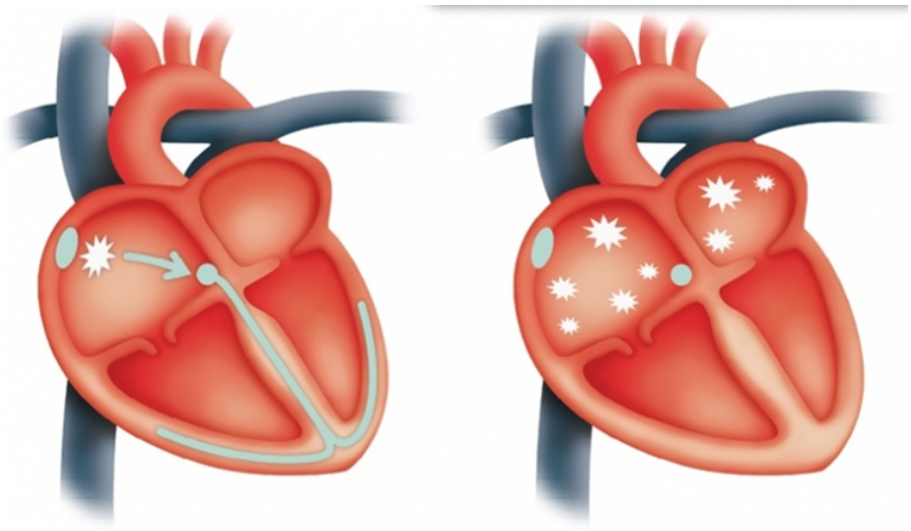

Figure 8: Schematic showing: (a) the one electrical signal starts a heartbeat, (b) a lots of random signals make it hard for you heart to beat steadily [120].

Premature ventricular contractions, or PVCs, are a type of abnormal heartbeat. Normally, a

special group of cells start the signal to start your heartbeat. These cells are in the sinoatrial (SA) node in the right atrium. The signal quickly travels down your heart's conducting system. It travels to the left and right ventricle. As it travels, the signal triggers nearby parts of your heart to contract. This allows your heart to squeeze in a coordinated way. In a premature ventricular contraction, the signal to start your heartbeat comes from one of the ventricles instead. This signal is premature, meaning it happens before the SA node has had a chance to fire. The signal spreads through the rest of your heart, causing a heartbeat. If this happens very soon after the previous heartbeat, your heart will push out very little blood. This causes a feeling of a pause between beats. If it happens a little later, your heart pushes out an almost normal amount of blood. This leads to a feeling of an extra heartbeat. So, the heart has a random "premature" heartbeat sandwiched between many other normal heartbeats [138]. PVCs are somewhat more common in people with some kind of heart disease. Only rarely do PVCs cause problems on their own. The appearance of ghost stochastic resonance phenomenon induced by noise, could indicate the presence of a malfunctioning of the hearth, and indicate some emergency measure to take.

I.5 Contribution of the thesis

In this research field, the main challenge is to improve the amount of energy harvested by the scavenger in order to increase his application field. It is well known in the literature that, when the nonlinear system is subjected to the combination of the harmonic excitation and the random force, many phenomena can be observed such as the stochastic resonance and the ghost-stochastic resonance. These two phenomena are characterized by the large amplitude of vibration. Indeed, the stochastic resonance occurs when the frequency of system's vibration is present in the frequency bandwidth of the harmonic excitation. However, when the maximum amplitude of the system is reached for a frequency of vibration absent in the frequency bandwidth of the harmonic force, this phenomenon is called a ghost-stochastic resonance. While one observes in the literature, a growing interest in the theoretical investigation of the ghost-stochastic resonance phenomenon in the nonlinear systems [22, 23, 24, 25, 26, 27, 28], the study of this phenomenon on the performance of the energy harvesting devices is not made. The first objective of this thesis is to investigated the performance of the proposed system when the ghost-stochastic resonance occurs.

One can also observes in the literature that, the energy harvesting systems using one mechanism of transduction and the hybrid models present the nonlinearity for the most, in the mechanical subsystem to warden the bandwidth of harvesters. However, the electrical part is composed of a lot of elements which can exhibit the nonlinearity such as: the coil, capacitor and resistor. From the model provided by Lefeuvre al.[121], we build the hybrid model combining piezoelectric and electromagnetic mechanisms where the magnetic circuit is composed of the nonlinear resistor. In fact, the nonlinear resistor can be realized using a block consisting of transistors [139, 140]. This resistor exhibiting the nonlinearity with a negative slope was used in Ref.[140] for the dynamics of self-sustained electromechanical transducer. The second objective of this thesis is to investigate the stochastic P-bifurcation phenomenon induced by the nonlinear resistor and the impact of the nonlinear resistor via the ghost-stochastic resonance under the system performance.

I.6 Conclusion

In this chapter, we present the generality on some energies sources available in our real environment and their mechanism of transduction. In fact, our real environment is doted of a lot of energies sources such as solar, wind, thermal and vibration energy. However, these energies sources are unevenly distributed over the surface of the globe consequently, does not have the same energy density. Here, we are interested in the energies of vibrations and thanks to their omnipresence in the environment. In addition, we present the motivations what have leaded at the development of the energy scavenging devices allowing thereby to power wearable appliances or detecting heart malfunctioning. A literature review on the energy scavenging devices is also made. The limits of applications of the models encountered in this research field are presented. From these limits, we give the contribution of this thesis.

CHAPTER II

MODELING AND MATHEMATICAL METHODS

II.1 Introduction

In the previous chapter, we presented the main physical phenomena and applications of energy harvesting with a direct link of the topics covered in this thesis. We gived a general introduction of energy harvesting in order to present the motivations that lead to the development of renewable energy, the potential energy source and then focused on energy harvesting from vibration motion with piezoelectric materials. In this previous chapter, we also exposed a description of the state of the art in terms of energy harvesting. In the present chapter, our focus will be on the description of the different physical systems used in this thesis with the model equations. The modeling is derived from fundamental formula in order to have a general form describing the hybrid energy harvester. The aim of this chapter is to present methods, mathematical tools and numerical techniques used, for the analysis of non linear hybrid energy harvester proposed.

II.2 Probabilistic analysis and Ghost-Stochastic resonance of a hybrid energy harvester under Gaussian White noise

The modelling, analysis and design of energy harvesters are already made complex by the fact that the systems combine elements from different domains. Nonlinearity adds to this complexity. The behaviour of linear systems is broadly well understood, and the tools available for their analysis are readily applied. With the introduction of nonlinearity, even apparently simple systems can give rise to highly complex behaviour. This can include the presence of coexisting solutions, sudden qualitative changes in behaviour with parameter variation, various forms of instability and the intricate patterns of behaviour known as chaos. The combination of nonlin-

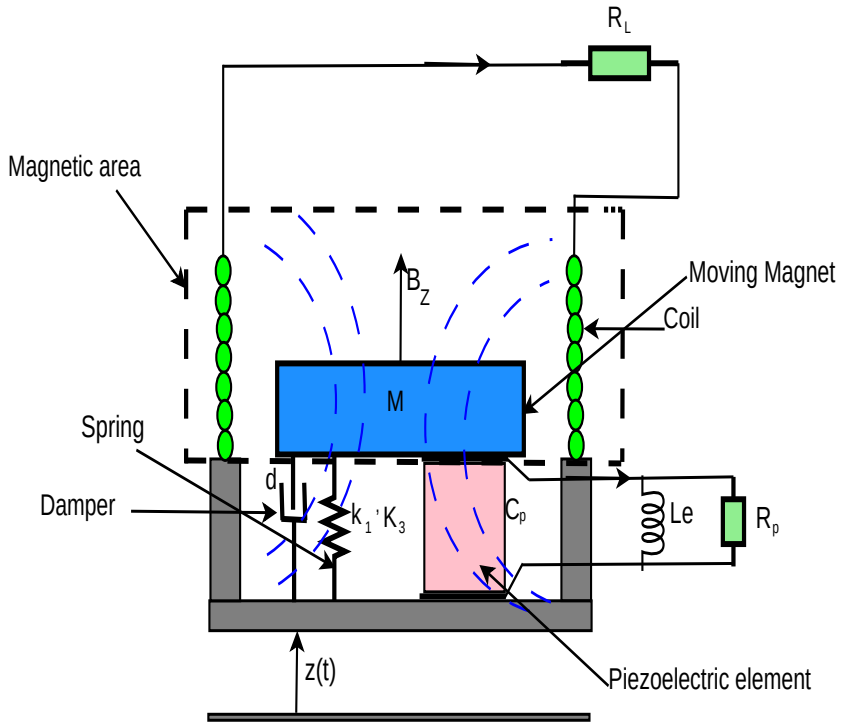

Figure 9: Schematic of the hybrid energy harvester.

earity with stochastic excitation brings still further complexity.For thorough understanding and optimal design of energy harvesting systems, it is necessary to take account of the presence of nonlinearity, both desired and undesired, with in these systems.

The considered hybrid energy harvesting system in this thesis, including the piezoelectric transduction and the electromagnetic induction, is shown in fig.9. We used the energy scavenger build by Lefeuvre in Ref.[121] with some modifications, by changing the rigid mass by a permanent magnet rod, and by adding a coil, in oder to enhance the output power and enlarge its application field.

II.2.1 Description of the physical model

The conception of energy scavenging device combining two mechanisms of transduction of ambient energy presents two main parts namely the mechanical and the electrical part. In order to improve the amount of energy harvested by Lefeuvre et al. [121], we construct the present model by changing on the model proposed in Ref.[121], the rigid mass by permanent magnet, which allow us to build the hybrid model enhancing thus the application field of the harvester build by Lefeuvre (Ref.[121]). It is worth noting that, in the schematic model, the mechanical part is composed of:

• a nonlinear spring with the linear stiffness coefficient k_1 and nonlinear stiffness coefficient k_3. Indeed, in a broad sense, kinetic energy harvesters can convert any mechanical motion energy (like fluid flows, pressure variations and ambient vibrations) into electrical energy to power systems located in the environs of this 'free' mechanical energy [141]. In this purpose, it is necessary to take account of the presence of nonlinearity, both desired and undesired. Nonlinearities appear through nonlinearity in the spring force [142] and impact nonlinearities. A number of recent contributions seek to use nonlinearity in a novel way to improve performance [13, 14, 15, 16]. Designers are exploring the use of nonlinearity to widen the bandwidth and reduce the ambient frequency sensitivity of such harvesters [17].

• a linear damping characterized by the damping coefficient d. Indeed, a much simpler and traditional approach to piezoelectric energy harvesting systems consists of using a linearized lumped parameter model. This model has been widely used for piezoelectric benders or cantilevers as in [143, 144, 145] and also for less common diaphragm piezoelectric harvesters [146, 147]. In most cases, these harvesters placed in a viscous medium with friction (also called damping or dissipation) are designed to collect vibrational energy and thus work at resonance to amplify their displacements. Therefore, models have to include time or frequency-dependent terms such as inertial and damping forces. Since there are always some losses due to dissipation in a realistic mechanical system, we simply add a linear damper to the system to accommodate these losses. The damping force depends on the mobile mass velocity and sometimes, on the displacement [148], but in practice, the model for damping is more complex (e.g. nonlinear squeeze film damping [149]. Because of the difficulties in modeling the damping, in most studies this force is considered linear.

The electrical part presents two subsystems namely the piezoelectric circuit and the electromagnetic circuit. The piezoelectric circuit is composed of the piezoelectric element and the load resistance R_p. The electromagnetic circuit has a permanent magnet of mass M, that produces a magnetic field B_z, the coil, connected to the rigid housing representing the stator is characterized by an inductance L_e. The load resistance of magnetic circuit is R_L. When the harvester is subjected to the external excitation $Z(t)$, the displacement of the magnetic mass M induces in the piezoelectric circuit, the deformation of piezoelectric element giving rise to the electrical field across the piezoelectric element. However, in the magnetic circuit, the displacement of the magnetic mass M induces a fluctuation of the magnetic flux in the surface of the coil, and conse-

quently, a generation of electromotive force $f_m(i)$ is produced on the terminals of the coil can be expressed as $f_m(i) = B_z i L_{coil}$. In the mechanical part, while in the magnetic circuit, It should be mentioned the presence of electromagnetic coupling produces a force on the harvester, we can note the Lenz electromotive voltage which is given by $f_e(\dot{z}) = -B_z L_{coil}\dot{z}$ with z, L_{coil}, and i, the displacement, the length of the coil and the current that flows in the coil respectively, B_z being the magnetic field generated by the permanent magnet. According to Newton's second law of motion, the sum of the force on the rigid mass then generates the governing equation(13) of the system ($spring + mass + piezo + damper + electromagnetic$) is given by the following equation:

$$M\ddot{z} + d\dot{z} + k_1 z + k_3 z^3 + Bil_{coil} - \theta_2\, v = Z\,(t) \tag{13}$$

where θ_2 is the electromechanical coupling coefficient. Applying to,the Kirchhoff's current law,the sum of the currents flowing through the electrical components is equal to the current flowing out from the piezoelement.The sum of currents flowing through the resistive load $\frac{v(t)}{R_p}$,to the internal piezoelement capacitance $C_p\dot{v}$ and to the switch is equal to the current from the current source $\theta_2\dot{z}$. Therefore, the governing equation for the piezoelectric transduction is:

$$C_p\dot{v} + \frac{v(t)}{R_p} + \theta_2\dot{z} = 0 \tag{14}$$

The voltage generated by the electromagnetic phenomenon is derived using Faraday's law of induction and Kirchhoff's law in the electromagnetic circuit by letting $\vec{B}_z = B\vec{u}_z$.

$$L_e\dot{i} + R_l i - Bl_{coil}\dot{z} = 0 \tag{15}$$

At summary , Using piezoelectric constitutive law and Newton's second law of motion, for such model of hybrid piezoelectric-inductive galloping harvesting system, we obtained motion equations given by:

$$M\ddot{z} + d\dot{z} + k_1 z + k_3 z^3 + Bil_{coil} - \theta_2\, v = Z\,(t)$$

$$C_p\dot{v} + \frac{v(t)}{R_p} + \theta_2\dot{z} = 0 \tag{16}$$

$$L_e\dot{i} + R_l i - Bl_{coil}\dot{z} = 0$$

Table 4: Physical parameters of hybrid model

Parameter	Value	Unit
L_{coil}	0.03	m
M	1	mg
k_1	-100	N/m
k_3	500	N/m
d	0.1	$-$
θ_2	0.1	$-$
R_L	1	kΩ
B	0.1	T
L_e	1	mH
C_p	4	F
R_p	500	Ω

where C_p is the capacity of the capacitor. The physical parameters used in this manuscript are given in table 1.

By using the time-transformation($t = \dfrac{\tau}{\omega}$), Eq.(16) gives rise to the following non-dimensional system:

$$\begin{aligned} &x'' + \mu a\, x' + \omega_0\, x - \beta_2\, y + \sigma\, x^3 + \beta 1\, r = N(\tau)\,(a) \\ &y' + \alpha_2 y - \beta_{22} x' = 0 (b) \\ &r' + \alpha_3\, r - \beta_{11}\, x' = 0 (c) \end{aligned} \tag{17}$$

with $N(\tau) = \sum_{i=1}^{m} f_0 \cos(\omega_i \tau) + \xi(\tau)$ where $\sum_{i=1}^{m} f_0 \cos(\omega_i \tau)$ is a harmonic excitation, with f_0 the amplitude of coherence force, $\omega_i = (k + i - 1)\,\omega_0$ is the frequency of the coherence force with k a constant took here equal to 2. ω_0 is the fundamental frequency. The variable $\xi(\tau)$, is the Gaussian white noise verifying the statistics properties: $< \xi(\tau) >= 0$, $< \xi(\tau)\,\xi(s) >= 2D\delta(\tau)$. The dimensionless parameters are given as follow:

$$\begin{aligned} &\mu_a = -\tfrac{\omega\, d}{k_1}; \sigma = -\tfrac{l^2 k_3}{k_1}; \beta_2 = -\tfrac{\theta_2 v_o}{l k_1}; \beta_1 = -\tfrac{B L_{coil} i_o}{l k_1} \\ &\alpha_2 = \tfrac{1}{\omega\, C_p R_p}; \beta_{22} = -\tfrac{\theta_2 l}{v_o C_p}; \beta_{11} = \tfrac{l B L_{coil}}{L i_o}; \alpha_3 = \tfrac{R_L}{\omega\, L_e}; \end{aligned} \tag{18}$$

$$z = lx\,(t\omega)\,; v = vo\,y\,(t\omega)\,; i = io\,r\,(t\omega)\,;$$
$$N\,(\tau) = -Z\left(\tfrac{\tau}{\omega}\right) l^{-1}{k_1}^{-1} \tag{19}$$

$$\mu_a = -\tfrac{\omega\, d}{k_1}; \sigma = -\tfrac{l^2 k_3}{k_1}; \beta_2 = -\tfrac{\theta_2 v_o}{l k_1}; \beta_1 = -\tfrac{BL_{coil} i_o}{l k_1}$$

$$\alpha_2 = \tfrac{1}{\omega\, C_p R_p}; \beta_{22} = -\tfrac{\theta_2 l}{v_o C_p}; \beta_{11} = \tfrac{lBL_{coil}}{Li_o}; \alpha_3 = \tfrac{R_L}{\omega\, L_e}; \tag{20}$$

$$z = lx\,(t\omega)\,; v = vo\,y\,(t\omega)\,; i = io\,r\,(t\omega)\,;$$

$$N\,(\tau) = -Z\left(\tfrac{\tau}{\omega}\right) l^{-1}{k_1}^{-1}$$

II.2.2 Mathematical methods for the determination of system response

a)Stochastic averaging method

Among various approaches nonlinear random vibration, the stochastic averaging method is a powerful approximate technique for the prediction of response of nonlinear system subject to external and parametric random excitations.

The stochastic averaging method has been extensively used in the field of random vibration and serves as a convenient tool to obtain the (approximate) stationary or non-stationary responses of stochastic dynamical systems [150]. This method simplifies the problem by introducing a dimensional reduction of the original system, but the essential behavior of the system is retained. Then, a numerical solution or even analytical solution of the low-dimensional Fokker-Planck-Kolmogorov (FPK) equation can be obtained. Following [151], the original method of stochastic averaging was introduced by Stratonovich in 1963[152] which may be viewed as an extension of the deterministic averaging procedure of Mitropolsky. This technique, known under the name of the classical stochastic averaging compared to its deterministic counterpart the effects of some nonlinear inertia terms and nonlinear stiffness terms, in the governing second order differential equation of motion of a single degree of freedom system are absent in the approximate solutions. It is worth noting that the effects of the nonlinear terms on the stochastic system cannot be studied by applying the classical stochastic averaging method. In Ref. [151],

they authors suggested that in order to reveal the effects of the nonlinear terms, a second order averaging is required. Let us Consider a set of differential equations in standard form:

$$\frac{dz_j}{dt}=\varepsilon \mathrm{f}_j\left(Z,t\right)+\varepsilon^{1/2}\mathrm{g}_{jr}\left(Z,t\right)\zeta_r\left(t\right) \tag{21}$$

where $j=1,2,..n$; $r=1,2,..m$; ϵ is a small positive parameter Z is a n-dimension random vector process of response state and z_j is its $j'th$ component; f_j and g_{jr} are deterministic nonlinear functions, while $\zeta_r(t)$ is the $r'th$ component of the stationary random excitation vector $\zeta\left(t\right)$. Elements of the latter vector are of zero mean and have cross correlation matrix $\Gamma(\tau)$ whose elements are $\Gamma_{rv}(\tau)=<\zeta_r(t)\zeta_v(t+\tau)>$ If the maximum of correlation times of the random excitations is much smaller than the minimum of the relaxation times of the multiple degree of freedom system, the state vector Z weakly converges to a diffusive $Markov$ vector $Z^{(0)}$ with transition probability density $p(Z^{(0)},t/Z_0^{(0)},t_0)$ or simply p, where the subscript 0 denotes at time t_0 . The governing FPK equation is:

$$\frac{\partial p}{\partial t}=-\varepsilon\frac{\partial\left(a_j p\right)}{\partial z_j^{(0)}}+\frac{\varepsilon}{2}\frac{\partial\left(b_{jk}p\right)}{\partial z_j^{(0)}\partial z_k^{(0)}} \tag{22}$$

where the drift and diffusion coefficients, a_j and b_{jk} are given, respectively by:

$$\mathrm{a}_j\left(z_k^{(0)}\right)=\mathrm{T}_s^{av}\left\{<f_j\left(z^{(0)},s\right)>+I_{av}\right\} \tag{23}$$

in which

$$I_{av}=T_s^{av}\left\{\int_{-\infty}^{0}<\frac{\partial g_{jr}\left(z^{(0)},s\right)}{\partial z_k^{(0)}}g_{kv}\left(z^{(0)},s+\tau\right)\zeta_r\left(s\right)\zeta_v\left(s+\tau\right)>d\tau\right\} \tag{24}$$

and

$$b_{jk}\left(z^{(0)}\right)=T_s^{av}\left\{\int_{-\infty}^{+\infty}<g_{jr}\left(z^{(0)},s\right)g_{kv}\left(z^{(0)},s+\tau\right)\zeta_r\left(s\right)\zeta_v\left(s+\tau\right)>d\tau\right\} \tag{25}$$

in which $T_{t_0}^{av}\{.\}$ denotes deterministic averaging of the enclosing quantity with respect to time s. That is,

$$T_{t_0}^{av}\{.\}=\lim_{T\to\infty}\frac{1}{T}\int_{t_0}^{t_0+T}\{.\}dt \tag{26}$$

The $Markov$ vector process $Z^{(0)}$ can be described by the following set of Itô's stochastic differ-

ential equations

$$\mathrm{dz}_j^{(0)}=\varepsilon \mathrm{m}_j\left(z^{(0)}\right)\mathrm{dt}+\varepsilon^{1/2}\sigma_{jr}\left(z^{(0)}\right)\mathrm{dW}_r\left(t\right) \tag{27}$$

where the unit Wiener processes are defined by $dW_r\left(t\right)=\zeta_r\left(t\right)dt$. The drift coefficients m_j and diffusion coefficients σ_{jr} of Eq.(27) are related to a_j and b_{jk} of the FPK equation (Eq.(22)) by:

$$\mathrm{m}_j\left(z^{(0)}\right)=\mathrm{a}_j\left(z^{(0)}\right);\sigma_{jr}\left(z^{(0)}\right)\sigma_{kr}\left(z^{(0)}\right)=\mathrm{b}_{jk}\left(z^{(0)}\right) \tag{28}$$

b) $Ito's$ **equation and probability density**

In many problems that involve modeling the behavior of some system, we lack sufficiently detailed information to determine how the system behaves, or the behavior of the system is so complicated that an exact description of it becomes irrelevant or impossible. In that case, a probabilistic model is often useful.Probability and randomness have many different philosophical interpretations, but, whatever interpretation one adopts, there is a clear mathematical formulation of probability in terms of measure theory, due to Kolmogorov. Probability is an enormous field with applications in many different areas. For example, for Dynamic systems subject to stochastic excitations, probabilistic approach employing the theory of stochastic bifurcation is essential, in order to examine their response and stability. The main purpose of this heading is to provide the statistic response of the harvester using the stochastic averaging technique developed by Stratonovich [152]. The success of the stochastic averaging method is mainly due to the reduction of dimensions of the FPK equation while the essential behavior of the system is retained. Here we simply aim to provide the statistic response of the harvester through the $Fokker-Planck-Komogorov$ equation. We will do so finding the Ito stochastic differential equations associated with the system (Eq.(27)).

we assume that, $f_0=0$. In the quasi-harmonic regime, the solution of the mechanical system (17) is of the form:

$$x\left(\tau\right)=a(\tau)\left(\tau\right)\cos\left(\theta\right);\quad x'(\tau)=-\omega a(\tau)\left(\tau\right)\sin\left(\theta\right) \tag{29}$$

where $\theta=\omega\tau+\psi(\tau)$ with ψ, the phase angle and $a(\tau)$ the amplitude. Substituting Eq.(29) into Eq.(17) (b)-(c), the solution of obtained equation can be written as follow:

$$y(\tau) = C_1 \mathrm{e}^{-\alpha 2\,\tau} + \frac{\beta_{22}\, a(\tau)\omega\,(\omega\,\cos(\theta) - \alpha_2\,\sin(\theta))}{\omega^2 + {\alpha_2}^2}$$
$$r(\tau) = C_2 \mathrm{e}^{-\alpha_3\,\tau} + \frac{a(\tau)\beta_{11}\omega\,(\omega\,\cos(\theta) - \alpha_3\,\sin(\theta))}{\omega^2 + {\alpha_3}^2} \tag{30}$$

In the steady state, Equations (30 a)-(b) can be rewritten as:

$$y(\tau) = \frac{\beta_{22}\, a(\tau)\omega\,(\omega\,\cos(\theta) - \alpha_2\,\sin(\theta))}{\omega^2 + {\alpha_2}^2} \quad (a)$$
$$r(\tau) = \frac{a(\tau)\beta_{11}\omega\,(\omega\,\cos(\theta) - \alpha_3\,\sin(\theta))}{\omega^2 + {\alpha_3}^2} \quad (b) \tag{31}$$

where

$$\omega\,\cos(\theta) - \alpha_2 \sin(\theta) = \sqrt{\omega^2 + {\alpha_2}^2}\cos\left(\theta + \arctan\left(\frac{\alpha_2}{\omega}\right)\right)$$
$$\omega\,\cos(\theta) - \alpha_3 \sin(\theta) = \sqrt{\omega^2 + {\alpha_3}^2}\cos\left(\theta + \arctan\left(\frac{\alpha_3}{\omega}\right)\right) \tag{32}$$

Thus, the amplitudes of steady-state current and charge are given by:

$$Y = \frac{\beta_{22}\, a\omega}{\sqrt{\omega^2 + {\alpha_2}^2}}; R = \frac{a\beta_{11}\,\omega}{\sqrt{\omega^2 + {\alpha_3}^2}} \tag{33}$$

Substituting Eq.(29) and Eq.(31) into Eq.(17), and applying the determinist averaging method in the determinist part of the obtained system, we have:

$$a' = -\frac{\gamma_{22} N(\tau)\sin(\theta)}{2\omega\,\gamma_{55}} - \frac{\gamma_{11} a}{2\omega\,\gamma_{55}}$$
$$\varphi' = \frac{\gamma_{33} N(\tau)\cos(\theta)}{\gamma_{44} a} + \frac{a^2\gamma_{12}}{\gamma_{44}} + \frac{\gamma_{13}}{\gamma_{44} a} \tag{34}$$

where

$$\begin{aligned}
\gamma_{11} &= {\beta_1}^2\omega^3\alpha_3 - {\beta_2}^2\omega^3\alpha_2 + \mu a\,\omega^3{\alpha_3}^2 + \mu a\,\omega^5 \\
&+\mu a\,\omega\,{\alpha_2}^2{\alpha_3}^2 + \mu a\,\omega^3{\alpha_2}^2 - {\beta_2}^2\omega\,\alpha_2\,{\alpha_3}^2 + {\beta_1}^2\omega\,\alpha_3\;{\alpha_2}^2 \\
\gamma_{22} &= 2\,{\alpha_2}^2\omega^2 + 2\,{\alpha_2}^2\,{\alpha_3}^2 + 2\,\omega^2{\alpha_3}^2 + 2\,\omega^4 \\
\gamma_{33} &= -8\,{\alpha_2}^2{\alpha_3}^2 - 8\,\omega^4 - 8\,\omega^2{\alpha_3}^2 - 8\,{\alpha_2}^2\omega^2 \\
\gamma_{44} &= 8\,\omega^5 + 8\,\omega^3{\alpha_3}^2 + 8\;\omega^3{\alpha_2}^2 + 8\,\omega\,{\alpha_2}^2{\alpha_3}^2 \\
\gamma_{55} &= \omega^4 + \omega^2{\alpha_3}^2 + {\alpha_2}^2\omega^2 + {\alpha_2}^2{\alpha_3}^2 \\
\gamma_{12} &= 3\,\sigma\,\omega^2{\alpha_3}^2 + 3\,\sigma\;{\alpha_2}^2\omega^2 + 3\,\sigma\,\omega^4 + 3\,\sigma\;{\alpha_2}^2{\alpha_3}^2 \\
\gamma_{13} &= -4\,\omega^2{\alpha_2}^2{\alpha_3}^2 + 4\,{\beta_1}^2\omega^4 - 4\,\omega^4{\alpha_2}^2 - 4\;\omega^6 - 4\,{\beta_2}^2\omega^4 \\
&-4\,\omega^4{\alpha_3}^2 + 4\,{\beta_1}^2\omega^2{\alpha_2}^2 - 4\,{\beta_2}^2\omega^2{\alpha_3}^2 \\
&+4\,\omega_0{\alpha_2}^2{\alpha_3}^2 + 4\,\omega_0{\alpha_2}^2\omega^2 + 4\,\omega_0\omega^2{\alpha_3}^2 + 4\,\omega_0\omega^4
\end{aligned} \tag{35}$$

Finally, applying the stochastic averaging method, in Eq. (34) , we obtain the Ito equation defined as:

$$\begin{aligned}
da &= \left(-\tfrac{2\gamma_{11}a}{\omega\,\gamma_{55}} + \tfrac{D}{2a\omega^2}\right)dt + \sqrt{\tfrac{D}{\omega^2}}\,dB_1 \\
d\theta &= \tfrac{\left(\gamma_{12}a^2+\gamma_{13}\right)dt}{\gamma_{44}} + \sqrt{\tfrac{D}{\omega^2a^2}}\,dB_2
\end{aligned} \tag{36}$$

where B_1 and B_2 are the normalized wiener process. We observe in Eq. (**??**) that a and θ are independent. Thus, we can provided the probability density for the amplitudes(a), rather than a joint probability density for θ. The probability density $P(a,\tau)$ of the instantaneous amplitude

a satisfies the Fokker-Planck-Kolmogorov equation:

$$\begin{aligned}\frac{\partial}{\partial\tau}p\left(a,\tau\right) &= -\left(-\frac{\gamma_{11}}{2\omega\,\gamma_{55}} - \frac{D}{\omega^2 2a^2}\right)p\left(a,\tau\right)\\ &-\left(-\frac{\gamma_{11}a}{2\omega\,\gamma_{55}} + \frac{D}{2a\,\omega^2}\right)\frac{\partial}{\partial a}p\left(a,\tau\right) + \frac{(D)\frac{\partial^2}{\partial a^2}p(a,\tau)}{2\omega^2}\end{aligned} \tag{37}$$

In the stationary state, the solutions of Eqs.(37) is given by:

$$p\left(a\right) = Na\mathrm{e}^{-\frac{\gamma_{11}a^2\omega}{(2D)(\omega^2+{\alpha_3}^2)(\omega^2+{\alpha_2}^2)}} \tag{38}$$

where N is the normalization constant which can be assessed numerically using Simpson's method. Through a transformation from variable (a,θ), to the original variables (x,x'), an expression for the stationary densities function of x and x' can be derived as:

$$P_n\left(x,x'\right) = \frac{P(a,\theta)}{2\pi\,a} \tag{39}$$

$$p\left(a\right) = \frac{N}{2\pi}\exp\left(-\frac{\gamma_{11}\omega\left(x^2+\frac{{x'}^2}{\omega^2}\right)}{2D\left(\omega^2+\alpha_3^2\right)\left(\omega^2+\alpha_2^2\right)}\right) \tag{40}$$

Thus, the expected value of the mean square electric current and charge can be calculated following this formula:

$$\begin{aligned}\left\langle y^2\left(\tau\right)\right\rangle = \left\langle Y^2\right\rangle &= \left(\frac{\beta_{22}\omega}{\sqrt{\omega^2+\alpha_2^2}}\right)^2 \times \left\langle a^2\right\rangle\\ &= \left(\frac{\beta_{22}\omega}{\sqrt{\omega^2+\alpha_2^2}}\right)^2 \int_0^{+\infty} a^2 p\left(a\right)da\end{aligned} \tag{41}$$

$$\left\langle Y^2\right\rangle = \frac{2\beta_{22}^2\omega D\left(\omega^4+\omega^2\left(\alpha_3^2+\alpha_2^2\right)+\alpha_2^2\alpha_3^2\right)}{\gamma_{11}\left(\omega^2+\alpha_2^2\right)}$$

and

$$\begin{aligned}\left\langle r^2\left(\tau\right)\right\rangle = \left\langle R^2\right\rangle &= \left(\frac{\beta_{11}\omega}{\sqrt{\omega^2+\alpha_2^2}}\right)^2 \times \left\langle a^2\right\rangle\\ &= \left(\frac{\beta_{11}\omega}{\sqrt{\omega^2+\alpha_3^2}}\right)^2 \int_0^{+\infty} a^2 p\left(a\right)da\end{aligned} \tag{42}$$

$$\left\langle R^2\right\rangle = \frac{2\beta_{11}^2\omega D\left(\omega^4+\omega^2\left(\alpha_3^2+\alpha_2^2\right)+\alpha_2^2\alpha_3^2\right)}{\gamma_{11}\left(\omega^2+\alpha_3^2\right)}$$

II.3 Resistance induced P-bifurcation and Ghost-Stochastic resonance of a hybrid energy harvester under colored noise

II.3.1 Description of Negative Resistance Devices

It is known in the literature that the invention of the dynatron in 1918 proves that it is possible for a 2-terminal device with no internal power supplies to possess a differential negative resistance [153, 154, 155, 156]. This discovery was initially greeted with fascination by some and scepticism by others because it seems to violate the conservation of energy. This paradox was of course quickly resolved upon recognizing that so long as the $v - i$ curve lies in the first and the third quadrants, the device will remain passive. Consequently, any point on the v-i curve having a negative slope must necessarily lie in the first or the third quadrant. Many vacuum tube devices exhibiting a negative differential resistance have since been invented and used in numerous application [157, 158, 159]. A lot of techniques can be used to build negative resistance. In fact, the invention of the transistor in 1948 has naturally triggered a search for solid state negative resistance devices. Unlike vacuum tubes, however, the physics of solid state devices is much more complex. It was not until 1958 that the first negative resistance solid state device, called the tunnel diode, was invented by Esaki [160]. In fact, so exotic was the physical mechanism responsible for the negative resistance that a Nobel prize in physics was awarded to Esaki in 1973. It took another 8 years before another promising 2-terminal solid state negative resistance device, called the Gunn diode, was invented [161, 162]. Another approach for inventing new solid state negative resistance devices is to combine two or more bipolar transistors with resistors [159].

II.3.2 Description of the system with the model equation

In the previous work, Mokem at al.[163], presented a hybrid energy harvester. The main objectives of their paper was to:

• show the impact of the colored noise parameters (correlation time, and noise intensity) on the performance of the proposed hybrid model,

• show the interest of studying the stochastic bifurcation phenomenon in this domain of research which was induced by the transduction material (piezoelectric material),

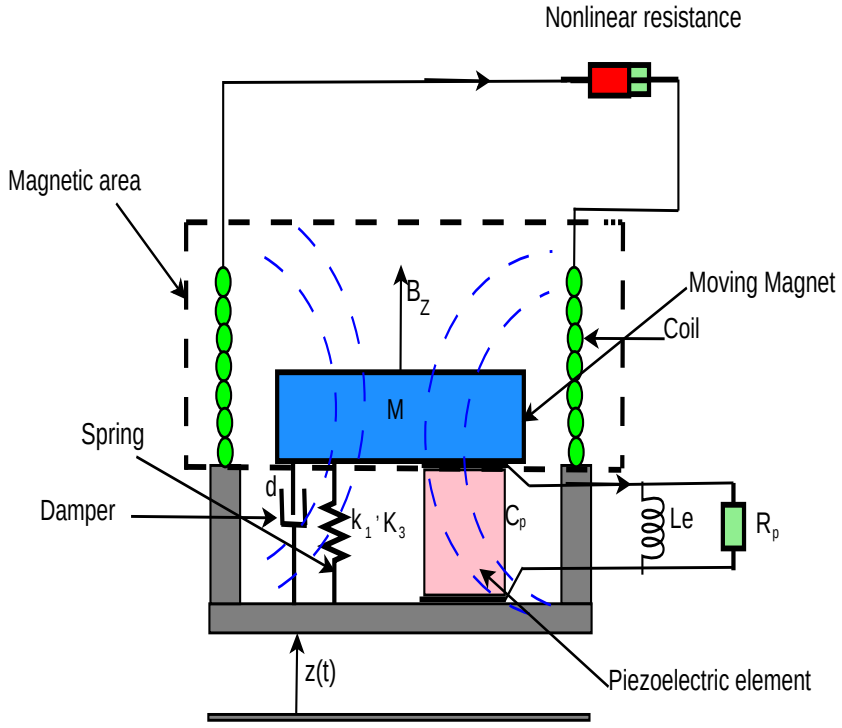

Figure 10: Schematic of the hybrid energy harvester.

•show that by placing the energy harvesting device in an environment where a coherent source (harmonic excitation) and random source coexists, the phenomenon of stochastic resonance can appear and improve the performance of the system. However, in the literature, the coherent force can be modeled by $\sum_{i=1}^{m} f_0 \cos(\omega_i \tau)$ with $\omega_i = (k + i - 1)\,\omega_0$ is the frequency of the coherence force with k a constant took here equal to 2. ω_0 is the fundamental frequency while m is integer number. We note in this expression of harmonic force, an absence of the fundamental frequency in the frequency's spectrum. This present work study the performance of the energy harvester when the fundamental frequency is absent in the harmonic excitation. In addition, in the context of energy harvesting, the resistance of load are crucial elements in integrated circuits and are used extensively in many electronic systems. Some of these resistors can exhibit a nonlinear behavior, i.e. the current-voltage characteristic curve $u = f(i)$ is not linear. We consider in this thesis a nonlinear resistance and we investigate its impact on the performances of the system. This impact of nonlinear resistance on the performance of the proposed model is observed through the bifurcation phenomenon, which is not the case in other works where this phenomenon was induced by the transduction material (piezoelectric material). In addition, in this thesis, although the natural frequency of the vibrations of the mechanical subsystem is absent in the frequency band of the coherent force, there is a value of the control parameter D for

which the amplitude of the system is maximum. This corresponds to the phenomenon of ghost-stochastic resonance which has not been studied in the model before, applied to the areas we mentioned in the preceding chapter. In this subsection of the thesis, we consider that, the load resistance of magnetic circuit in the previous model proposed is considered as nonlinear where the Ohm's law is given by $U_R = -R_0 i_0 \left[\left(\frac{i}{i_0} \right) - \frac{1}{3} \left(\frac{i}{i_0} \right)^3 + \frac{1}{5} \left(\frac{i}{i_0} \right)^5 \right]$ [164], with R_0 and i_0, the normalized resistance and current respectively while i be the value of the current corresponding to the limit resistor voltage. Let us notice that, the nonlinear resistor can be realized using a block consisting of two transistor [164, 165]. Thus, by taking into account this consideration, system (16) becomes:

$$
\begin{aligned}
& M\ddot{z} + d\dot{z} + k_1 z + k_3 z^3 + BiL_{coil} - \theta\, v = Z\,(t) \\
& C_p \ddot{v} + \frac{\dot{v}}{R_p} + \frac{v}{L_e} + \theta \ddot{z} = 0 \\
& L_m \ddot{i} - R_0 i_0 \left[\frac{\dot{i}}{i_0} - \frac{i^2 \dot{i}}{i_0^3} + \frac{i^4 \dot{i}}{i_0^5} \right] - BL_{coil} \ddot{z} = 0
\end{aligned}
\tag{43}
$$

where all parameters appearing in system (43) are defined in the previous system (Eq.(16)). By using the time-transformation($t = \frac{\tau}{\omega}$), Eq.(43) gives rise to the following non-dimensional system:

$$
\begin{aligned}
& \ddot{x} + \mu_a \dot{x} + \omega_0 x - \beta_2 y + \sigma x^3 + \chi r = N(\tau) \\
& \ddot{y} + \alpha_2 \dot{y} + \mu_{33} y - \beta_{22} \ddot{x} = 0 \\
& \ddot{r} + \mu_1 \dot{r} + \mu_2 r^2 \dot{r} + \mu_3 r^4 \dot{r} - \beta_{11} \ddot{x} = 0 = 0
\end{aligned}
\tag{44}
$$

with $N(\tau) = \sum_{i=1}^{m} f_0 \cos(\omega_i \tau) + \xi(\tau)$ where $\sum_{i=1}^{m} f_0 \cos(\omega_i \tau)$ is a harmonic excitation, with f_0 the amplitude of coherence force, $\omega_i = (k + i - 1)\,\omega_0$ is the frequency of the coherence force with k a constant took here equal to 2. ω_0 is the fundamental frequency . The variable $\xi(\tau)$, is the colored noise verifying the statistics properties: $< \xi(\tau)\,\xi(s) >= \frac{D}{\tau_1} \mathrm{e}^{-\frac{|\tau - s|}{\tau_1}}$ with D and τ_1, the parameters characterizing the colored noise and denote the intensity and the correlation times of the noise. The variables x, y and r denote respectively the displacement of the mechanical subsystem, the voltage and current of piezoelectric and electromagnetic circuits. The dimensionless

parameters are giving as follow:

$$\mu_a = -\frac{\omega\, d}{k_1}; \sigma = -\frac{l^2 k_3}{k_1}; \beta_2 = -\frac{\theta\, vo}{l k_1}$$

$$\chi = -\frac{BL_{coil}\, io}{l k_1}; f(\tau) = -\tfrac{1}{l k_1} u\left(\frac{\tau}{\omega}\right); \alpha_2 = \frac{1}{\omega\, C_p R_p}$$

$$\beta_{22} = -\frac{\theta\, l}{vo\, C_p}; \beta_{11} = \frac{BL_{coil} l}{io\, L_m}; \mu_1 = -\frac{Ro}{\omega\, L_m}; \mu_2 = \frac{io^2 Ro}{\omega\, L_m io^2}; \tag{45}$$

$$\mu_3 = -\frac{io^4 Ro}{\omega\, L_m io^4}; \mu_{33} = \frac{1}{\omega^2 C_p Le}; M = -\frac{k_1}{\omega^2}$$

$$z = lx(t\omega); v = vo\, y(t\omega); i = io\, r(t\omega)$$

II.3.3 Mathematical methods for the determination of system response

Ito's equation and probability density

In this heading, we use the stochastic averaging method to provide the statistic response of the harvester. In the quasi-harmonic regime, the solution of the harvesting energy divice (44) is of the form [163]:

$$\begin{aligned} x(\tau) &= a_1(\tau)(\tau)\cos(\theta_1); \quad x'(\tau) = -\omega a_1(\tau)(\tau)\sin(\theta_1) \\ y(\tau) &= a_2(\tau)(\tau)\cos(\theta_2); \quad y'(\tau) = -\omega a_2(\tau)(\tau)\sin(\theta_2) \\ r(\tau) &= a_3(\tau)(\tau)\cos(\theta_3); \quad r'(\tau) = -\omega a_3(\tau)(\tau)\sin(\theta_3) \end{aligned} \tag{46}$$

where $\theta_j = \omega\tau + \psi_j(\tau)$ with ψ_i, the phase angle and $a_i(\tau)$ the amplitude with the integer number varying between $1...3$. Substituting Eq.(46) into Eq.(44), and applying the stochastic averaging method in the obtained system, we obtained the following equations so called Ito's equations:

$$
\begin{aligned}
da_1 &= \left(-\frac{\mu_a}{2}a_1 + \frac{D}{2\omega_1^2 a_1\left(\tau_1^2+1\right)}a_1 \right) d\tau + \sqrt{\frac{D}{\omega_1^2\left(\tau_1^2+1\right)}}dw_1(a) \\
da_2 &= \left(-\frac{\alpha_2}{2}a_2 + \frac{\beta_{22}^2 D}{2\omega_2^2 a_2\left(\tau_1^2+1\right)} \right) d\tau + \sqrt{\frac{\beta_{22}^2 D}{\omega_2^2\left(\tau_1^2+1\right)}}dw_2(b) \\
da_3 &= \left(\Omega_{11} + \frac{\beta_{11}^2 D}{2\omega_3^2 a_3\left(\tau_1^2+1\right)} \right) d\tau + \sqrt{\frac{\beta_{11}^2 D}{\omega_3^2\left(\tau_1^2+1\right)}}dw_3(c) \\
d\varphi_1 &= \left(\frac{3a_1^2\sigma}{8\omega_1} - \frac{\omega_1}{2} + \frac{\omega_0}{2\omega_1} \right) d\tau + \sqrt{\frac{D}{\omega_1^2 a_1^2\left(\tau_1^2+1\right)}}dw_4(d) \\
d\varphi_2 &= \left(-\frac{\beta_{22}\beta_2}{2\omega_2} - \frac{\omega_2}{2} \right) d\tau + \sqrt{\frac{\beta_{22}^2 D}{\omega_2^2 a_2^2\left(\tau_1^2+1\right)}}dw_5(e) \\
d\varphi_3 &= \left(\frac{\beta_{11}\beta_1}{2\omega_3} - \frac{\omega_3}{2} \right) d\tau + \sqrt{\frac{\beta_{11}^2 D}{\omega_3^2 a_3^2\left(\tau_1^2+1\right)}}dw_6(f)
\end{aligned}
\tag{47}
$$

where $\Omega_{11} = -\frac{\mu_3}{16}a_3^5 - \frac{\mu_2}{8}a_3^3 - \frac{\mu_1}{2}a_3$ while w_1, w_2, w_3, w_4, w_5 and w_6 are the normalized wiener process. Is is worth noting that, in Eq. (47), $a_1, a_2, a_3, \varphi_1, \varphi_2$ and φ_3 are independent. Thus, we can provided the probability density for the amplitudes(a_1, a_2, a_3), rather than a joint probability density for φ_1, φ_2 and φ_3 . The probability density $P(a_1, \varphi_1), P(a_2, \varphi_2)$ and $P(a_3, \varphi_3)$ of the instantaneous amplitude a_1, a_2 and a_3 satisfies the Fokker-Planck-Kolmogorov equations:
For the mechanical subsystem:

$$
\begin{aligned}
&\frac{\partial p\left(a_1,\tau\right)}{\partial\tau} = \frac{\partial}{\partial a_1}\left[\left(-\frac{\mu_a a_1}{2} + \frac{D}{2\omega_1^2 a_1\left(\tau_1^2+1\right)} \right) p\left(a_1,\tau\right) \right] + \\
&\frac{\partial^2}{2\partial a_1^2}\left[p\left(a_1,\tau\right)\left(\frac{D}{\omega_1^2\left(\tau_1^2+1\right)} \right) \right]
\end{aligned}
\tag{48}
$$

For the electrical subsystems:

-Piezoelectric circuit

$$
\begin{aligned}
&\frac{\partial p\left(a_2,\tau\right)}{\partial\tau} = \frac{\partial}{\partial a_2}\left[\left(-\frac{\alpha_2 a_2}{2} + \frac{\beta_{22}^2 D}{2\omega_2^2\left(\tau_1^2+1\right)} \right) p\left(a_2,\tau\right) \right] + \\
&\frac{\partial^2}{2\partial a_2^2}\left[p\left(a_2,\tau\right)\left(\frac{\beta_{22}^2 D}{\omega_2^2\left(\tau_1^2+1\right)} \right) \right]
\end{aligned}
\tag{49}
$$

- Electromagnetic circuit

$$
\begin{aligned}
&\frac{\partial p\left(a_3,\tau\right)}{\partial\tau} = \frac{\partial}{\partial a_3}\left[\left(\Omega_{11} + \frac{\beta_{11}^2 D}{2\omega_3^2 a_3\left(\tau_1^2+1\right)} \right) p\left(a_3,\tau\right) \right] + \\
&\frac{\partial^2}{2\partial a_3^2}\left[p\left(a_3,\tau\right)\left(\frac{\beta_{11}^2 D}{\omega_3^2\left(\tau_1^2+1\right)} \right) \right]
\end{aligned}
\tag{50}
$$

In the context of energy harvesting systems, we are primarily interested in the long-term system behavior, we then have to obtain stationary probability density function. Hence, the stationary solutions of Eqs.(48)-(50) of electrical and mechanical part respectively are obtained as:

$$p\left(a_1,\tau\right)=C_1 a_1 \exp\left(-\frac{\mu_a a_1^2\omega_1^2\left(\tau_1^2+1\right)}{2D}\right) \tag{51}$$

$$p\left(a_2,\tau\right)=C_2 a_2 \exp\left(-\frac{\alpha_2 a_2^2\omega_2^2\left(\tau_1^2+1\right)}{2\beta_{22}^2}\right) \tag{52}$$

$$p\left(a_3,\tau\right)=C_3 a_3 \exp\left(-\frac{a_3^2\omega_3^2\left(\tau_1^2+1\right)\left(\mu_3 a_3^4+3\mu_2 a_3^2+24\mu_1\right)}{48D\beta_{11}^2}\right) \tag{53}$$

where C_1, C_2 and C_3 are the constant of normalization assessed numerically.

Through a transformation from variable (a_1,θ_1), (a_2,θ_2) and (a_3,θ_3) to the original variables $\left(x,\dot{x}\right)$,$\left(y,\dot{y}\right)$ and $\left(r,\dot{r}\right)$, an expression for the stationary densities function of x and $\dot{x}$, y and $\dot{y}$ and r and $\dot{r}$ can be derived as

$$p_{1n}\left(x,\dot{x}\right)=\frac{1}{2\pi\omega_1 a_1}p_1\left(a_1\right) \tag{54}$$

$$p_{1n}\left(x,\dot{x}\right)=\frac{C_1}{2\pi\omega_1}\exp\left[-\frac{\mu_a\omega_1^2\left(\tau_1^2+1\right)\left(x^2+\frac{\dot{x}^2}{\omega_1^2}\right)}{2D}\right] \tag{55}$$

$$p_{2n}\left(y,\dot{y}\right)=\frac{1}{2\pi\omega_2 a_2}p_2\left(a_2\right) \tag{56}$$

$$p_{2n}\left(y,\dot{y}\right)=\frac{C_2}{2\pi\omega_2}\exp\left[-\frac{\alpha_2\omega_2^2\left(\tau_1^2+1\right)\left(y^2+\frac{\dot{y}^2}{\omega_2^2}\right)}{2\beta_{22}^2}\right] \tag{57}$$

$$p_{3n}\left(r,\dot{r}\right)=\frac{1}{2\pi\omega_3 a_3}p_3\left(a_3\right) \tag{58}$$

$$p_{3n}\left(r,\dot{r}\right)=\frac{C_3}{2\pi\omega_3}\exp\left[\frac{\Lambda_{12}\left(r^2+\frac{\dot{r}^2}{\omega_3^2}\right)\left(\Lambda_{11}+24\mu_1\right)}{48D\beta_{11}^2}\right] \tag{59}$$

where $\Lambda_{12}=\omega_3^2\left(\tau_1^2+1\right)$ and $\Lambda_{11}=\mu_3\left(r^2+\frac{\dot{r}^2}{\omega_3^2}\right)^2+3\mu_2\left(r^2+\frac{\dot{r}^2}{\omega_3^2}\right)$, while $a_1=\sqrt{x^2+\frac{\dot{x}^2}{\omega_1^2}}$; $a_2=\sqrt{y^2+\frac{\dot{y}^2}{\omega_2^2}}$ and $a_3=\sqrt{r^2+\frac{\dot{r}^2}{\omega_3^2}}$

II.3.4 Stability analysis of the harvester

In the order to investigated the stability of the system, a rewriting of Eq.(47)(a)-(c) is required.

$$\begin{aligned}
da_1&=\frac{dV\left(a_1\right)}{da_1}+\sqrt{\frac{D}{\omega_1^2\left(\tau_1^2+1\right)}}dw_1\\
da_2&=\frac{dV\left(a_2\right)}{da_1}+\sqrt{\frac{\beta_{22}^2D}{\omega_2^2\left(\tau_1^2+1\right)}}dw_2\\
da_3&=\frac{dV\left(a_3\right)}{da_1}+\sqrt{\frac{\beta_{11}^2D}{\omega_3^2\left(\tau_1^2+1\right)}}dw_3
\end{aligned} \tag{60}$$

with $V\left(a_1\right),V\left(a_2\right)$ and $V\left(a_3\right)$, the effective potentials of mechanical and two electrical (piezoelectric and electromagnetic circuit) subsystem respectively. The expression of these potentials are given as follow:

$$\begin{aligned}
V\left(a_1\right)&=\frac{\mu_a a_1^2}{4}-\frac{D\ln\left(a_1\right)}{2\omega_1^2\left(\tau_1^2+1\right)}(a)\\
V\left(a_2\right)&=\frac{\alpha_2 a_2^2}{4}-\frac{\beta_{22}^2D\ln\left(a_2\right)}{2\omega_2^2\left(\tau_1^2+1\right)}(b)\\
V\left(a_3\right)&=\frac{\mu_3 a_3^6}{96}+\frac{\mu_2 a_3^4}{32}+\frac{\mu_1 a_3^6}{4}-\frac{\beta_{11}^2D\ln\left(a_3\right)}{2\omega_3^2\left(\tau_1^2+1\right)}(c)
\end{aligned} \tag{61}$$

II.3.5 Stochastic P-bifurcation induced by load resistance

The stochastic P-bifurcation is a stochastic bifurcation phenomenon that occurs in a random system. The stochastic bi- furcation contains the D-bifurcation and the P-bifurcation problems. The D-bifurcation focuses on the stochastic bifurcation point in the probability one sense which is measured by the maximal Lyapunov exponent [18]. The P-bifurcation studies the mode of the stationary probability density function or the invariant measure of the stochastic process. The stochastic P-bifurcation takes place when the mode of the stationary probability density function

changes in nature. It indicates the jump of the distribution of the random variable in probability sense. The D-bifurcation and the P-bifurcation are independent. There is no direct relation between these two stochastic bifurcation phenomena [18]. It is also judicious to notice that, D bifurcation is a dynamical concept, which is similar in nature to deterministic bifurcations, while p bifurcation is a static concept. This heading is consecrated to the investigation of the P-bifurcation phenomenon in the harvester most particulary in the magnetic circuit constituted of the nonlinear resistor. First and foremost, it is worth reminding that, stochastic P-bifurcation takes place when the mode of the stationary probability density function changes in nature [163]. It indicates the jump of the distribution of the random variable in probability sense. We provide in this subsection of the thesis, the condition for which this phenomena can be observed in the system most particulary in the electromagnetic circuit. For reaching our objective, we let, $\frac{dp\left(a_3\right)}{da_3}=0$. The extrema of distribution Eq. (53) are the roots of equations:

$$\omega_3^2\left(1+\tau_1^2\right)\left(-\frac{\mu_3 a_3^6}{8}-\frac{\mu_2 a_3^4}{4}-\mu_1 a_3^2\right)+D\beta_{11}^2=0 \tag{62}$$

II.4 Numerical simulation

Numerical simulation is a technique of major importance in various technical and scientific fields. Used to understand diverse physical phenomena or to design everyday objects, it plays a major role in innovation in the industrial sector. Whilst engineering curricula now include training courses dedicated to it, numerical simulation is still not well-known in some economic sectors, and even less so among the general public. Simulation involves the mathematical modeling of the real world, coupled with the computing power offered by modern technology. Designed to perform virtual experiments, digital simulation can be considered as an "art of prediction".This heading aims at presenting the numerical mathematic models used to integrate numerically the different physical models, in order to predict the systems responses of the different models proposed in this thesis.

II.4.1 Euler version algorithm

In mathematics and computational science, the Euler method (also called forward Euler method) is a first-order numerical procedure for solving ordinary differential equations (ODEs) with a

given initial value. The Euler method is named after Leonhard Euler, who treated it in his book Institutionum calculi integralis published 1768 [166]. The Euler method is a first-order method, which means that the local error (error per step) is proportional to the square of the step size, and the global error (error at a given time) is proportional to the step size.

$$\dot{X} = \quad f\left(t, X\right) + g\left(t, X\right) \times \gamma, X\left(t_0\right) = X_0 \tag{63}$$

where the fisrt term is drift function and second, the diffusion term while $\gamma = \frac{dW}{dt}$ where W(t) is Weiner process. Eq.(63) can be written as:

$$dX = \quad f\left(t, X\right) dt + g\left(t, X\right) \times dW, X\left(t_0\right) = X_0 \tag{64}$$

Integrating Eq.(64)from 0 to t, we have Itô integral equation:

$$X(t) = \quad X_0 + \int_0^t f\left(s, X(s)\right) ds + \int_0^t g\left(s, X(s)\right) dWs \tag{65}$$

One-step Euler-Maruyama method will be derived by setting t=$\tau_{j+r}, r = 0, 1$in the integral Eq.(65)

$$X(t) = \quad X_0 + \int_0^t f\left(s, X(s)\right) ds + \int_0^t g\left(s, X(s)\right) dWs \tag{66}$$

This gives

$$X(\tau_j) = \quad X_0 + \int_0^{\tau_j} f\left(s, X(s)\right) ds + \int_0^{\tau_j} g\left(s, X(s)\right) dWs \tag{67}$$

$$X(\tau_{j+1}) = \quad X_0 + \int_0^{\tau_{j+1}} f\left(s, X(s)\right) ds + \int_0^{\tau_{j+1}} g\left(s, X(s)\right) dWs \tag{68}$$

Eq.(67)-(68)$\Longrightarrow$

$$X(\tau_{j+1}) = \quad X_{\tau_j} + \int_{\tau_j}^{\tau_{j+1}} f\left(s, X(s)\right) ds + \int_{\tau_j}^{\tau_{j+1}} g\left(s, X(s)\right) dWs \tag{69}$$

II.4.2 Box-Muller algorithm

One of the most useful methods for generating random numbers with a normal distribution is the Box-Müller transform, which was suggested by George Edward Pelham Box and Mervin Edgar Müller (1958). The method was in fact first mentioned explicitly by Raymond E. A. C. Paley and Norbert Wiener in 1934 [167]. Altogether, the Box-Müller method [167] takes independent standard uniform random variables U_1 and U_2 and produces independent standard normals X_1 and X_2 using the formulas:

$$\theta = 2\pi U_1, \quad R = \sqrt{-2\ln(U_2)},\ X_1 = R\cos(\theta), X_2 = R\sin(\theta) \tag{70}$$

In other words, from two random numbers $u_1, u_2 \in [0, 1]$ (generated by a uniform distribution), we produce two independent standard normally distributed numbers W_1 and W_2, namely

$$W_1 = \sqrt{-2\ln(u_1)}\cos(2\pi u_1) \quad , W_2 = \sqrt{-2\ln(u_2)}\sin(2\pi u_2) \tag{71}$$

It has been proven that the random variables X_1 and X_2 are independent, given that they incorporate the same R and θ. Here the independence property is analytically and computationally satisfied.

II.4.3 Algorithm of colered noise

For simplicity, we consider a stochastic equation with a single variable:

$$\dot{x} = \quad f(x) + \xi(t) \tag{72}$$

in which x is the variable of interest, $f(x)$ is a driving force and $\xi(t)$ denotes the colored noise variable, solution of this stochastic equation:

$$\dot{\xi(t)} = \quad -\lambda\xi(t) + \eta(t) \tag{73}$$

the colored noise has the properties [168, 18]:

$$< \xi(t) >= 0; \quad \{< \xi(t)\xi(s) >\} = D\lambda\exp(-\lambda D\,|t - s|) \tag{74}$$

where λ is the inverse of the correlation time for the colored noise τ and D is the noise strengh of the colored noise. $\eta(t)$ represent Gaussian random white noise which verify the statistic properties:

$$< \eta(\tau) >= 0; \quad < \eta(t)\eta(s) >= 2D\lambda\delta(t-s) \tag{75}$$

$< ... >$ indicates the white-noise average and $\{...\}$ indicates averaging over the distribution of initial condition ξ_0 values which is given by :

$$P(\xi_0) = \quad \frac{1}{\sqrt{2\pi D\lambda}} \exp(-\frac{\xi_0^2}{2D\lambda}) \tag{76}$$

This secondary averaging is essential for the stationary correlation given in Eq.(76). The Box Mueller algorithm [167, 168] can be used to generate Gaussian noise from two random numbers which are uniformly distributted on the unit interval, $\Delta t, \eta(t)$ is defined as $\eta(t) = \sqrt{-4D\Delta t \log(a)} \times \cos(2\pi b)$ where a=random number, b=random number We use for the initial distribution of ξ,

$$\xi(0) = \quad \sqrt{-2D\lambda \log(r1)} \times \cos(2\pi r_2) \tag{77}$$

where r_1=random number, r_2=random number. To start the simulation, an initial value for $\xi$is needed and is obtained in accord with the previous equations. After that the algorithm to generate colored noise is obtained by integrating eq.(73), and we have:

$$\xi(t) = \quad \xi(0)\exp(-\lambda t) + \lambda \int_0^t \exp[-\lambda(t-s)]\eta(s)ds \tag{78}$$

$$\xi(t+\Delta t) = \quad \xi(0)\exp[-\lambda(t+\Delta t)] + \lambda \int_0^{t+\Delta t} \exp[-\lambda(t+\Delta t-s)]\eta(s)ds \tag{79}$$

Consequently,

$$\xi(t+\Delta t) = \quad \xi(t)\exp[-\lambda\Delta t] + \lambda \int_t^{t+\Delta t} \exp[-\lambda(t+\Delta t-s)]\eta(s)ds \tag{80}$$

$$\xi(t+\Delta t) = \quad \xi(t)\exp[-\lambda\Delta t] + h(t,\Delta t) \tag{81}$$

in which h(t,Δt)=$\lambda \int_{t}^{t+\Delta t} \exp[-\lambda(t+\Delta t-s)]\eta(s)ds$

It is worth noting that h(t,Δt) is Gaussian and has zero mean.Therefore all of its properties are determined by its second moment, $< h^2(t,\Delta t) >= D\lambda(1-E)$ where $E = \exp(-2\lambda\Delta t)$. The exponentially colored noise is obtained by the lines:

$$h = \sqrt{-2D\lambda(1-E^2)\log(m)} \times \cos(2\pi n) \tag{82}$$

$$\xi \mid t+\Delta t = \xi(t)E + h(t,\Delta t) \tag{83}$$

$$\xi \mid t+\Delta t = \xi(t)E + h(t,\Delta t) \tag{84}$$

The Euler version of the integration of eq.(72) and eq.(73) given by: r_1=random number, r_2=random number

$$\xi = \sqrt{-2D\lambda\log(r_1)} \times \cos(2\pi r_2) \tag{85}$$

m=random number, n=random number, p=f(x)+ξ

$$x \mid t+\Delta t = x + p\Delta t \tag{86}$$

$$\xi \mid t+\Delta t = \xi(t)E + h(t,\Delta t) \tag{87}$$

II.4.4 Ghost stochastic resonance phenomenon

Noise is often thought of as interfering with signal detection and information transmission. Static on a radio station, ancillary conversations in a crowded room and flashing neon light along a busy thoroughfare all tend to obscure or distract from the desired information [169]. Now, it has been realized that certain noise-induced phenomena are of great use in various contexts. One such noise-induced phenomenon which has a wide range of applications in various branches of science and engineering is ghost stochastic resonance [169]. Indeed, the ghost stochastic resonance (GSR) phenomenon is the nonlinear effect in which the noise is able to make favorable the transmission of the useful signal. This effect can take various forms, depending on the types

considered for noise, the wanted signal, the nonlinear transmission system, and the performance measurement which is improved by adding noise. It cannot occur in a linear system. It is well known in the literature that ghost stochastic resonance phenomenon is observed in a lot of systems namely the electronic circuits [169]. This phenomenon is similar to the stochastic resonance phenomenon [170] who was first introduced by the Italian physicists Benzi et al. [171] to explain the periodicity of earth's ice ages. The eccentricity of the orbit of the earth varies with a periodicity of about 10^5 years, but according to current theories the variation is not strong enough to cause a dramatic climate change. Suppose the ice-covered and water-covered earth correspond to the two local minima. The variation of eccentricity with the period 10^5 years is too weak to induce the transition from ice-covered to water-covered earth and vice-versa. By introducing a bi-stable potential, Benzi et al. [171] suggested that a cooperative phenomenon between the weak periodic variation in the eccentricity (the signal) and the other random fluctuations might account for the strong periodicity observed. It is worth noting that, the stochastic resonance occurs when the frequency of system's vibration is present in the frequency bandwidth of the harmonic excitation. However, when the maximum amplitude of the system is reached for a frequency of vibration absent in the frequency bandwidth of the harmonic force, this phenomenon is called a ghost stochastic resonance. As the stochastic resonance phenomenon, the ghost stochastic resonance phenomenon requires three basic ingredients namely an energetic activation barrier, this energetic barrier can be encountered in the double or triple potential well of a bi-stable system or tri-stable; a weak coherent input (periodic signal) and a source of noise that is inherent to the system. In the scientific literature, there are many a methods for characterizing the ghost stochastic resonance for example the Mean Residence Time (TMR).

II.4.5 Mean Resident Time (TMR)

The Mean resident time (TMR) is one of the signature of the ghost stochastic resonance phenomenon. It can be defined as the average over a large number of residence times although the resident time is defined as a time duration spent by the system in it before switching to another well. In the system presenting the nonlinearities and exhibiting the ghost stochastic resonance phenomenon, When the noise is suppressed, the motion of the system is confined to a well or an equilibrium state. That is, before the noise-induced dynamics, the residence time of the system in each well is infinite. When we enhance the noise intensity D, we observe that, for a certain value

of the noise intensity called here D_c, the system begins to visit the other well also. For D values, just above D_c, TMR of the system in a well is very large. Thus, $TMR \gg \frac{T_0}{2}$ with $T_0 = \frac{2\pi}{\omega}$, the inverse of the fundamental frequency of the system. When $TMR = T_0/2$, the ghost stochastic resonance phenomenon occurs and consequently, the amplitude response reaches his maximum. This maximum observed characterizes the ghost stochastic resonance (GSR) phenomenon.

II.4.6 Mathematical formula for determining the ghost-stochastic resonance phenomenon

In this thesis, the ghost-stochastic resonance is investigated in order to know the amount of energy harvested by the hybrid system. For reaching our objective, we consider that, the two models are subjected to the combination of the harmonic and the random excitation defined as follow:

$$F(\tau) = \sum_{i=1}^{m} f_0 \cos(\omega_i \tau) + \xi(\tau) \tag{88}$$

with $\sum_{i=1}^{m} f_0 \cos(\omega_i \tau)$ is a harmonic excitation, with f_0 the amplitude of coherence force, $\omega_i = (k + i - 1)\omega_0$ is the frequency of the coherence force with k a constant took here equal to 2. ω_0 is the fundamental frequency. $\xi(\tau)$ is the random excitation. It is worth noting that, the equations of the two models are nonlinear and should exhibit many frequency components. For the large value of time($\tau \to \infty$), the asymptotic solution of equations for the different models can be given as follows:

$$< x(\tau) >_{as} = \sum_{j} x_m(j\omega_i) \cos[j\omega_i \tau - \psi_m(j\omega_i)] \tag{89}$$

where j is a non-negative constant which may be in integer or fractional form, $X_m(j\omega_i)$ and $\psi_m(j\omega_i)$ are the mean response amplitude and phase lag respectively at the frequency $j\omega_i$. The mean amplitude response is defined as in Ref. [163, 172]:

$$X_m = \sqrt{A_s^2 + A_c^2} \tag{90}$$

where A_s and A_c are the jth sine and cosine components of the Fourier coefficients defined as follows:

$$\begin{aligned} A_S &= \frac{2}{nT}\int_0^{nT} x(\tau)\sin(\omega_i\tau)d\tau \\ A_c &= \frac{2}{nT}\int_0^{nT} x(\tau)\cos(\omega_i\tau)d\tau \end{aligned} \tag{91}$$

where $n = 500$, while $T = \dfrac{2\pi}{\omega_i}$ is the period harmonic excitation.

II.4.7 Efficiency in power conversion of the harvester

The efficiency conversion of energies dispersed in the environment by the electricity's generator is the one of the fundamental elements for evaluating the system's performance. Thus, the efficiency of the hybrid model is assessed by using this formula:

$$\eta = \frac{P_e}{P_m} \times 100 \tag{92}$$

with P_e and P_m, are respectively, the electrical and the mechanical power effective value. It is well known in the literature that the power effective value is defined as:

$$p_t = \sqrt{\frac{1}{\tau}\int_0^{\tau} \left(p_t^{ins}\right)^2 d\tau} \tag{93}$$

where p_t^{ins} is the instantaneous power and τ is the time.

II.5 Discrete schematic of the different models

II.5.1 Probabilistic analysis and Ghost-Stochastic resonance of a hybrid energy harvester under Gaussian White noise

The numerical scheme used in this thesis is based on the Euler version algorithm. By letting $\dot{x} = u$, Eq.(44) can be rewritten as follow:

$$\begin{aligned} x' &= u \\ u' &= -\mu_a u - \omega_0 x + \beta_2 y - \sigma x^3 - \beta_1 r + N(\tau) \\ y' &= -\alpha_2 y + \beta_{22} u \\ r' &= -\alpha_3 y + \beta_{11} u \end{aligned} \tag{94}$$

The discrete equations can be written as:

$$\begin{aligned} x_{i+1} &= x_i + u_i h \\ u_{i+1} &= u_i + \left[-\mu_a u_i - \omega_0 x_i + \beta_2 y_i - \sigma x_i^3 - \beta_1 r_i \right] h + \zeta_k(\tau) \\ y_{i+1} &= y_i + \left[-\alpha_2 y_i + \beta_{22} u_i \right] h \\ r_{i+1} &= r_i + \left[-\alpha_3 y_i + \beta_{11} u_i \right] h \end{aligned} \tag{95}$$

II.5.2 Resistance induced P-bifurcation and Ghost-Stochastic resonance of a hybrid energy harvester under colored noise

The numerical scheme used in this model is based on the Euler version algorithm. By letting $\dot{x} = u$, $\dot{y} = w$ and $\dot{r} = z$, Eq.(44) can be rewritten in the following form:

$$\begin{aligned} \dot{x} &= u \\ \dot{u} &= -(\mu_a u + \omega_0 x - \beta_2 y + \chi r + \sigma x^3) + N(\tau) \\ \dot{y} &= w \\ \dot{w} &= -(\alpha_2 w + \mu_{33} y + \beta_{22} \dot{u}) \\ \dot{r} &= z \\ \dot{z} &= -\left(\left(\mu_1 + \mu_2 r^2 + \mu_3 r^4 \right) z - \beta_{11} \dot{u} \right) \end{aligned} \tag{96}$$

The discrete equations can be written as:

$$\begin{aligned} x_{k+1} &= x_k + h u_k \\ u_{k+1} &= u_k + \left[-(\mu_a u_k + \omega_0 x_k - \beta_2 y_k + \chi r_k + \sigma x_k^3) \right] h \\ &\quad - \left[\sigma\, x_k^3 + \eta_1 y_k \right] h + \xi_k(\tau) \\ y_{k+1} &= y_k + h w_k \\ w_{k+1} &= w_k + \left[-(\alpha_2 w_k + \mu_{33} y_k + \beta_{32} u_{k+1}) \right] h \\ r_{k+1} &= r_k + h z_k \\ z_{k+1} &= z_k + \left[-(\mu_1 + \mu_2 r_k^2 + \mu_3 r_k^4)\, z_k - \beta_{11} u_{k+1}) \right] h \end{aligned} \tag{97}$$

II.6 Conclusion

This chapter of the thesis aimed to describe the mathematical modeling for the different models used. First of all, we have presented some analytical methods, following by the numerical methods used. These two techniques are used to provide the results presented in the following chapter. Using the stochastic average method, the $Fokker - Planck - Kolmogorov$ equation is built. From this equation, the statistic response of the harvester is derived following of the study of stochastic p-bifurcation phenomenon in the proposed models. Besides, the stability analysis of the harvester is also made. The following chapter is consecrated to numerical simulation of the mathematic model obtained from the physical model proposed in this present chapter.

CHAPTER III

RESULTS AND DISCUSSIONS

III.1 Introduction

This present chapter aims to present and discuss the main results of this thesis using the numerical simulations. Firstly, we present the results of probabilistic analysis and Ghost-Stochastic resonance phenomenon of a hybrid energy harvester under Gaussian White noise. Here, the probability density function is plotted following the mean square voltage in current. We also study in this section, the ghost-stochastic resonance phenomenon. In the second section, we present the results of resistance induced P-bifurcation and Ghost-Stochastic resonance of a hybrid energy harvester under colored noise. This heading of the thesis aims to study the stochastic p-bifurcation following stability analysis and the study of ghost-stochastic resonance phenomenon.

III.2 Probabilistic analysis and Ghost-Stochastic resonance of a hybrid energy harvester under Gaussian White noise

III.2.1 Numerical simulation of the probability density function and mean square intensity and voltage

In the purpose to compare the analytical results obtained via the stochastic averaging method, the numerical simulation is made for the harvester. Fig.11, shows the good agreement between the numerical results and those obtained analytically. We also draw in fig.12, the $3D$ representation of probability density of harvester. It emerges from these results that, the probability distribution is unimodal.

We plotted in fig.13 (a)-(b), the mean square current of electromagnetic circuit and the mean square voltage of the piezoelectric circuit versus coupling coefficient β_{11} and β_{22} for diverse values of the electrical impedances α_{11} and α_{22}. Here, the means square represent the

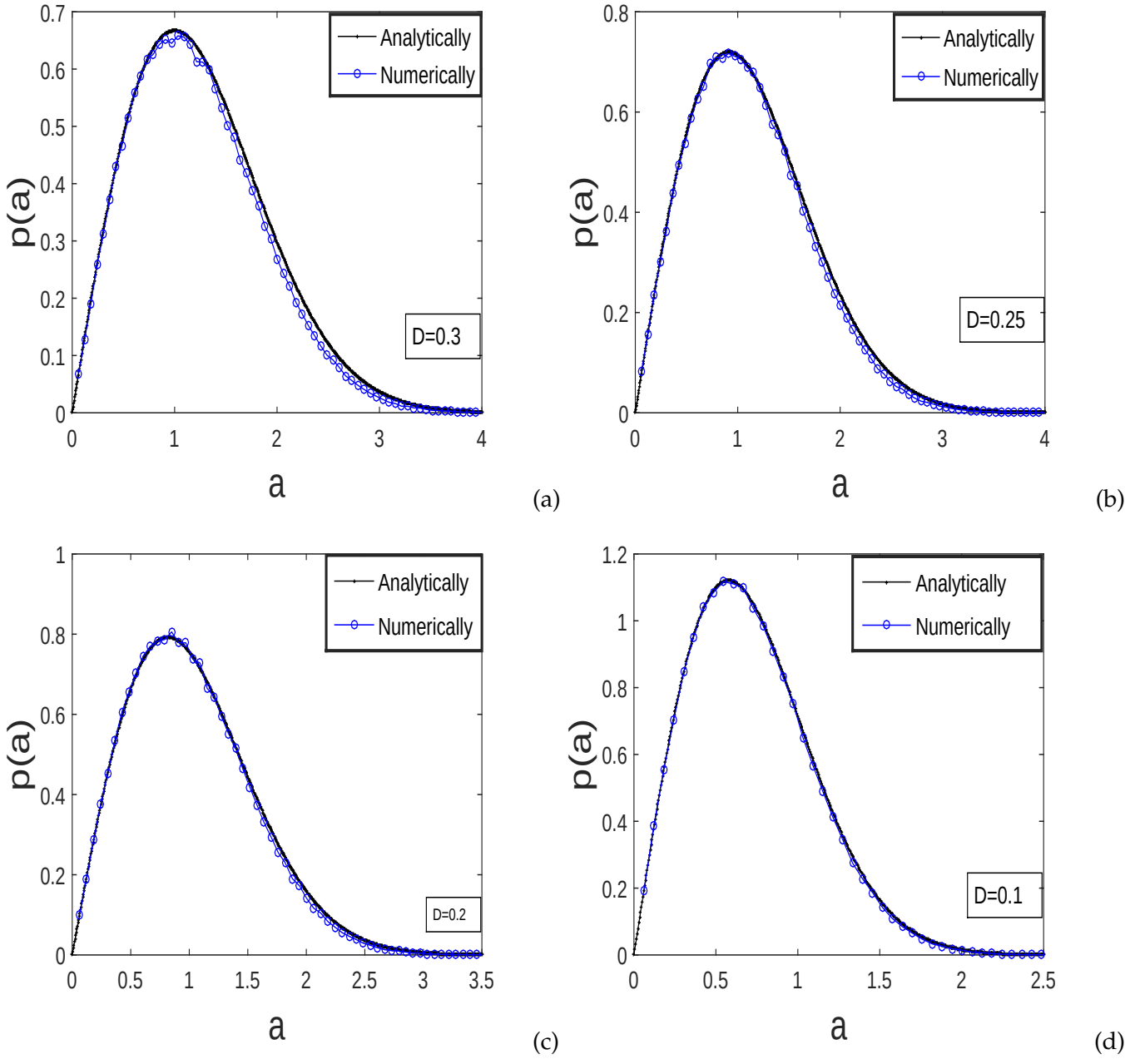

Figure 11: Stationary probability density for different values of noise intensity for $\mu_a = 0.3$, $\beta_2 = 0.005$, $\beta_1 = 0.003$, $\alpha_2 = 0.000001$, $\beta_{22} = -0.005$, $\beta_{11} = 0.003$, $\alpha_3 = 0.0003$, $\sigma = 0.05$, $\omega_0 = 1$.

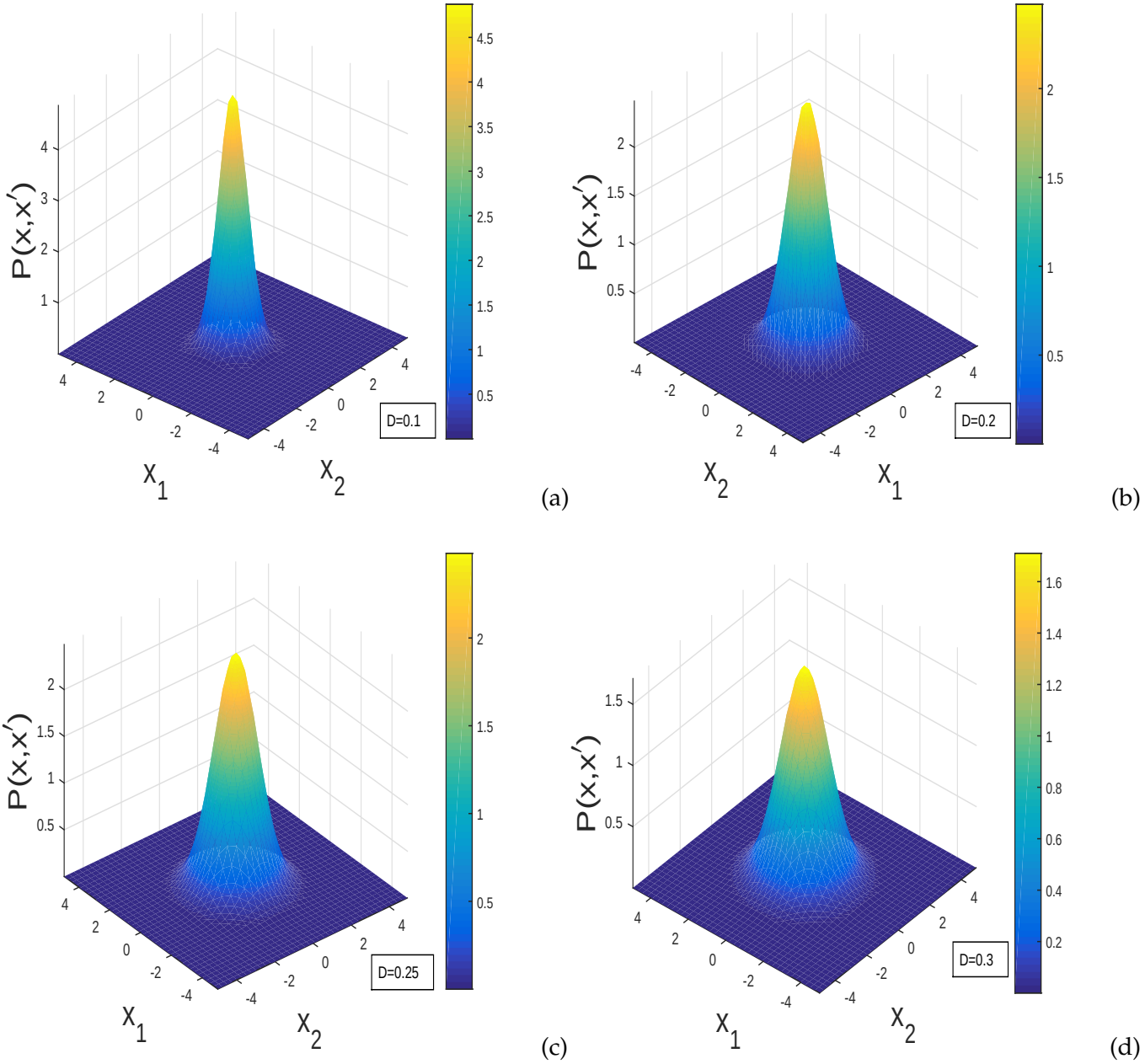

Figure 12: Stationary probability density of the system in 3D representation for: for $\mu_a = 0.3$, $\beta_2 = 0.005$, $\beta_1 = 0.003$, $\alpha_2 = 0.000001$, $\beta_{22} = -0.005$, $\beta_{11} = 0.003$, $\alpha_3 = 0.0003$, $\sigma = 0.05$, $\omega_0 = 1$.

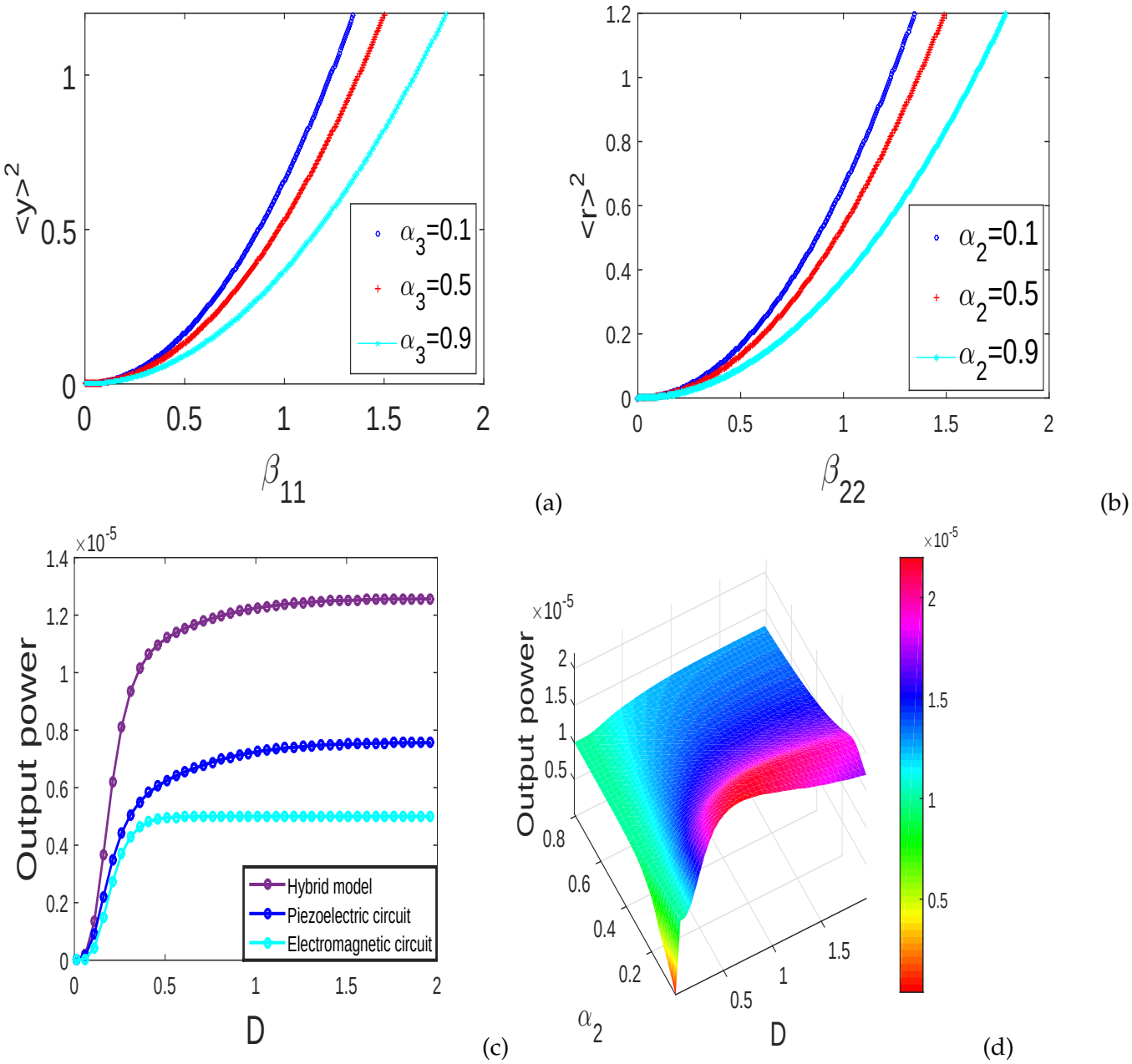

Figure 13: (a) Evolution of mean square voltage of piezoelectric circuit versus coefficient β_{11},(b) Evolution of mean square current of magnetic circuit versus coefficient β_{22}, (c) Output power versus noise intensity D, (d) 3D-representation of the Output power of hybrid model versus noise intensity D and piezoelectric coupling coefficient for $\mu_a = 0.3$, $\beta_2 = 0.005$, $\beta_1 = 0.003$, $\alpha_2 = 0.000001$, $\beta_{22} = -0.005$, $\beta_{11} = 0.003$, $\alpha_3 = 0.0003$, $\sigma = 0.05$, $D = 0.1$, $\omega_0 = 1$.

output voltage generated by the two electrical circuits (magnetic and piezoelectric circuit). We observe in these figures that, for the fixed value of the coupling coefficient, the amount of energy harvested by the system decreases when the electrical impedance increases.

In fig.13 (c)-(d), we compare the output power generated by the hybrid model and those obtained by the piezoelectric and electromagnetic model respectively. We notice that the energy harvested by the hybrid model is higher than the one harvested by the piezoelectric or electromagnetic circuit. We provide in fig.13(d), the $3D$-representation of the output power of the hybrid model versus noise intensity and electrical impedance of piezoelectric circuit α_2. We observe that, for a fixed value of noise intensity D, the maximum of output power decreases when α_2 increases.

III.2.2 Numerical simulation of the mean amplitude response and ghost stochastic resonance phenomenon

In this heading, we assume that, $f_0 \neq 0$. Thus, the harvester is subjected to the combination of the coherence excitation $\sum_{i=1}^{m} f_0 \cos(\omega_i \tau)$ and the random force $\zeta_k(\tau)$. In the purpose to get a deep understanding of the observed dynamics and the influence of noise, we can assess the mean residence time and mean amplitude response.

Fig.14(a) shows the evolution of the numerically computed $x_m(\omega)$ for $\omega = \omega_0$, $\omega = \omega_1 = 2\omega_0$ and $\omega = \omega_2 = 3\omega_0$ as a function of the noise intensity D. A typical noise-induced resonance is realized with theses frequencies. ω_1 and ω_2 are present in the input signal. The resonance observed with these frequencies is the usual stochastic resonance [173, 174]. The resonance associated with the missing frequency ω_0 is ghost-stochastic resonance. The ghost-stochastic resonance occurs at $D = D_{max} = 0.3$. This can be corroborated in fig.14(b) by plotting the mean residence time. Indeed, in fig.14(b), when the noise intensity D is equal to $D = 0.05$, the size of the orbit increases when the value of D increases. However, the orbit remains in the right well. For $D \geq 0.05$, the orbit visits the left well and gives rise to the ghost-stochastic resonance phenomenon when the noise intensity takes the value $D = D_{max} = 0.3$.

III.2.3 Numerical simulation of efficiency in power conversion of the harvester

In fig.14(c)-(d), we drawn the efficiency conversion of the piezoelectric and electromagnetic subsystem versus noise intensity D. It emerges from these figures that, when $\omega = \omega_0$, the ef-

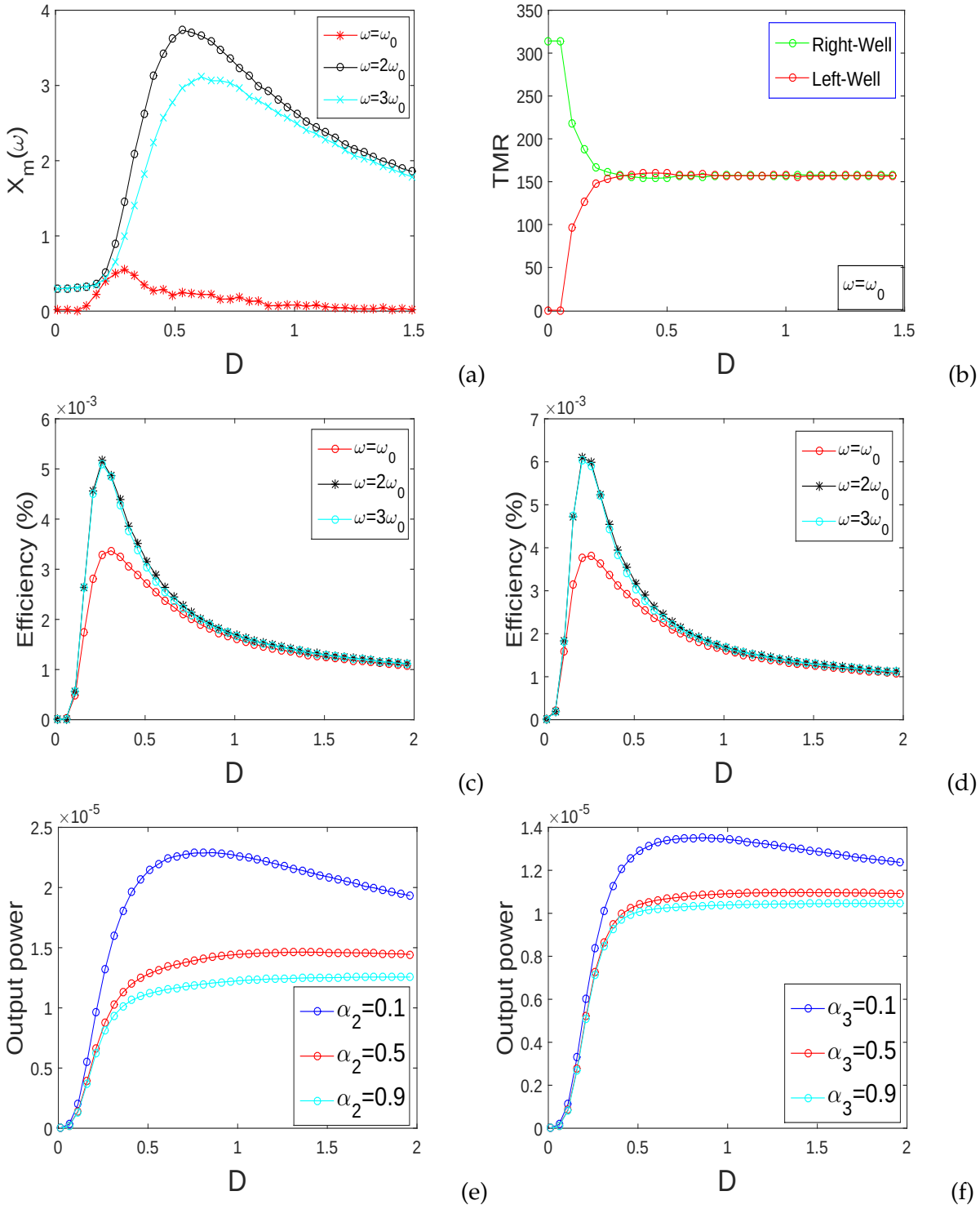

Figure 14: (a) Mean amplitude response $x_m(\omega)$ versus noise intensity D , (b) Mean residence time versus noise intensity D, (c)-(d) Efficiency versus noise intensity D for $\alpha_3 = 0.0003$,$\alpha_2 = 0.000001$, (e)-(f) Output voltage versus noise intensity for $\mu_a = 0.3$, $\beta_2 = 0.005$, $\beta_1 = 0.003$, $\beta_{22} = -0.005$, $\beta_{11} = 0.003$, $\sigma = 0.05$, $f_0 = 0.39$, $\omega_0 = 1$.

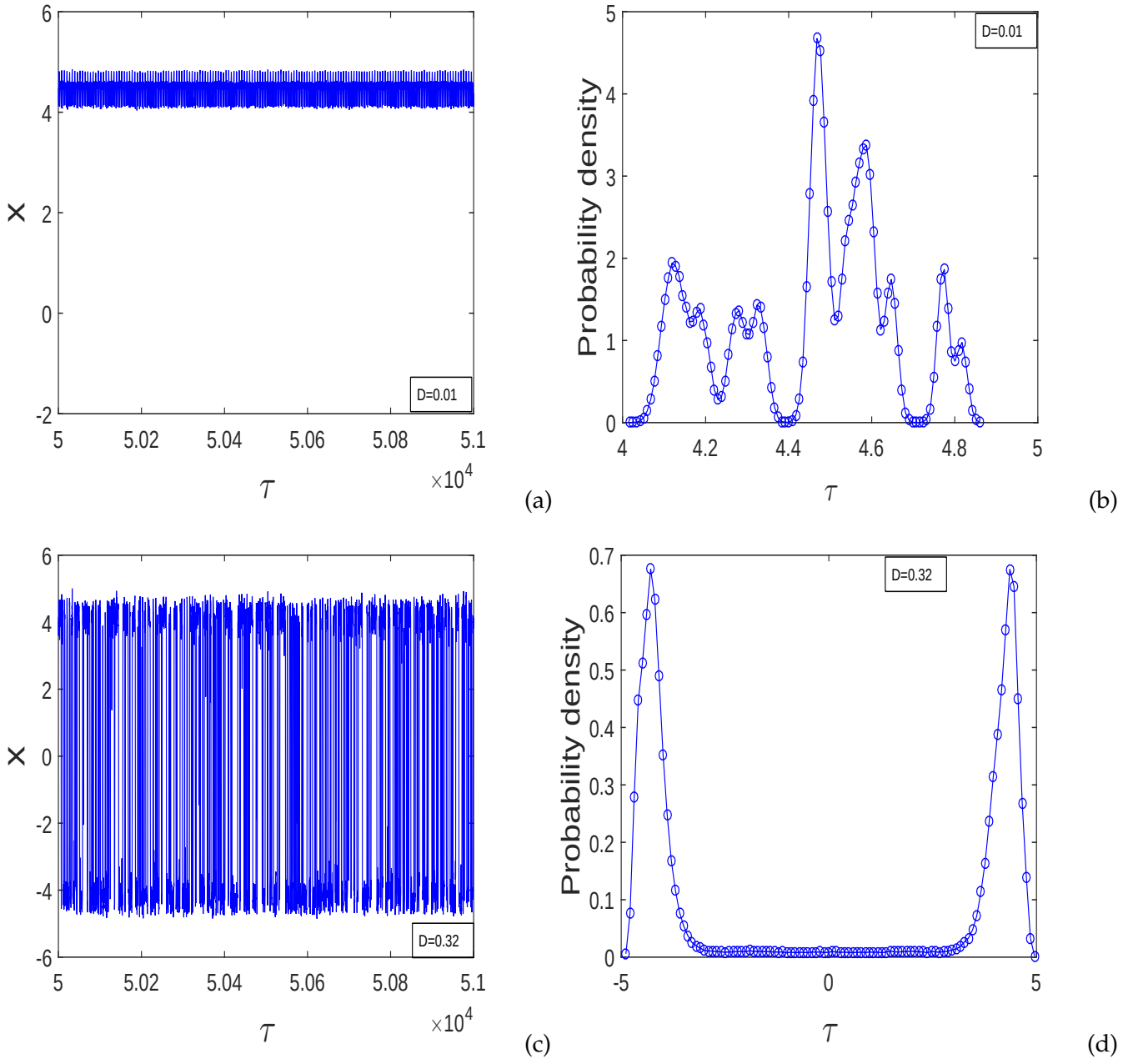

Figure 15: (a), (c), Time series of the mechanical subsystem, (b), (d), Probability distribution of the mechanical subsystem for for $\mu_a = 0.3$, $\beta_2 = 0.005$, $\beta_1 = 0.003$, $\alpha_2 = 0.000001$, $\beta_{22} = -0.005$, $\beta_{11} = 0.003$, $\alpha_3 = 0.0003$, $\sigma = 0.05$, $f_0 = 0.39$, $\omega_0 = 1$.

ficiency increases for $D < D_{max}$, reaches a maximum for $D = D_max = 0.3$ when the ghost-stochastic resonance occurs, and decreases for $D > D_{max}$. We also provided in fig.14(e)-(f), the output power for $\omega = \omega_0$, for different values of electrical impedance of the piezoelectric α_2 and magnetic circuit α_3. We observe in these figures that, while the fundamental frequency is absent in the input signal, the harvester can generated a significative energy. In addition, we also notice in these figures fig.14(e)-(f) that, an enhancing the α_2 and α_3 lead to decrease the output power.

We plotted in fig.15, the time series of the harvester, with the corresponding probability distribution. In fig.15(a) and (b), we observe that the system vibrates in the right-well and presents a lot of maximum and minimum. No any transition is observed in this condition. However, in fig.15(c), the transition phenomenon is observed. The system vibrates around the position X = 0 between the positions X = -4.29 and X = 4.359. This is corroborated by fig.15(d). We plot in fig.16(a)-(d), the voltage of the piezoelectric subsystem and the magnetic current of the magnetic circuit versus the time, corresponding to the probability density function plotted in fig.15(b) and (d). We notice in fig.16, the amplitude of the voltage of the piezoelectric circuit and magnetic current of the magnetic circuit is higher when the ghost-stochastic resonance occurs. Thus, when the ghost-stochastic resonance occurs, the piezoelectric output power and the magnetic output power will be maximized, and consequently, improves the amount of energy harvested by the scavenger. This shows the correlation between the peaks location in the probability density function and the output power.

III.3 Resistance induced P-bifurcation and Ghost-Stochastic resonance of a hybrid energy harvester under colored noise

III.3.1 Numerical simulation of probability density function and steady state analysis

In the purpose to validate the efficiency of the analytical method used in this subsection of the thesis, the numerical simulation is made.

Fig.17(a)-(h) show the probability density function of the electromagnetic circuit (Eq.(53)) with its corresponding effective potential (Eq.(61)(c)) configurations when we modify the intensity of the colored noise. We observe in these figures, two-well effective potential for certain values of D with two stable points A_1 and A_3 while A_2 represents the unstable equilibrium

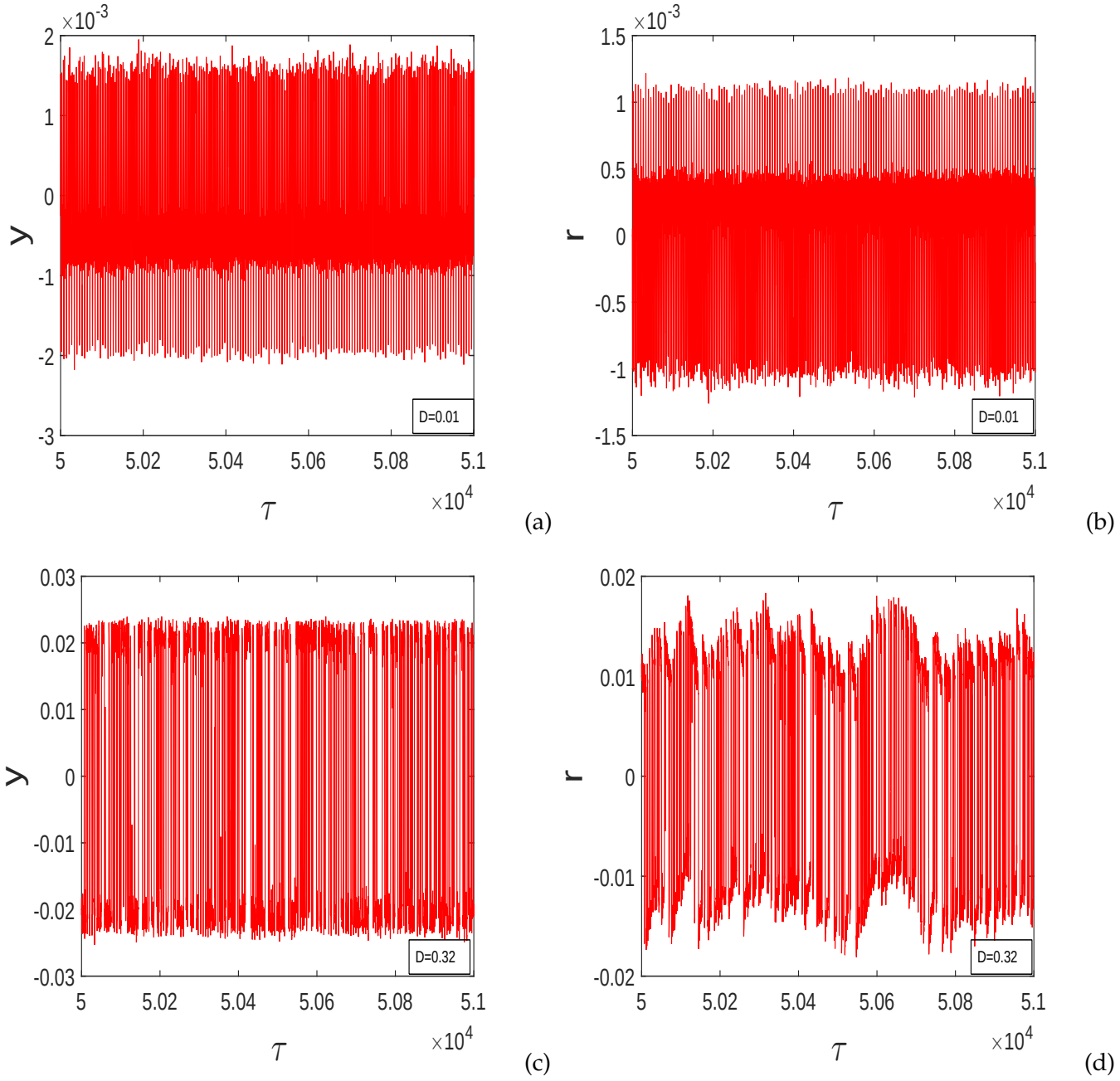

Figure 16: Time series of the piezoelectric voltage and magnetic current, (a)Voltage of piezoelectric circuit before the ghost-stochastic resonance, (a)Magnetic current of the magnetic circuit before the ghost-stochastic resonance,(c) Voltage of piezoelectric circuit when the ghost-stochastic resonance occurs, (d) Magnetic current of the magnetic circuit when the ghost-stochastic resonance, for for $\mu_a = 0.3$, $\beta_2 = 0.005$, $\beta_1 = 0.003$, $\alpha_2 = 0.000001$, $\beta_{22} = -0.005$, $\beta_{11} = 0.003$, $\alpha_3 = 0.0003$, $\sigma = 0.05$, $f_0 = 0.39$, $\omega_0 = 1$.

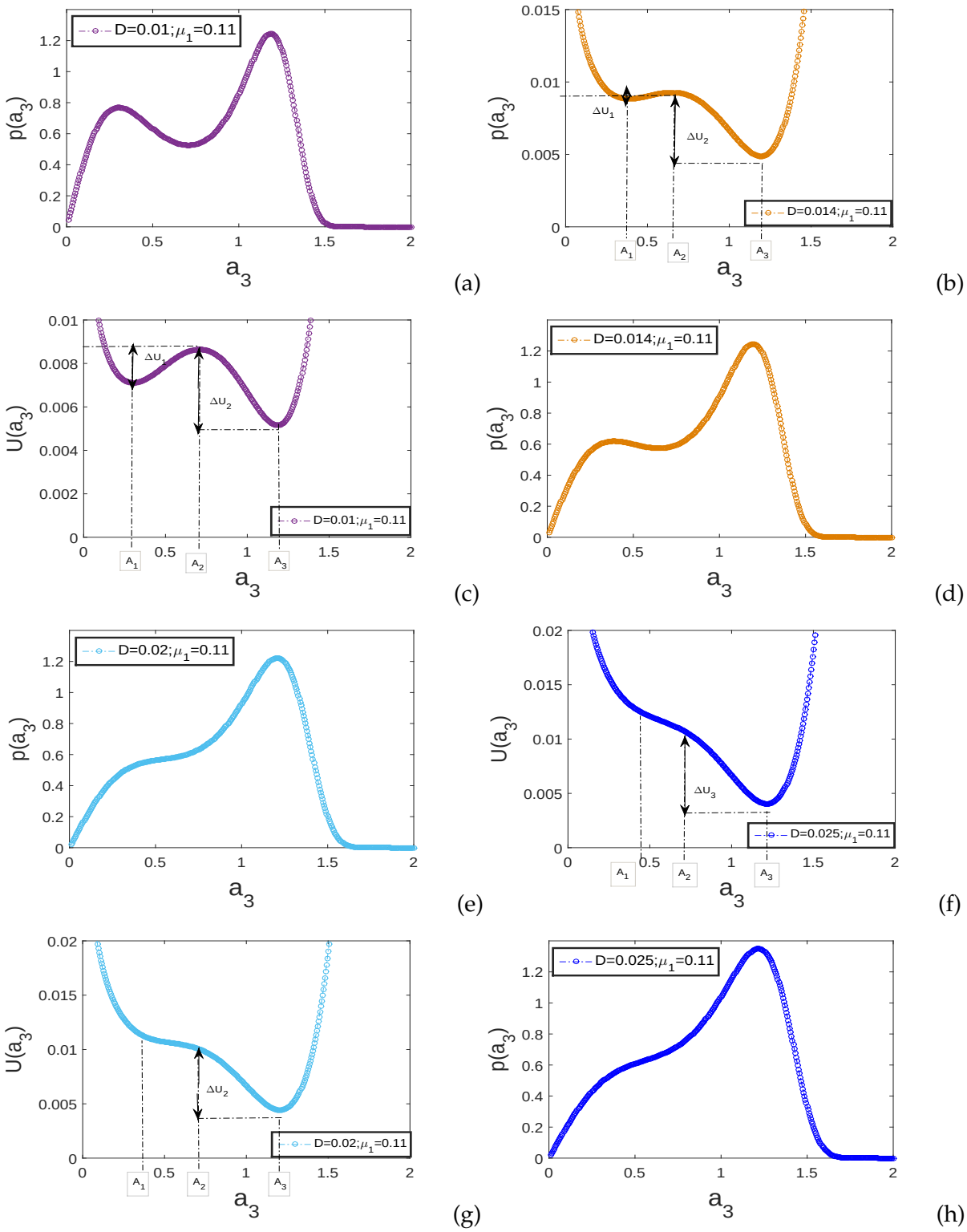

Figure 17: Stationary probability density of the magnetic circuit (Eq. (53)) with its corresponding effective potential of the system: for $\mu_a = 0.11$,$\mu_2 = 0.06$, $\beta_2 = 0.1$, $\mu_3 = 1$, $\alpha_2 = 0.06$, $\beta_{22} = -0.01$, $\mu_1 = 0.11$, $\mu_1 = 0.11$,$\mu_2 = -1$,$\mu_3 = 1$,$\chi = 0.003$,$\sigma = 0.05$, $\omega_3 = 1$,$\beta_{11} = 0.00003$.

point(fig.17 (b,c,g,f)). A disappearance of equilibrium point (A_1) is observed when we increase the intensity of colored noise. In addition, by enhancing the noise intensity, an asymmetric effective potential is destructed at detriment of the monostable effective potential (see fig.17(f)). Let us notice that, when the effective potential presents two stable equilibrium points, the probability density function $p(a_3)$ as a function of amplitude of current a_3 exhibits two peaks (fig.17(a), (d) and (g)) at different equilibrium points A_1 and A_3. It is worth reminding that, in the stochastic models, the peaks of the probability density function correspond to attractors, and troughs correspond to repellers. Moreover, an equilibrium point is more stable (high resilience) if the probability density function peak is large in comparison with another equilibrium point which is less stable (low resilience) as the probability density function peak is small.

III.3.2 Stochastic P-bifurcation induced by load resistance

Fig.18(a) show the bifurcation diagram drawn in the parameter plan (μ_1, D). It emerges from this result that, the probability distribution is unimodal in the white area and bimodal in the colored domain while the blue line corresponds to the threshold of the bimodality. Let's notice that, the bimodality area allow us to know the interval of the variation of the linear resistance for which the amount of harvested energy can be improved. This result is corroborated by plotting in fig.18(b), the corresponding probability density.

Fig.18(c) show the probability density function obtained from eq.(51). The agreement between these tow results is observed.

We also plotted in figure 18(d), the amplitude of the dimensionless current for different value of noise intensity. By varying the dimensionless linear resistance μ_1, figure 18(d) presents the domain of bimodality of the electromagnetic circuit. The two modes observed for certain values of linear resistance (see fig.18(d)), correspond to the two maximal values of the probability density (see figure 17(a), (d) and (g)), corresponding to two stable limits cycle.

We provided in fig.19(a)-(f), and fig.20(g)-(l), the joint stationary probability density (normalized $p_{n3}(r_1, r_2)$, and unormalized $p(r_1, r_2)$) of the magnetic circuit(Eq.(53)) for divers values of dimensionless linear resistance μ_1 and noise intensity D. Fig.19(a)-(c) show the bimodality distribution. In this condition, the amplitude of the electrical current flowing in the load resistance of the magnetic circuit presents two limit circles whose the first has an amplitude close to ≈ 0.05 and the second near to ≈ 1.05. However, from fig.19(d)-(f) to 20(g)-(l), we observe a disappear-

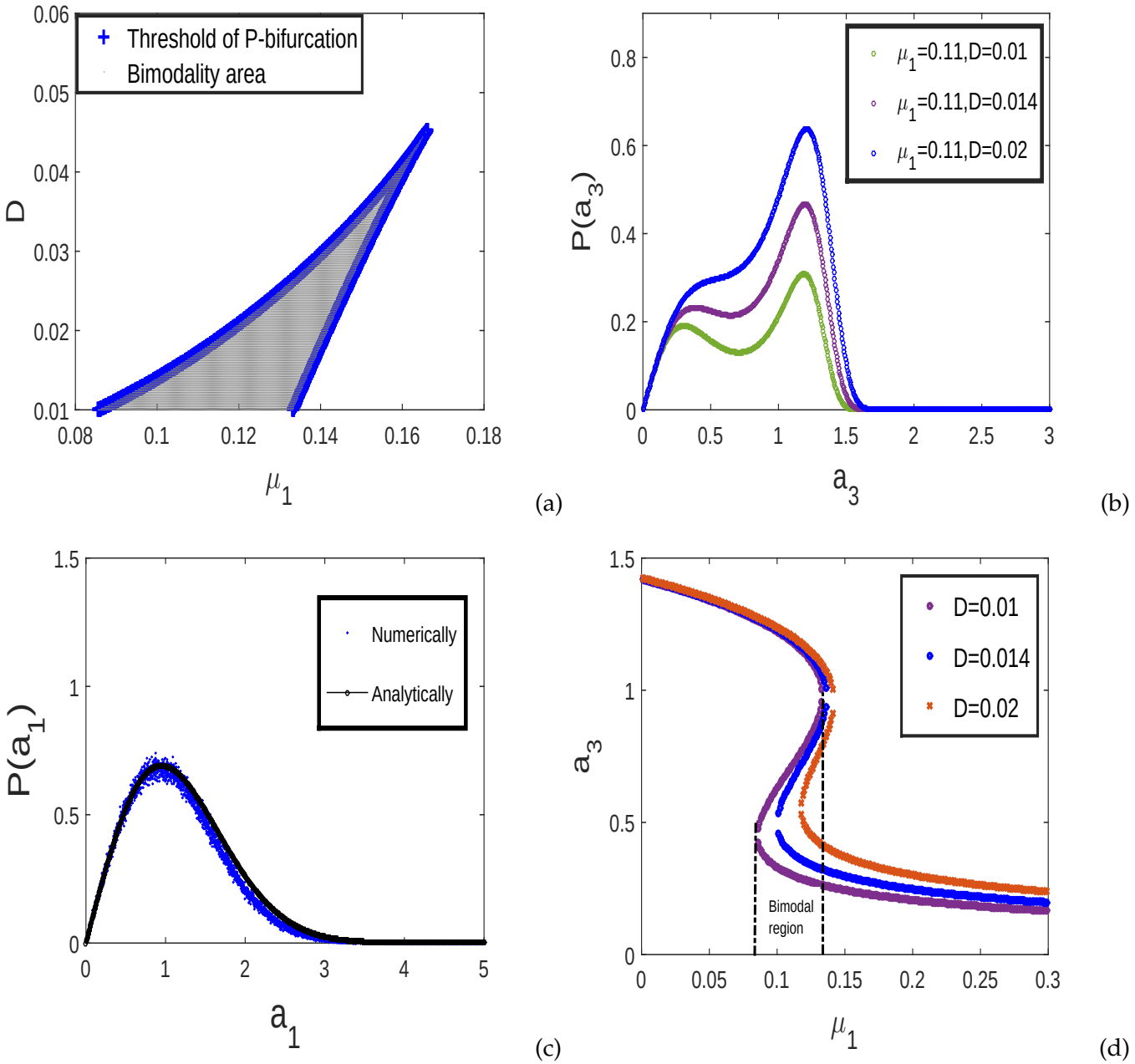

Figure 18: (a)Bifurcation diagram, (b) Stationary probability density of electrical subsystem for different values of noise intensity, (c) Stationary probability density of the mechanical subsystem (eq.(s13)), (d) Amplitude of voltage of the magnetic (Eq.(62)) and piezoelectric (Eq.(62))circuit for different values of noise intensity D for $\mu_a = 0.11$,$\alpha_2 = 0.06$, $\beta_2 = 0.1$, $\mu_{33} = 1$, $\beta_{22} = -0.01$, $\mu_1 = 0.11$,$\mu_2 = -1$,$\mu_3 = 1$,$\chi = 0.003$,$\sigma = 0.05$, $\omega_0 = 1$,$\beta_{11} = 0.00003$.

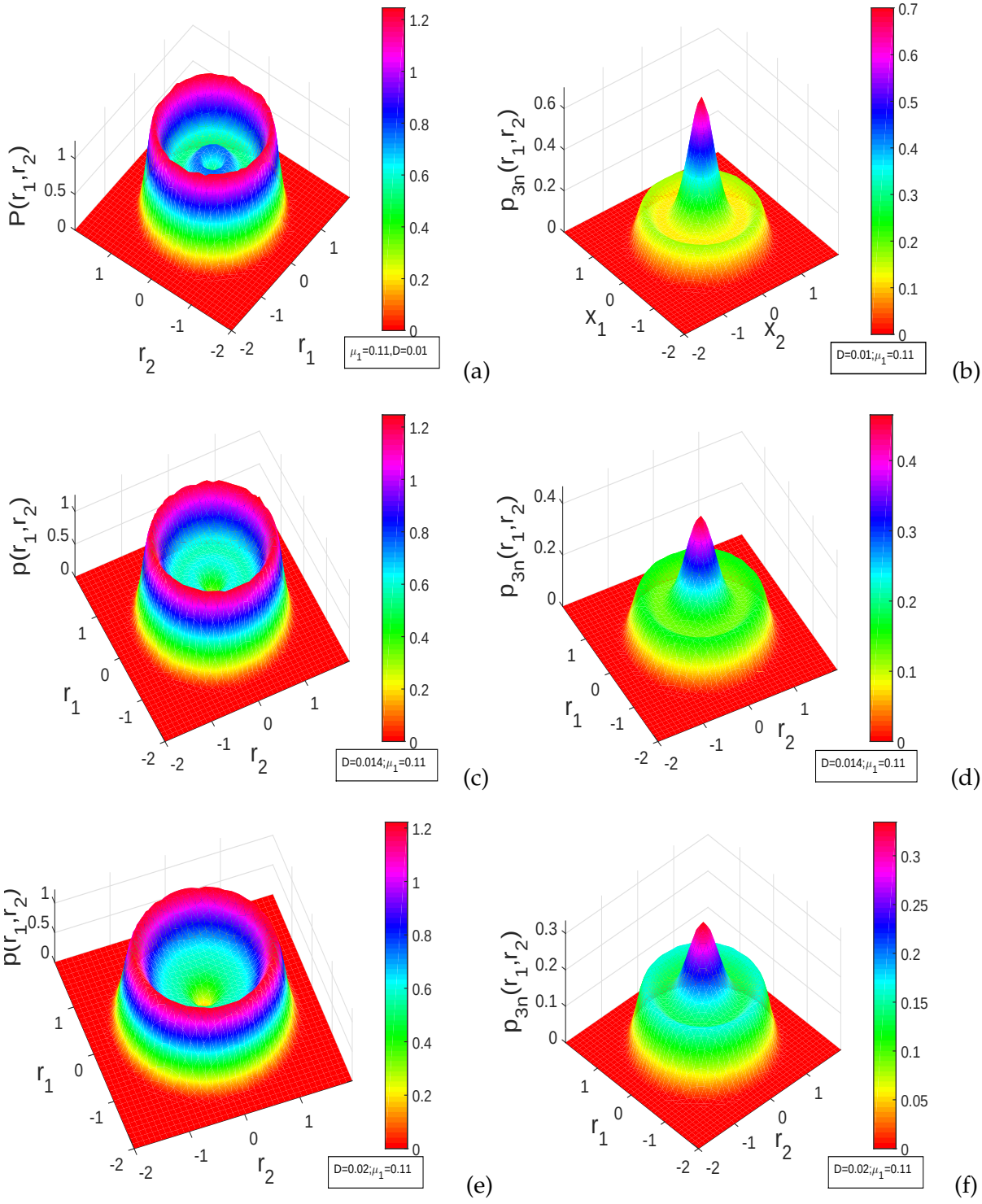

Figure 19: 3-D representation of the stationary probability density of Eq.(53) for different values of noise intensity for $\mu_a = 0.11$,$\alpha_2 = 0.06$, $\beta_2 = 0.9$, $\mu_{33} = 1$, $\beta_{22} = -0.01$, $\mu_1 = 0.11$,$\mu_2 = -1$,$\mu_3 = 1$,$\chi = 0.003$,$\sigma = 0.05$, $\omega_0 = 1$,$\beta_{11} = 0.00003$,$\tau_1 = 0.01$.

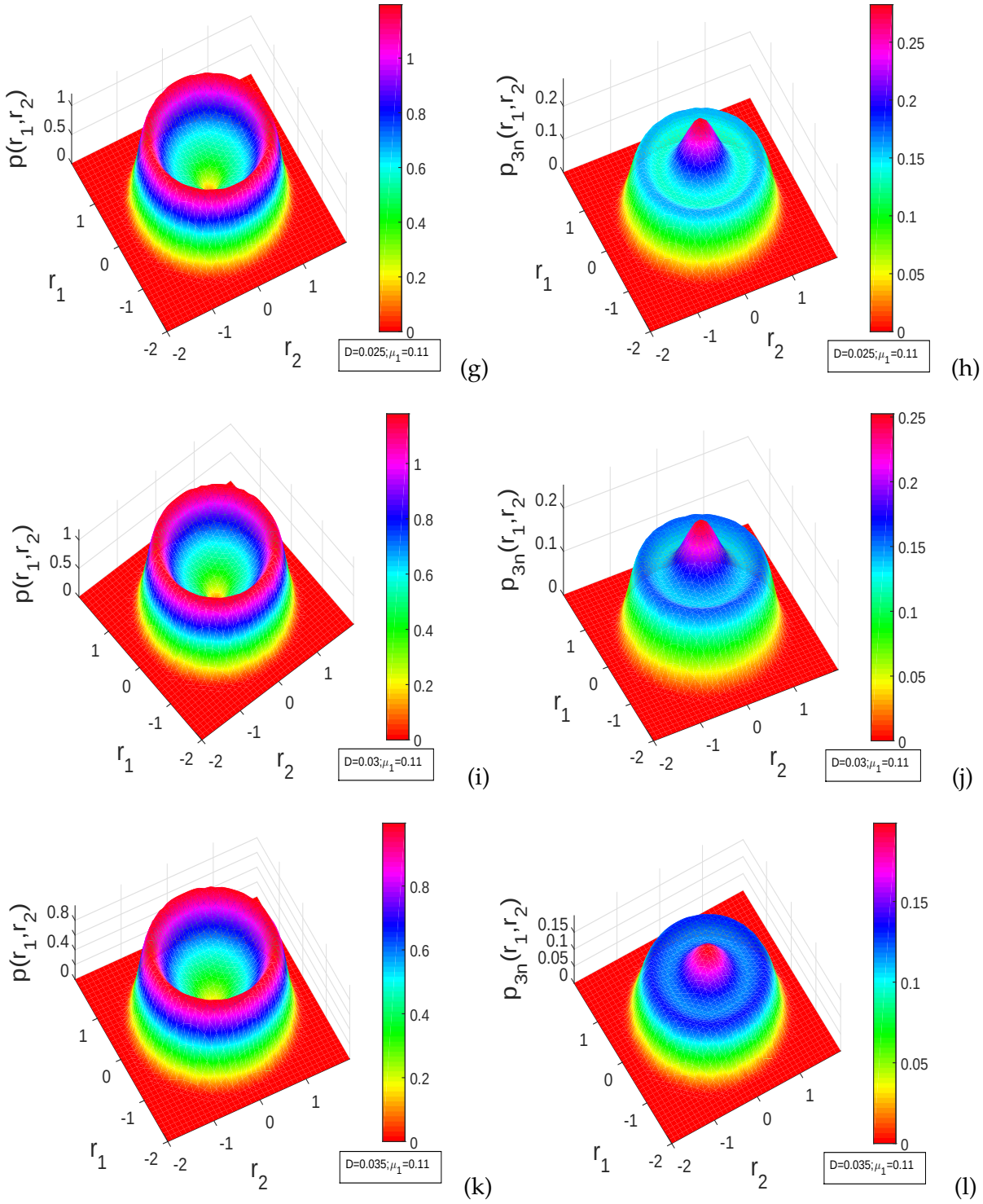

Figure 20: 3-D representation of the stationary probability density of Eq.(53) for different values of noise intensity for $\mu_a = 0.11$,$\alpha_2 = 0.06$, $\beta_2 = 0.9$, $\mu_{33} = 1$, $\beta_{22} = -0.01$, $\mu_1 = 0.11$,$\mu_2 = -1$,$\mu_3 = 1$,$\chi = 0.003$,$\sigma = 0.05$, $\omega_0 = 1$,$\beta_{11} = 0.00003$,$\tau_1 = 0.01$.

ance of the first limit circle and a high probability of the appearance of the second limit circle. The distribution is unimodal.

III.3.3 Mean residence time and ghost-stochastic resonance

Fig.21(a) and (c) show the mean amplitude response $X_m(\omega_i)$ versus the intensity of the colored noise D and the amplitude of the coherence force f_0 for $\omega_i = \Omega = \omega_0$. We observe in fig.21 that, while the fundamental frequency (ω_0) is absent in the frequency's spectrum of the harmonic excitation force $\omega_i = \Omega$, it exists one value of the noise intensity D for which the system response is optimum. The appearance of the maximum in fig.21 (a) at $D = Dmax = 0.31$ and its corresponding amplitude of mechanical subsystem $X_m = 2.713$ in absence of ω_0 within the frequency's spectrum of harmonic excitation corresponds to the ghost stochastic resonance. This can be corroborate by plotting in fig.21(b), the mean residence time (TMR). The same phenomenon is observed when f_0 vary (see fig.21(c)). Let us notice that, when the ghost-stochastic resonance occurs, the output power of the harvester is maximal (see fig.22(b)-(f)).

We provided in fig.21(e), the amplitude response $X_m(\omega_i)$ for $\Omega = \omega_0$, $\Omega = \omega_1 = 2\omega_0$, $\Omega = \omega_2 = 3\omega_0$ versus noise intensity D. A typical noise-induced resonance is realized with theses frequencies. $\Omega = \omega_1$ and $\Omega = \omega_2$ are present in the input signal. The resonance observed with these frequencies is the usual stochastic resonance which is largely study in this research field [163]. The resonance associated with the missing frequency $\Omega = \omega_0$ is ghost-stochastic resonance. Fig.21(f) shows the $3D$-representation of the mean amplitude response $X_m(\omega_i)$ versus noise intensity D and m. We note in this figure that, when m and D increase, the variation of the maximum amplitude of $X_m(\Omega)$ is not perceptible.

We plotted in fig.22(a)-(b), the mean amplitude voltage $y_m(\Omega)$ and the mean square voltage $y_m(\Omega)^2$ of the piezoelectric circuit when f_0 varies with $\Omega = \omega_0$, $\Omega = \omega_1 = 2\omega_0$, $\Omega = \omega_2 = 3\omega_0$. We observe in these figures that, for a given value of $\Omega = \omega_i$, it exists one value of f_0 for which the mean amplitude voltage $y_m(\Omega)$ and the mean square voltage $y_m(\Omega)^2$ rapidly increase. Fig.22(c) shows the 3D-representation of the mean square current $r_m(\Omega)^2$ versus D and m. It emerges from this result that, regardless of the value of m, the resonance, characterized by a peak is observed.

We also provided in fig.22(d)-(f), the mean square current of the magnetic circuit versus D for divers values of the coefficient of linear μ_1 and nonlinear (μ_2, μ_3) resistance. Fig.22(d) shows the impact of linear resistance on the amount of energy collected by the system. It emerges from

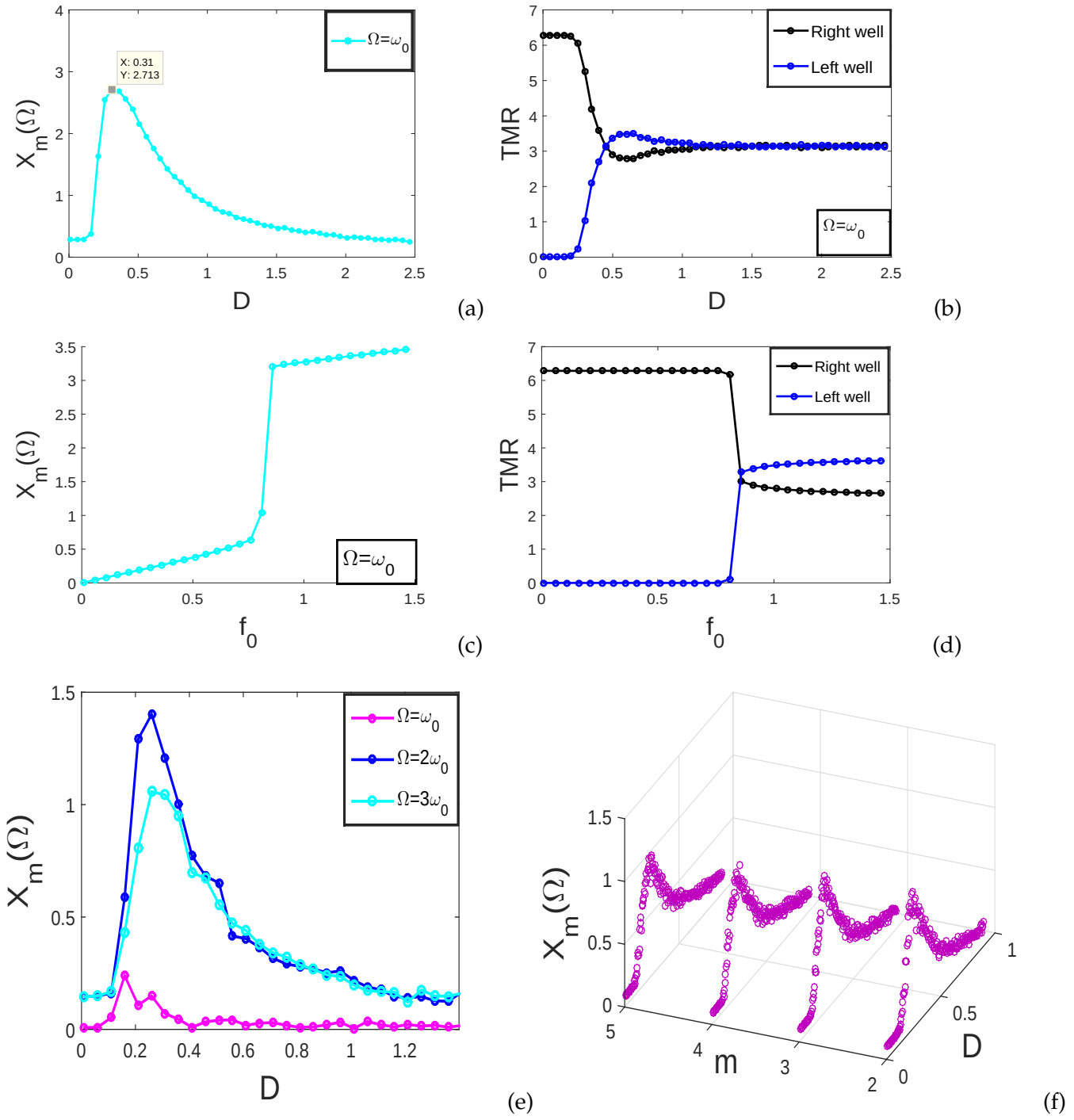

Figure 21: (a)-(d) Mean amplitude response $X_m(\omega)$ and Mean residence time versus noise intensity D for $f_0 = 0.38$, (e)-(f) Mean amplitude response $X_m(\omega)$ and Mean residence time versus noise intensity f_0, (a) Mean amplitude response $X_m(\omega_i)$ versus noise intensity D for different value of $\Omega = \omega_i$, (b) $3D$-representation of Mean amplitude response $X_m(\omega_i)$ versus m and noise intensity D for $D = 0.01$, The other system parameters are given as follow: for $\mu_a = 0.11$,$\alpha_2 = 0.06$, $\beta_2 = 1$, $\mu_{33} = 1$, $\beta_{22} = -0.001$, $\mu_1 = 0.11$,$\mu_2 = -1$,$\mu_3 = 1$,$\chi = 0.003$,$\sigma = 0.05$, $\omega_0 = 1$,$\beta_{11} = 0.003$,$\tau_1 = 0.01, m = 2$.

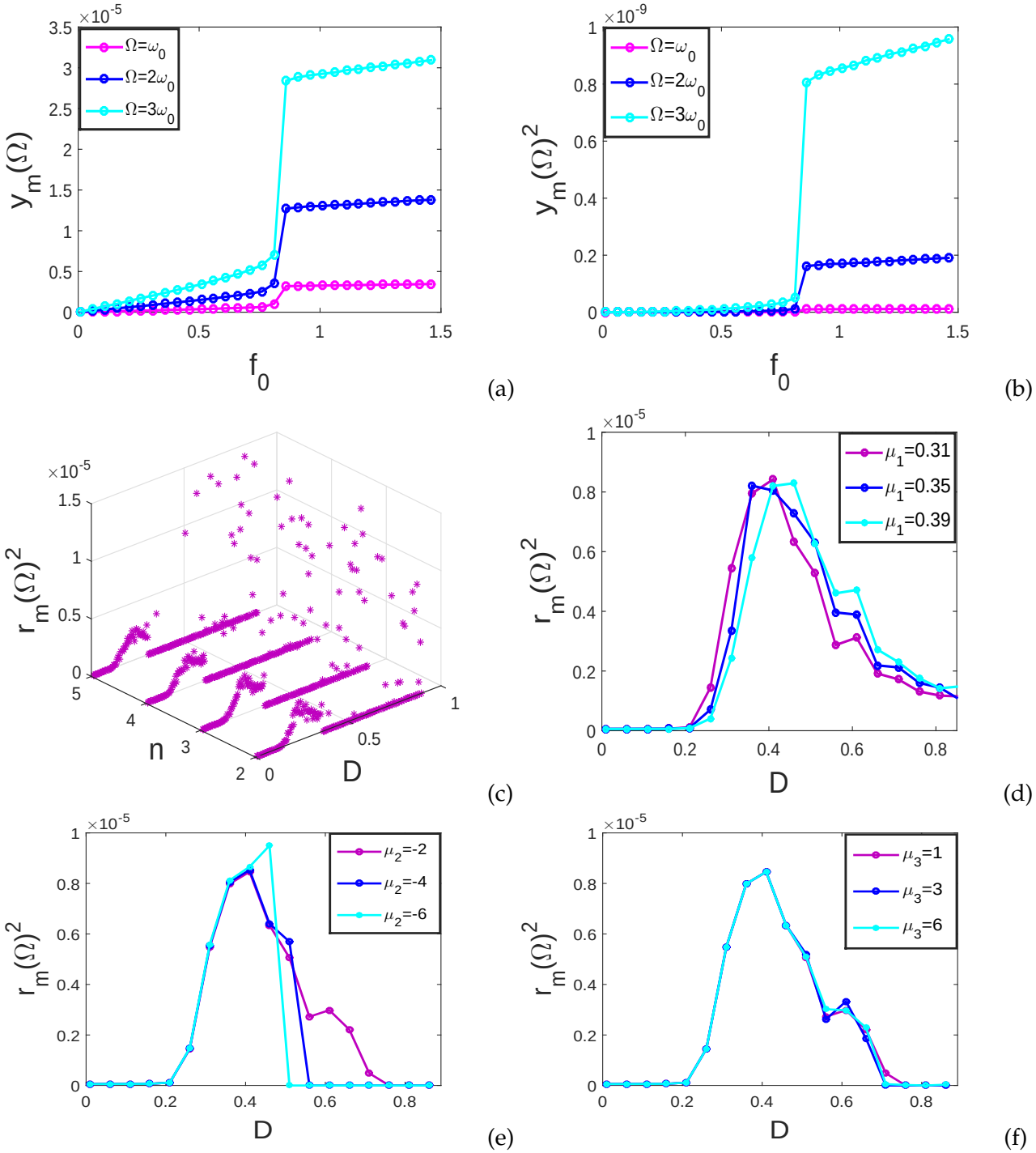

Figure 22: (a)-(b) Mean amplitude response $y_m(\Omega)$ and mean square voltage $y_m(\Omega)^2$ of the piezoelectric circuit for diverse values of Ω with $D = 0.01$, $\mu_1 = 0.31$, (c)-(d) 3D-representation of mean square current $y_m(\Omega)^2$ of the magnetic circuit versus D and m, and mean square current $y_m(\Omega)^2$ of the magnetic circuit versus D for $\Omega = 2\omega_0$, $\mu_2 = 1$ $\mu_3 = -1$, (e)-(f) Mean square current $y_m(\Omega)^2$ of the magnetic circuit versus D for diverse value of μ_2 for $\mu_1 = 0.31$,$\mu_3 = -1$, mean square current $y_m(\Omega)^2$ of the magnetic circuit versus D for diverse values of μ_3 for $\Omega = 2\omega_0$,$\mu_1 = 0.31$, $\mu_2 = 1$ with $\mu_a = 0.11$,$\alpha_2 = 0.06$, $\beta_2 = 0.1$, $\mu_{33} = 1$, $\beta_{22} = -0.01$, $\chi = 0.003$,$\sigma = 0.05$, $\omega_0 = 1$,$\beta_{11} = 0.00003$,$\tau_1 = 0.01$.

this result that, when the coefficient of the dimensionless resistance μ_1 increases, the peak of the output power of the magnetic circuit which is proportional to the peak of the mean square current increases by shifting towards the large value of noise intensity D. However, in fig.22(c)-(d), when the value of the dimensionless nonlinear coefficient of resistance enhances (μ_2 and μ_3), the change on the amount of the harvested energy is not perceptible.

Fig.23 shown the evolution of mean amplitude response of the mechanical subsystem $X_m(\Omega)$, the mean amplitude response $Y_m(\Omega)$ of the piezoelectric circuit and the output power generated by the device versus noise intensity D for diverse values of the relaxation time τ with $\Omega = 2\omega_0$ and $\Omega = 3\omega_0$. We observed in fig.23(a) that, when the noise parameter D increases, the exists a one value of $D = D_max$ for which the amplitude response reaches its maximum. The appearing of this maximum corresponds to the stochastic resonance phenomenon, characterized by the largest amplitude oscillation for a given excitation level, and reflects the transition in the system response from single potential well to double well oscillations characteristics with hopping between the two potential wells. This phenomenon contributes to the improvement of system performance. We can also noted in this figure (fig.23(a)) that, an increasing of the relaxation time τ leads to the enhancement of the maximum of amplitude response $X_m(\Omega)$ of the mechanical subsystem by shifting its maximum value towards the high value of noise intensity D. Fig.23(b)-(c) showed the evolution of amplitude response of the piezoelectric circuit $Y_m(\Omega)$ and the output power generated by the device. It emerges from the results obtained that, when the noise intensity D increases, the amplitude response $Y_m(\Omega)$ of the piezoelectric circuit and the output power increase, reaches a maximum and decreases while and increasing of the correlation time leads to the enhancing of the peak of output power by shifting this peak toward the high value of the parameter of noise D. The same phenomenon is observed in the fig.23(d)-(f) when $\Omega = 2\omega_0$.

In the purpose to corroborate the stochastic resonance observed in previous figures (fig.23), we plotted in fig.24, the amplitude of displacement of mechanical subsystem, the voltage of the piezoelectric subsystem and the magnetic current of the magnetic circuit versus the time. We notice in this figure (fig.24) that, the amplitude of displacement of mechanical subsystem, the amplitude of the voltage of piezoelectric circuit and magnetic current of the magnetic circuit is higher when the stochastic resonance phenomenon occurs. Thus, when the stochastic resonance occurs, the piezoelectric output power and the magnetic output power will be maximized, and

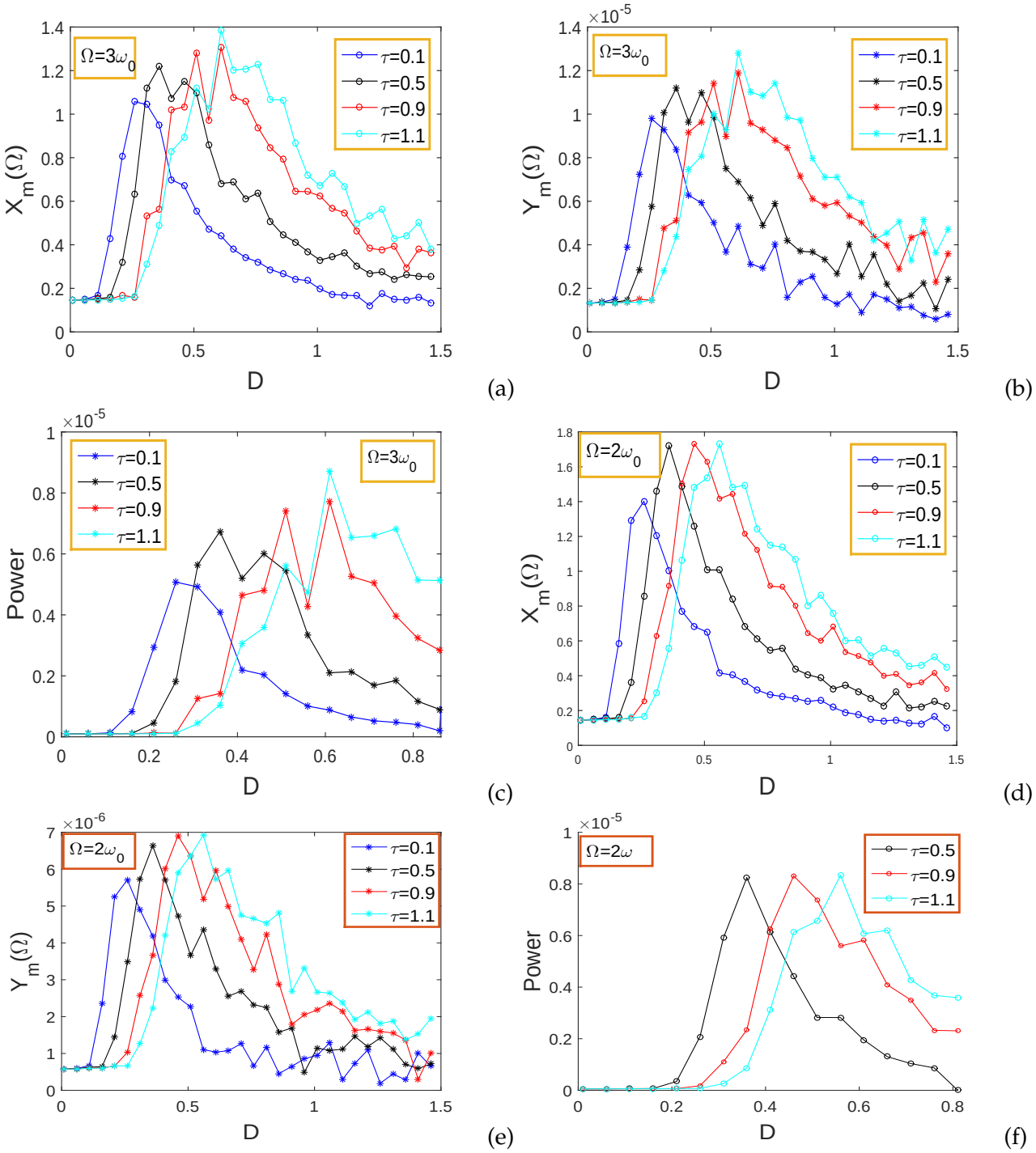

Figure 23: (a)-(c) Mean amplitude response $X_m(\Omega)$ of the mechanical subsystem; mean amplitude response $Y_m(\Omega)$ of the piezoelectric circuit subsystem and output power of the hybrid model versus noise intensity D for diverse values of the correlation time τ with $\Omega = 3\omega_0$, (d)-(f) Mean amplitude response $X_m(\Omega)$ of the mechanical subsystem; mean amplitude response $Y_m(\Omega)$ of the piezoelectric circuit subsystem and output power of the hybrid model versus noise intensity D for diverse values of the correlation time τ with $\Omega = 3\omega_0$ for $\mu_1 = 0.031$, $\mu_2 = 1$ with $\mu_a = 0.11$,$\alpha_2 = 0.06$, $\beta_2 = 0.1$, $\mu_{33} = 1$, $\beta_{22} = -0.01$, $\chi = 0.003$,$\sigma = 0.05$, $\omega_0 = 1$,$\beta_{11} = 0.00003$,$\tau_1 = 0.01$.

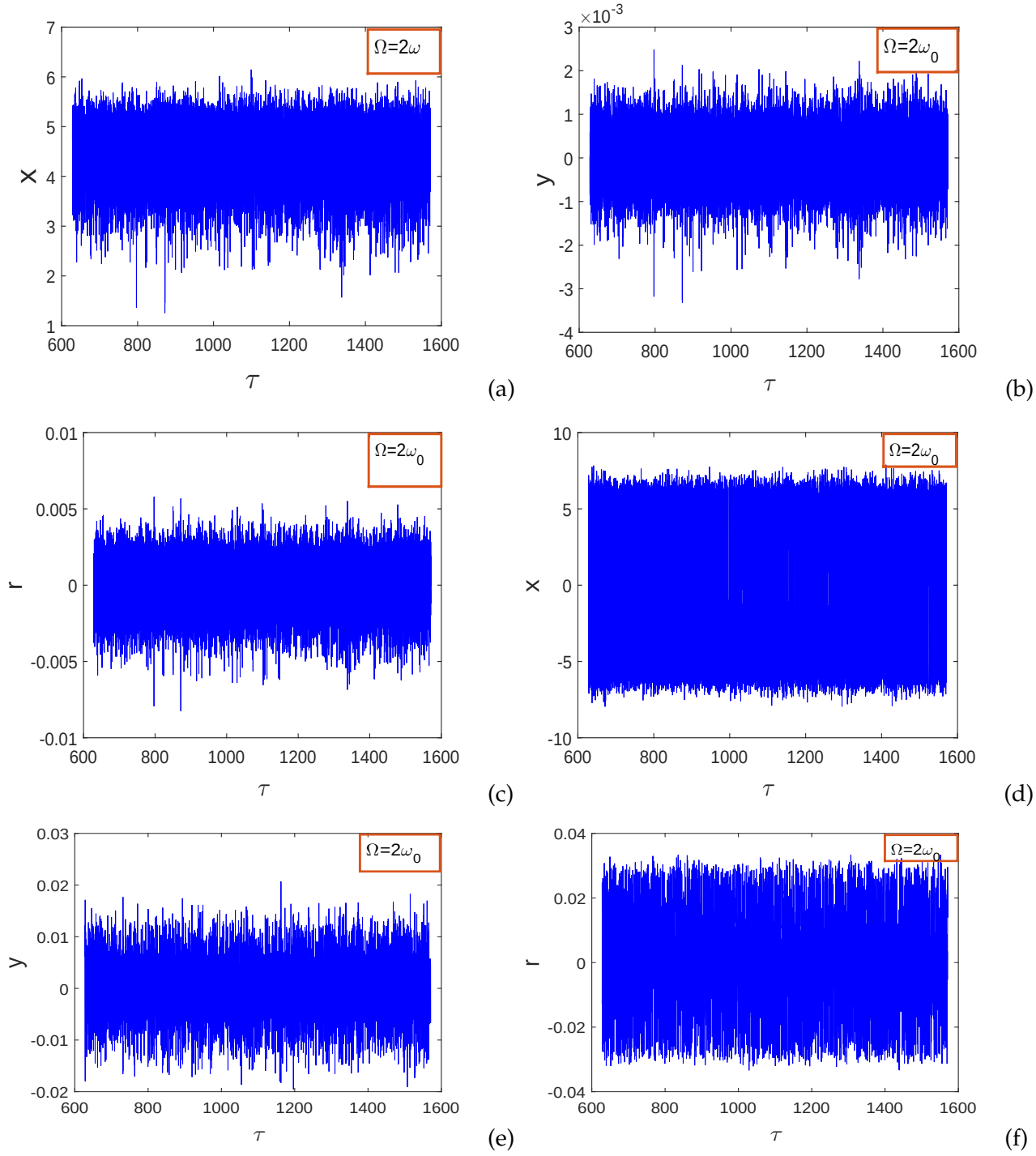

Figure 24: (a)-(c): Time series of displacement of the mechanical subsystem x, the voltage of the piezoelectric and current of the magnetic circuit for $\Omega = 2\omega_0$ and $D = 0.1$ before the stochastic resonance phenomenon. (d)-(f): Time series of displacement of the mechanical subsystem x, the voltage of the piezoelectric and current of the magnetic circuit for $\Omega = 2\omega_0$ and $D = 0.28$ after appearing of the stochastic resonance phenomenon, for the correlation time $\tau = 0.1$ with $\Omega = 2\omega_0$ for $\mu_1 = 0.031$, $\mu_2 = 1$ with $\mu_a = 0.11$,$\alpha_2 = 0.06$, $\beta_2 = 0.1$, $\mu_{33} = 1$, $\beta_{22} = -0.01$, $\chi = 0.003$,$\sigma = 0.05$, $\omega_0 = 1$,$\beta_{11} = 0.00003$,$\tau_1 = 0.01$.

consequently, improves the amount of energy harvested by the device.

We also plotted in fig.25, the amplitude of displacement x of mechanical subsystem, the voltage of the piezoelectric subsystem y and the magnetic current r of the magnetic circuit versus the time for $\Omega = 3\omega_0$. We also notice in this figure (fig.25) that, the amplitude response of mechanical and electrical subsystem are improved when the stochastic resonance occurs.

III.4 Discussion

In a broad sense and as we show in this work, kinetic energy harvesters can convert any mechanical motion (like fluid flows, pressure variations and ambient vibrations) into electrical energy to power systems located in its environs [175]. In this purpose, it is necessary to take account of the presence of nonlinearity, both desired and undesired. Nonlinearities appear through nonlinearity in the spring force [176] and others component's nonlinearities. A number of recent contributions seek to use nonlinearity in a novel way to improve the harvesters performances (see [177, 178, 179]), thus justifying the consideration of nonlinearity in this work.

This work shows that for our device, the maximum power of the hybrid model is greater than that of the piezoelectric and electromagnetic models independently. As pointed in [180], hybridization of two conversion mechanisms in a single system improved the functionality of the harvester in the low frequency range (such as vehicle motion, human motion, and wave heave motion, which usually occur at low frequencies ($< 20Hz$) [181, 182, 183]). It is seen that the results are qualitatively in rather good agreement with those from [184], that noticed that the total synergistically extracted power from the hybrid harvester is more than the power obtained from each independently. Many authors [185, 186, 187] have pointed that, hybridization could be deliberately exploited within a mechanical system for optimized energy harvesting. Experimental results from [184] confirms that the extracted power at various loading conditions for available ambient excitations is greater.

In this thesis, the harmonic excitation is combined with Gaussian white noise. As we mentioned in the preceding sections, the type of energy harvester system under study, could be subjected to noise, coming from many sources (such as physical structure-generated noise [188], environmental and transportation noise [189, 190, 191] and pneumatic noise [192, 193, 194].

The results obtained in this work, shows an improvement of the system performance when the noise intensity is around $D \approx 0.3$ (See fig. 14(c), (d)) for a frequency of vibration

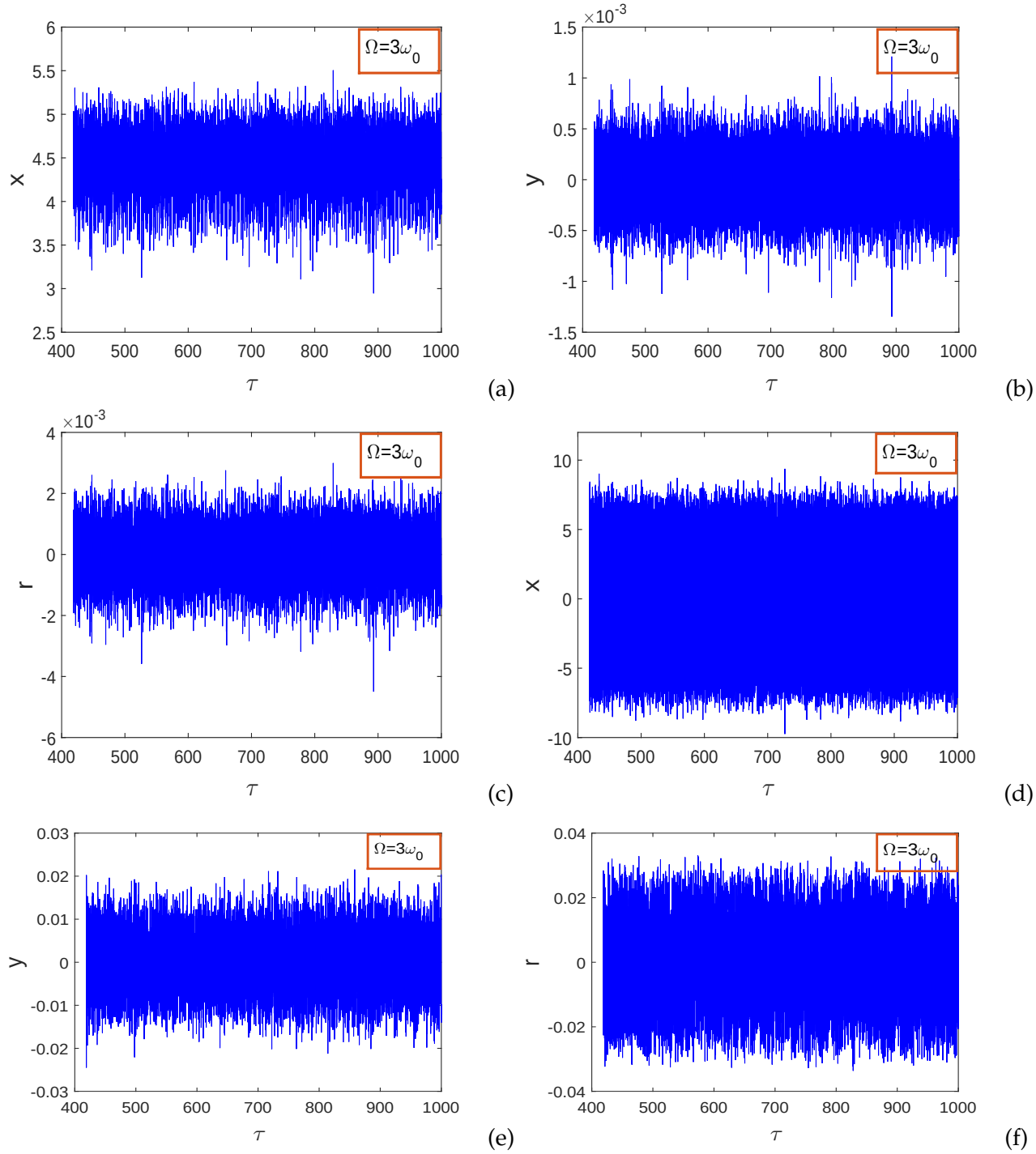

Figure 25: (a)-(c): Time series of displacement of the mechanical subsystem x, the voltage of the piezoelectric and current of the magnetic circuit for $\Omega = 3\omega_0$ and $D = 0.05$ before the stochastic resonance phenomenon. (d)-(f): Time series of displacement of the mechanical subsystem x, the voltage of the piezoelectric and current of the magnetic circuit for $\Omega = 3\omega_0$ and $D = 0.4$ after appearing of the stochastic resonance phenomenon, for the correlation time $\tau = 0.1$ with $\Omega = 2\omega_0$ for $\mu_1 = 0.031$, $\mu_2 = 1$ with $\mu_a = 0.11$,$\alpha_2 = 0.06$, $\beta_2 = 0.1$, $\mu_{33} = 1$, $\beta_{22} = -0.01$, $\chi = 0.003$,$\sigma = 0.05$, $\omega_0 = 1$,$\beta_{11} = 0.00003$,$\tau_1 = 0.01$.

absent in the frequency bandwidth of the harmonic force. It is known in the literature that, when the nonlinear system is subjected to the combination of the harmonic excitation and the random force, many phenomena can be observed such as the stochastic resonance and the ghost-stochastic resonance. These two phenomena are characterized by the large amplitude of vibration [195, 196, 197]. Zheng at al. [198, 199] in their work, have indicated that the available power generated under stochastic resonance is noticeably higher than the power that can be collected under other harvesting conditions. As in this study this resonance occurs and the maximum amplitude of the system is reached for a frequency of vibration absent in the frequency bandwidth of the harmonic force, this phenomenon is called a ghost-stochastic resonance [200, 201, 202, 203].

III.5 Conclusion

In this chapter, we investigates the stochastic $p-bifurcation$ and $Ghost-Stochastic$ resonance phenomenon in the energy harvesting systems. Firstly, we present the results of probabilistic analysis and Ghost-Stochastic resonance phenomenon of a hybrid energy harvester under Gaussian White noise. Here, we plotted the probability density function which allows to estimate the high limits cycle characterizing a maximum energy. The mean square voltage and current are investigated for diverse values of electrical impedance. It emerges from these results that, and increasing of the electrical impedance leads to the decreasing of the amount of energy harvested by the system. We also study in this part of the thesis, the ghost-stochastic resonance phenomenon. It emerges from these results that, when it occurs, the performance is improved. In the second part of the thesis, we present the results of resistance induced P-bifurcation and Ghost-Stochastic resonance of a hybrid energy harvester under colored noise. The stochastic p-bifurcation is studied following stability analysis and the study of ghost-stochastic resonance phenomenon. The agreement between the analytical and numerical results validated the efficiency of the analytical method proposed. The results obtained in this chapter reveal that, while the natural frequency is absent in the coherent excitation, the system performance can be improved for certain value of the noise intensity

General Conclusion

Main results

In this thesis, we proposed two physical models aiming to harvest the vibrations energy in order to energize directly the microelectronic devices or stocked for future utilization. These two proposed systems are subjected to the harmonic and random excitation (Gaussian white noise and colored noise).

•First of all, the probabilistic analysis and $Ghost - Stochastic$ resonance of a hybrid energy harvester under Gaussian White noise is studied. Using the stochastic averaging method, we constructed the $Fokker - Plank - Kolmogorov$ equation whose the solution in the stationary state is the probability density. From this statistic response, we assessed the output power of the piezoelectric and electromagnetic circuit under the form of mean square voltage and current. The impact of electrical impedance of piezoelectric and electromagnetic subsystem is presented with detail. It emerges from these results that, the output power of the two electrical circuit enhance when the coupling parameters increase while a enhancing of the electrical impedances lead to the reduction of the output power. In addition, combining the coherence force with Gaussian white noise, the $ghost - stochastic$ resonance phenomenon is observed characterized by the large amplitude of vibration allowing thus to harvest more energy while fundamental frequency be absent in the harmonic signal. The agreement between the analytical and numerical results validated the efficiency of the analytical method proposed. The results obtained in this model reveal that, while the natural frequency is absent in the coherent excitation, the system performance can be improved for certain value of the noise intensity.

•Besides, a resistance induced $P - bifurcation$ and $Ghost - Stochastic$ resonance of a hybrid energy harvester under colored noise is also investigated. In this part of the thesis, we also investigate the $ghost - stochastic$ resonance resulting of the combination of colored noise and harmonic force. The appearing of this phenomenon improves the amount of energy harvested by the hybrid model. Using the numerical simulations, the Mean Residence Time (TMR) is pro-

vided in the goal to measure the $ghost - stochastic$ phenomenon. In addition, the stochastic $P - bifurcation$ induced by the resistor is also investigated. By using the stochastic averaging method, the $Fokker - Planck - Kolmogorov(FPK)$ equations of the mechanical and the two electrical circuits are constructed. We discuss the stability of the harvester by plotting the probability density function. The system is more stable if the peak of the probability density is large and less stable in the contrary case. We also discuss the effective potential of the electromagnetic subsystem and it interaction with noise intensity D, in order to predict the activation energy necessary for switching between two probable stationary states or limit cycle that was recorded as greatly increasing the efficacy of electromagnetic transduction. We also studied the mode of the stationary probability density function. It emerges from this result that the electrical subsystem undergoes qualitative changes called stochastic $P - bifurcation$. The impact of linear and nonlinear resistance is studied in this thesis showing the important of the nonlinear resistor in this research field.

Perspectives

Like future work based in this thesis, we have:

• Make an experimental investigation in order to completely validate the results obtained through the analytical and numerical simulation.

•Study the impact of memory effect in the system performance.

List of Publications

1- **G. J. Fezeu**, I.S. Mokem Fokou, C. Nono Dueyou Buckjohn, M. Siewe Siewe and C. Tchawoua. *Probabilistic analysis and ghost-stochastic resonance of a hybrid energy harvester under Gaussian White noise*. Meccanica (2020), https://doi.org/10.1007/s11012-020-01204-3.

2- **G. J. Fezeu**, I.S. Mokem Fokou, C. Nono Dueyou Buckjohn, M. Siewe Siewe and C. Tchawoua. *Resistance induced P-bifurcation and Ghost-Stochastic resonance of a hybrid energy harvester under colored noise*. Physica A (2020),
doi: https://doi.org/10.1016/j.physa.2020.124857.

Bibliography

[1] Mitcheson P. D. ,Miao P., Stark B. H., Yeatman E. M., Holmes A. S., Green T. C., MEMS electrostatic micropower generator for low frequency operation, Sensors and Actuators A, 115:523-529 (2014)

[2] Sari I., Balkan T., Kulah H., An electromagnetic micro power generator for wideband environmental vibrations, Sensors and Actuators, 145:405-413 (2008)

[3] Nono D. B. C., Siewe S. M., Mokem F. I. S., Tchawoua C. , Investigating bifurcations and chaos in magnetopiezoelastic vibrating energy harvesters using Melnikov theory, Physica Scripta, 88:015006 (2013)

[4] Ko W. H., Piezoelectric energy converter for electronic implants, US Patent 3456134, july 15, 1969 WEN 0 3,456,134

[5] Schroeppel E. A., Pacing lead with piezoelectric power generating means, US Patent 4690143, July 19, 1984, 632,457

[6] Goto H., Sugiura T., Harada Y., et al, Feasibility of using the automatic generating system for quartz watches as a leadless pacemaker power source, Medical and Biological Engineering and Computing, 37: 377-380 (1999)

[7] Hansen A., van L. S., Stevels A., Design of a fuel cell powered radio, a feasibility study in alternative power sources for portable products, Proceedings of the 2000 IEEE International Symposium on Electronics and the Environment (Cat. No.00CH37082)

[8] Iskos D., Lurie K., Sakaguchi S., Benditt, Termination of implantable pacemeker ther- apy: Experience in five patients. Ann. Intern. Med., 126:787-790 (1997)

[9] Starner T., Human-powered wearable computing, IBM Systems Journal 35:3-4 (1996)

[10] Williams, C.B. and Yates, R.B., Analysis of a Micro-electric Generator for Microsystems, Sensors and Actuators A, 52:811 (1996)

[11] Beeby S. P., Tudor M. J., W. N. M., Energy harvesting vibration sources for microsystems applications Meas. Sci. Technol., 17:175-195 (2006)

[12] Cedrik A. K., Litak G., Nataraj C., Nonlinear analysis of energy harvesting systems with fractional order physical properties Nonlinear Dyn., 80:491-501 (2015)

[13] And B., Baglio S., Trigona C., Dumas N., Latorre L., Nouet P., Nonlinear mechanism in MEMS devices for energy harvesting applications, Journal of Micromechanics and Microengineering, 20:1-12 (2010)

[14] Barton, D. A. W., Burrow, S. G., Clare, L. R., Energy harvesting from vibrations with a nonlinear oscillator. Journal of Vibration and Acoustics 132:021009 (2010)

[15] Erturk A., Hoffmann J., Inman, D. J., A piezomagnetoelastic structure for broadband vibration energy harvesting, Applied Physics Letters 94:3 (2009)

[16] Stanton S. C., McGehee C. C., Mann B. P., Nonlinear dynamics for broadband energy harvesting: Investigation of a bistable piezoelectric inertial generator. Physica D: Nonlinear Phenomena, 239:640-653 (2010)

[17] Zhu D., Tudor M. J., Beeby S. P., Strategies for increasing the operating frequency range of vibration energy harvesters: A review. Measurement Science and Technology, 21:022001 (2010)

[18] Yong X., Rencai G., Huiqing Z., Wei X., and Jinqiao D., Stochastic bifurcations in a bistable DuffingVan der Pol oscillator with colored noise,PHYSICAL REVIEW E, 83:056215 (2011)

[19] Jin X., Wang Y., Xu M., Huang Z., Semi-analytical solution of random response for nonlinear vibration energy harvesters. J Sound Vib., 340:26782 (2015)

[20] Zhao S., Erturk A., Deterministic and band-limited stochastic energy harvesting from uniaxial excitation of a multilayer piezoelectric stack Sens. Actuators A, 214:5865 (2014)

[21] Di L., Yong X., Junlin L., Probabilistic response analysis of nonlinear vibration energy harvesting system driven by Gaussian colored noise, Chaos Solitons and Fractals, 104:806-812 (2017)

[22] Berthet R., Petrosyan A., Roman B., Am. J. Phys., 70:744 (2002)

[23] Rowland D.R., Am. J. Phys., 72:758 (2004)

[24] Chialvo D.R., Calvo O., Gonzalez D.L., Piro O., Savino G.V., Phys. Rev. E, 65:050902 (2002)

[25] Chialvo D.R., Chaos, 13:1226 (2003)

[26] Buldu J.M., Chialvo D.R., Mirasso C.R., Torrent M.C., Garcia-Ojalvo J., Europhys. Lett., 64:178 (2003)

[27] Buldu J.M., Gonzalez C.M., Trull J., Torrent M.C., Garcia-Ojalvo J., Chaos, 15:013103 (2005)

[28] Van der Sande G., Verschaffelt G., Danckaert J., Mirrasso C.R., Phys. Rev. E, 72:016113 (2005)

[29] Juan C. A. W., Ambient Intelligence: Basic Concepts and Applications,Conference: ICSOFT 2006, First International Conference on Software and Data Technologies, Setbal, Portugal, September 11-14, (2006)

[30] Starner T.E., Powerful change part 1: batteries and possible alternatives for the mobile market, IEEE Pervasive Computing, 62:941-950(2002)

[31] Lal A. and Blanchard J., Daintiest dynamos [nuclear microbatteries], IEEE Spectrum, 41:36-41 (2004)

[32] Infinite Power Solutions: THINERGY micro-energy cell (MEC) product overview, DS1015 v1.2 11 July 2012, www.InfinitePowerSolutions.com

[33] Ekkaphol K., Yan Z., Ekachai L., Kittipong N., A dual-band rectifier for RF energy harvesting systems, 2014 11th International Conference on Electrical Engineering/Electronics, Computer, Telecommunications and Information Technology (ECTI-CON)

[34] Pavone D., Buonanno A., D'Urso M., and Della C. F., Design Considerations for Radio Frequency Energy Harvesting Devices, Progress In Electromagnetics Research B, 45:19-35 (2012)

[35] Simon H.K.W., Radio-Frequency Rectifier for Electromagnetic Energy Harvesting: Development Path and Future Outlook, November 2014, Proceedings of the IEEE 102(11):1667-1691

[36] Mahima A., Maryam S. B., Girish K., RF energy harvesting system from cell towers in 900MHz band, Published 2011 Materials Science, National Conference on Communications (NCC)

[37] Diego M., Alessandra C., Massimo D. P., Vittorio R., Genetic-based design of a tetra-band high-efficiency radio-frequency energy harvesting system, IET Microwaves, Antennas and Propagation, IET Microwaves Antennas and Propagation 7:1254-1263 (2013)

[38] Danilo D. D., Luca C., Luciano T., An UHF RFID Energy-Harvesting System Enhanced by a DC-DC Charge Pump in Silicon-on-Insulator Technology, Microwave and Wireless Components Letters, 23:315 - 317 (2013)

[39] Yildiz F., Potential Ambient Energy-Harvesting Sources and Techniques, Journal of technology studies, 35:40-48 (2009)

[40] Yildiz, Faruk, and Coogler K. L, Low Power Energy Harvesting with a Thermoelectric Generator through an Air Conditioning Condenser, 2014 121st ASEE Annual Conference and Exposition, Indianapolis, IN, Paper ID.10552

[41] Shancymol S., Kulkarni R.K, A Comprehensive Review of Energy Harvesting Techniques and its Potential Applications, International Journal of Computer Applications, 139:14-19 (2016)

[42] Chen M., Lu S. S. and Liao B., On the figure of merit of thermoelectric generators Trans. ASME J. Energy Resources Technol., 127 37-41 (2005)

[43] Saba A., Energy Harvesting for Wireless Sensor Networks Review, Published in: 2014 Federated Conference on Computer Science and Information Systems

[44] Shancymol S., Kulkarni R.K, A Comprehensive Review of Energy Harvesting Techniques and its Potential Applications, International Journal of Computer Applications, 139:14-19 (2016)

[45] Hunaidi, Osama, Traffic vibrations in buildings. Institute for Research in Construction, National Research Council of Canada. Institute for Research in Construction (2000)

[46] Jones C. J. C., and Block J. R., Prediction of ground vibration from freight trains. Journal of sound and vibration, 193:205-213 (1996)

[47] Sheng X., Jones C. J. C., and Thompson D. J., A comparison of a theoretical model for quasi-statically and dynamically induced environmental vibration from trains with measurements, Journal of Sound and Vibration, 267:621-635 (2003)

[48] Francesco B., Jonathan B. F., and Julien V., Blood flow mechanics in cardiovascular development, Cell Mol Life Sci. , 72:2545-2559 (2015)

[49] Johnson B.M., Garrity D.M., Dasi L.P., The transitional cardiac pumping mechanics in the embryonic heart, Cardiovasc Eng Tech., 4:246-255 (2013)

[50] Goetz J.G., Steed E., Ferreira R.R., Roth S., Ramspacher C., Boselli F., Charvin G, Liebling M, Wyart C, Schwab Y, Vermot J., Endothelial cilia mediate low flow sensing during zebrafish vascular development, Cell Rep., 6:799-808 (2014)

[51] Petter D., John-Peder E. K., Andreas S., Jan E., Ann F. B., Tino E., Assessment of fluctuating velocities in disturbed cardiovascular blood flow: in vivo feasibility of generalized phase-contrast MRI, J Magn Reson Imaging., 28:655-63 (2008)

[52] Van O. P., Potters W.V., Collins J., Carr M., Carr J., Malaisrie S.C., Fedak P.W., McCarthy P.M., Markl M., Barker A.J., Characterization of Abnormal Wall Shear Stress Using 4D Flow MRI in Human Bicuspid Aortopathy, Annals of biomedical engineering, 43:1385-1397 (2014)

[53] https://kidshealth.org/en/kids/heart-murmurs.html

[54] Breckenridge R.A., Anderson R.H., Elliott P.M., Isolated left ventricular non-compaction: the case for abnormal myocardial development, Cardiol Young. 17:124-129 (2007)

[55] Weiford B.C., Subbarao V.D., Mulhern K.M., Noncompaction of the ventricular myocardium, Circulation, 109:2965-2971 (2004)

[56] https://www.heartfoundation.org.nz/your-heart/heart-conditions/atrial-fibrillation

[57] Glynne-Jones P., Tudor, M.J., Beeby, S.P. and White, N.M., An Electromagnetic, Vibration-powered Generator for Intelligent Sensor Systems, Sensors and Actuators A, 110:344-349 (2004)

[58] Mitcheson, P., Miao, P., Start, B., Yeatman, E., Holmes, A. and Green, T., MEMS Electrostatic Micro-Power Generator for Low Frequency Operation, Sensors and Actuators A, 115:523-529 (2004)

[59] Roundy, S., Wright, P.K. and Rabaey, J.M., A Study of Low Level Vibrations as a Power Source for Wireless Sonsor Nodes, Computer Communications, 26:1131-1144 (2003)

[60] Khan, Farid U.I., State of the art in acoustic energy harvesting". Journal of Micromechanics and Microengineering. 25:023001 (2015)

[61] Glynne-Jones P., Tudor, M.J., Beeby, S.P. and White, N.M., An Electromagnetic, Vibration-powered Generator for Intelligent Sensor Systems, Sensors and Actuators A, 110:344-349 (2004)

[62] Mitcheson P., Miao P., Start B., Yeatman E., Holmes A. and Green T., MEMS Electrostatic Micro-Power Generator for Low Frequency Operation, Sensors and Actuators A, 115:523-529 (2004)

[63] Beeby S. P., Tudor M. J., and W. N. M., Energy harvesting vibration sources for microsystems applications, Meas. Sci. Technol., vol., 17:175-195 (2006)

[64] R. Amirtharajah and A. P. Chandrakasan, Self-powered signal processing using vibration-based power generation, IEEE J. Solid-State Circuits, 33:687-695 (1998)

[65] Beeby S. P., Tudor M. J., Torah R. N., Roberts S., Donnell T. O, Roy S., Microsyst. Technol, 13:1647 (2007)

[66] Mann B.P., Owens B.A., Investigations of a nonlinear energy harvester with a bistable potential well, Journal of Sound and Vibration, 329:1215-1226 (2010)

[67] Kulah H., Najafi K., IEEE Sens. J., 8:261 (2008)

[68] Zhu D., Roberts S., Tudor M. J., Beeby S. P., Sens. Actuators, A, 158:284 (2010)

[69] Avila A. G. B., Linares L. E.G., Appl. Math. Model. , 36:4728 (2012)

[70] Marin A., Bressers S., Priya S., J. Phys. D: Appl. Phys., 44:295501 (2011)

[71] Marin A., Turner J., Ha D. S., Priya S., Smart Mater. Struct. , 22:075008 (2013)

[72] H. Liu, Y. Qian, C. Lee, Sens. Actuators, A , 204:37 (2013)

[73] Oumbé Tékam G. T., Tchawou T. E. B., Kitio K. C. A., Woafo P., Analysis of an electromechanical energy harvester system with geometric and ferroresonant nonlinearities, Nonlinear Dyn., 76:15611568 (2014)

[74] Lin D., Andrew B. C., Congran J., Ian T., Zi C., and John X. J. Zhang, Vibration-Energy-Harvesting System: Transduction Mechanisms, Frequency Tuning Techniques, and Biomechanical Applications, Advanced Materials Technologies, 4:1900177 (2019)

[75] Meninger S., Mur-Miranda J. O., Amirtharajah R., Chandrakasan A., and Lang J., Vibration-to-Electric Energy Conversion. Very Large Scale Integration Systems, IEEE Transactions on, 9:64-76 (2001)

[76] Amirtharajah R., Meninger S., Mur-Miranda J. O., Chandrakasan A. P. A., and Lang J. H., BA micropower programmable DSP powered using a MEMS-based vibration-to-electric energy converter,2000 in Proc. IEEE Int. Conf. Solid State Circuits

[77] S. Roundy, K. S. J. Pister, and P. K.Wright: Micro-electrostatic vibration to electricity converters, 2002 in Proc. IMECE2002, ASME International Mechanical Engineering Congress and Exposition (ASME)

[78] Roundy S., Wright P. K., Pister K. S. J., ASME International Mechanical Engineering Congress and Exposition, 2002 IMECE2002, (ASME)

[79] Sterken T., Baert K., Puers R., Borghs G., and Mertens R., A new power MEMS component with variable capacitance, in Proc. Pan Pacific Microelectron. Symp., 4:2734 (2003)

[80] Blokhina E., Galayko D., Basset P., and Feely O., Steady-state oscillations in resonant electrostatic vibration energy harvesters, IEEE Trans. Circuits Syst., 4:14 (2012)

[81] Ma W., Zhu R., Rufer L., Zohar Y., and Wong M., An integrated floatingelectrode electric microgenerator, J. Microelectromech. Syst., 16:2937 (2007)

[82] Hoffmann D., Folkmer B., and Manoli Y., Fabrication, characterization and modelling of electrostatic micro-generators, J. Micromech. Microeng., 19:094001 (2009)

[83] Nye J.F., Physical Properties of Crystals: Their Representation by Tensors and Matrices. Oxford: Clarendon Press, (1985)

[84] Voigt,Woldemar, Lehrbuch der K., Berlin: B. G. Teubner, (1910)

[85] Liu, H., Zhong J.L., Chengkuo L., Seung-Wuk L. L., A comprehensive review on piezoelectric energy harvesting technology: Materials, mechanisms, and applications, Applied Physics Reviews, 5:041306 (2018)

[86] Jiashi Y. An introduction to the theory of piezoelectricity, Springer, (2005)

[87] Lee Y. R. Shin, Jae H.P., Il Song R., Kyehan C., Sang Kug, Energy harvesting based on acoustically oscillating liquid droplets, 2014 Sensors and Actuators A: Physical. Special Issue of the Micromechanics Section of Sensors and Actuators based upon contributions revised from the Technical Digest of the 27th IEEE International Conference on MICRO ELECTRO MECHANICAL SYSTEMS (MEMS)

[88] Cui Y., Zhang Q., Yao M., Dong W., Gao S. ,Vibration piezoelectric energy harvester with multi-beam, AIP Advances, 5:041332 (2015)

[89] KoW. H., Piezoelectric energy converter for electronic implants, US Patent 3456134, Jul 15, 1969. 4, 6 (1969)

[90] Elvin N.G., Elvin A.A., Spector M.A., self-powered mechanical strain energy sensor. Smart Materials and Structures, 10:293-299 (2001)

[91] Kim H.W., Priya S., Uchino K., Newnham R.E., Piezoelectric energy harvesting under high pre-stressed cyclic Vibrations, Journal of Electroceramics, 15:27-34 (2005)

[92] Zhao S., Erturk A., Deterministic and band-limited stochastic energy harvesting from uniaxial excitation of a multilayer piezoelectric stack,Sens. Actuators A, 214:58-65 (2014)

[93] Borowiec M., Litak G., Lenci S., Noise effected energy harvesting in a beam with stopper,International Journal of Structural Stability and Dynamics in press(08) (2014)

[94] Shrabani, Joydip D., Bidhan C. B., Fabio M., Autonomous stochastic resonance driven by colored noise, Phys. Rev. E, 98:012120 (2018)

[95] Tao Y., Qingjie C., Dynamics and energy generation of a hybrid energy harvester under colored noise excitations, Mechanical Systems and Signal Processing, 121:745-766 (2019)

[96] Vinicius L., Joo P., Americo C. J., The nonlinear dynamics of a bistable energy harvesting system with colored noise disturbances, 2019 Conference of Computational Interdisciplinary Science, Atlanta, United States (hal-02010224)

[97] Yanxia Z., Yanfei J., Pengfei X., Dynamics of a coupled nonlinear energy harvester under colored noise and periodic excitations, International Journal of Mechanical Sciences, 172:105418 (2020)

[98] Madinei H. , Haddad K. H., Adhikari S. , Friswell M. I., A hybrid piezoelectric and electrostatic vibration energy, harvester. In: Brandt A, Singhal R, editors. Shock, Vibration, Aircraft/Aerospace, Energy Harvesting Acoustics Optics, 9:18995 (2016)

[99] Fokou I. S. M., Buckjohn C. N. D., Siewe M. S., Tchawoua C., Probabilistic distribution and stochastic P-bifurcation of a hybrid energy harvester under colored noise Commun. Nonlinear Sci. Numer. Simulat., 56:177-197 (2018)

[100] Foupouapouognigni O., Nono Dueyou Buckjohn C., Siewe Siewe M., Tchawoua C., Hybrid Electromagnetic and Piezoelectric Vibration Energy Harvester with Gaussian white noise excitation, Physica A: Statistical Mechanics and its Applications, Elsevier, vol. 509:346-360 (2018)

[101] Zhenlong X., Xiaobiao S., Danpeng C., Tao X., A novel tunable multi-frequency hybrid vibration energy harvester using piezoelectric and electromag- netic conversion mechanisms, 6:10 (2016)

[102] Lee B., Wei L., Hybrid energy harvester based on piezoelectric and electromagnetic mechanisms. J. Micro/Nanolith. MEMS MOEMS, 9:023002 (2010)

[103] Wang C., Yanlong C., Jin X., Piezoelectric and electromagnetic hybrid energy harvester for powering wireless sensor nodes in smart grid. J. Mech. Sci.Technol., 29:4313 (2015)

[104] Madinei H., Haddad K.H., Adhikari S., Friswell M.I., A hybrid piezoelectric and electrostatic vibration energy, harvester. In: Brandt A, Singhal R, editors. Shock, Vibration, Aircraft/Aerospace, Energy Harvesting Acoustics Optics, 9:189-95 (2016)

[105] Elvin N., Erturk A., Advances in Energy Harvesting Methods, Springer, New York (2013)

[106] Daqaq M.F., Masana R., Erturk A., Quinn D.D., On the Role of Nonlinearities in Vibratory Energy Harvesting: A Critical Review and Discussion, Applied Mechanics Reviews 66:040801 (2014)

[107] Shenck N. S., Paradiso J. A., IEEE Micro, 21:30 (2001)

[108] Paradiso J. A., Starner T., IEEE Pervas. Comput., 4:18 (2005)

[109] Rome L. C., Flynn L., Goldman E. M., Yoo T. D., Biophysics: Generating electricity while walking with loads, Science, 309:1725-1728 (2005)

[110] Huang X., Wang L., Wang H., Zhang B., Wang X., Stening R. Y. Z., Sheng X., and Yin L., Materials Strategies and Device Architectures of Emerging Power Supply Devices for Implantable Bioelectronics, Small, 16:e1902827 (2019)

[111] Secord T.W., Audi M.C., A Tunable Resonance Cantilever for Cardiac Energy Harvesting. Cardiovasc Eng. Tech., 10:380-393 (2019)

[112] Aditya N. and Amin Karami M., Energy harvesting from arterial blood pressure for powering embedded micro sensors in human brain, Journal of Applied Physics 121:124506 (2017)

[113] Martin D., Elie L., Yanan Z., Marion W., Bertrand B., Renzo Dal M., Micro Blood Pressure Energy Harvester for Intracardiac Pacemaker, Journal of Microelectromechanical Systems, 23:651-660 (2014)

[114] Deterre M., Lefeuvre E. and Dufour-Gergam E., An active piezoelectric energy extraction method for pressure energy harvesting, Smart Mater. Struct., 21:085004 (2012)

[115] Romero E., Warrington R. O. and Neuman M., Physiol. Meas., 30:35-62 (2009)

[116] Goto H., Sugiera T., Harada Y. and Kazui T., Med. Biol. Eng. Comput. 37:377-80 (1999)

[117] Tashiro R., Kabei N., Katayama K., Tsuboi E. and Tsuchiya K., J. Artif. Organs, 5:0239 (2002)

[118] Canan D. et al., Conformal piezoelectric energy harvesting and storage from motions of the heart, lung, and diaphragm, in Proceedings of the National Academy of Sciences, 111:1927-1932 (2014)

[119] Lefeuvre E. et al., Energy Harvesting Devices as Long Lasting Power Sources for the Next Generation Pacemakers, 2013 In Proceeding of the IEEE 2013 International conference on Microelectronics (ICM)

[120] Martin D., toward an energy harvester for leadless pacemakers. These de Doctorat Soutenue le 9 Juillet (2013)

[121] Lefeuvre E., Badel A., Richard C., Petit L., Guyomar D., A comparison between several vibration-powered piezoelectric generators for standalone systems, Sensors and Actuators A 126:405-416 (2006)

[122] Pillatsch P., Yeatman E., Holmes A., Real world testing of a piezoelectric rotational energy harvester for human motion, 2013 Journal of Physics Conference Series 476(1):2010

[123] Elie L., Adrien B., Claude Richard and Daniel Guyomar, Piezoelectric Energy Harvesting Device Optimization by Synchronous Electric Charge Extraction, Journal of Intelligent Material Systems and Structures 16:865 (2005)

[124] Shashank P., Daniel J. I., Energy Harvesting Technologies, Springer Science and Business Media, New York, page 213 (2009)

[125] Nguyen D., Halvorsen E., Jensen G., Vogl, A., Fabrication and characterization of a wideband MEMS energy harvester utilizing nonlinear springs. Journal of Micromechanics and Microengineering, 20:125009 (2010)

[126] Elena Blokhina, Abdelali El Aroudi Eduard Alarcon, Dimitri Galayko, Nonlinearity in Energy Harvesting Systems Micro- and Nanoscale Applications, Springer International Publishing Switzerland, Cham, (2016)

[127] Secord T.W., Audi M.C., A Tunable Resonance Cantilever for Cardiac Energy Harvesting. Cardiovasc Eng Tech 10:380-393 (2019)

[128] Angel M. Dzhambov, Donka D. Dimitrova, Heart disease attributed to occupational noise, vibration and other co-exposure: Self-reported population-based survey among Bulgarian workers, Medycyna Pracy ,67:435-445 (2016)

[129] Ilona C., Michael G. S., Kerstin Persson Waye, Effects of train noise and vibration on human heart rate during sleep: an experimental study, BMJ Open 3:e002655 (2013)

[130] Patricia T., Mahnaz S., Sarah S., Arnaud E., Odile R., Alain M., Eur J Appl Physiol, 108:671-680 (2010)

[131] Sandra P., Elke De V., Raymond C., Nocturnal road traffic noise: A review on its assessment and consequences on sleep and health, Environment International 36:492-498 (2010)

[132] JosephGrayzel, Gallop rhythm of the heart: I. Atrial gallop, ventricular gallop and systolic sounds, The American Journal of Medicine, 28:578-592 (1960)

[133] Schmidt S.E., M.Graebe, Toft E., Struijk J.J., No evidence of nonlinear or chaotic behavior of cardiovascular murmurs, Biomedical Signal Processing and Control, 6:157-163 (2011)

[134] Thomas S.L., Makaryus A.N., Physiology, Cardiovascular Murmurs. [Updated 2019 Jun 3]. In: StatPearls [Internet]. Treasure Island (FL): StatPearls Publishing; Jan. Available from: https://www.ncbi.nlm.nih.gov/books/NBK525958

[135] James H. G., John Ross J.R., and Dean T. M., Patterns of Brachial Arterial Blood Flow in Conscious Human Subjects with and without Cardiac Dysfunction, Circulation, 34:833-848 (1966)

[136] Petter Dyverfeldt, Malenka Bissell,Alex J. Barker, Ann F. Bolger, Carl-Johan Carlhll, Tino Ebbers, Christopher J. Francios, Alex Frydrychowicz, Julia Geiger, Daniel Giese, Michael D. Hope, Philip J. Kilner, Sebastian Kozerke, Saul Myerson, Stefan Neubauer, Oliver Wieben, and Michael Markl, 4D flow cardiovascular magnetic resonance consensus statement, J Cardiovasc Magn Reson, 17:72 (2015)

[137] https://www.heartandstroke.ca/heart /conditions/ arrhythmia, consulted the 25-07-2020

[138] https://www.saintlukeskc.org/health-library/premature-ventricular-contractions, consulted the 25-07-2020

[139] Chedjou J. C., Woafo P., Damngang S., Jounal of Vibrations and Accoustics, 123:170 (2001)

[140] Yamapi R., Dynamics and sychronization of electromechanical devices with Duffing linearity,Physics [Physics]. Université de Abomey-Calavy, English (2003)

[141] Knight C., Davidson J., Behrens S., Energy options for wireless sensor nodes. Sensors, 8:8037-8066 (2008)

[142] Miki, D., Honzumi, M., Suzuki, Y., Kasagi, N., 2010 Large-amplitude mems electret generator with nonlinear spring. In Proceedings of IEEE Conference on Microelectromechanical Systems (MEMS)

[143] Roundy S. and Wright P. K., Smart Mater. Struct. 13:1131 (2004)

[144] Anton S., and Sodano H., Smart Mater. Struct. 16:1-21 (2007)

[145] Shu Y. C. and Lien I. C., Smart Mater. Struct. 15:1499 (2006)

[146] Minazara E., Vasic D., Costa F. and Poulin G., Ultrasonics 44:e699-703 (2006)

[147] Wang D. A. and Liu N. Z., Sensors Actuators A 167:449-58 (2011)

[148] Taylor, J. R., Classical mechanics. University Science Books, (2005)

[149] Senturia S. D., Microsystem design (Vol. 3). Boston: Kluwer Academic Publishers, (2001)

[150] Wei C., Leo D., Arvid N., Bernt J. L., A comparative study of the stochastic averaging method and the path integration method for nonlinear ship roll motion in random beam seas. Journal of Marine Science and Technology, 23:854-865 (2018)

[151] Cho W.S., Nonlinear random vibration analytical techniques and applications. New York: CRC Press Taylor and Francis Group, (2012)

[152] Stratonovich R.L., Topics in the theory of random noise volume I: general theory of random processes nonlinear transformations of signals and noise. New York: Gordon and Breach Science Inc. (1963)

[153] Hull A.W., The dynatron-a vacuum tube possessing negative electric resistance', Proc. Insriture of Radio Engineers, 6:5-35 (1918)

[154] Leon 0. Chua, Juebang Yu And Youying Yu, Negative resistance devices. Circuit theory and applications, 11:161-186 (1983)

[155] Spany V., 'Negative resistance of storage elements based on junction transistors', Slaboproudy Obzor., 21:403-408 (1960)

[156] Nagata M., A simple negative impedance circuit with no internal bias supplies and good linearity, ZEEE Trans. Circuit Theory, CT-12:433-434 (1965)

[157] Turner L. B., The kallirotron: an aperiodic negative resistance triode combination, Radio Rev., 1:317-329 (1920)

[158] Tonks L., Space charge as cause of negative resistance and its bearing on short wave generation, Physics Review, 30:501 (1927)

[159] Clarke G. T., Application of the dynatron, Wireless Engineer, 11:75 (1934)

[160] Esaki L., New phenomenon in narrow germanium p-n junctions, Phys. Rev., 109:603 (1958)

[161] Gunn J. B., Microwave oscillation of current in 111-V semiconductors, Solid Stare Carnm., 1:88 (1963)

[162] Kroemer H. Theory of the Gunn effect, 12:19-30 (1969)

[163] Fokou I.S.M., Buckjohn C.N.D., Siewe M.S., Tchawoua C., Probabilistic distribution and stochastic P-bifurcation of a hybrid energy harvester under colored noise Commun. Nonlinear Sci. Numer. Simulat. 56:177-197 (2018)

[164] Chedjou J. C., Woafo P., Damngang S., Jounal of Vibrations and Accoustics, 123:170 (2001)

[165] Yamapi R., Dynamics and sychronization of electromechanical devices with Duffing linearity,Physics [Physics]. Université de Abomey-Calavy, English (2003)

[166] Atkinson K.A., An Introduction to Numerical Analysis (2nd ed.). New York: John Wiley Sons. ISBN (1989)

[167] ZAHRI M., Colored-Noise-Like Multiple Itô Stochastic Integrals: Algorithms and Numerics, Journal of Numerical Mathematics and Stochastics, 7:48-69 (2015)

[168] Fox R.F., Gatland I.R., Roy R., Vemuri G.. Fast, accurate algorithm for numerical simulation of exponentially correlated noise. Phys., Rev. A 38:5938 (1988)

[169] Rajasekar S., Miguel A.F., Sanjuan Nonlinear Resonances-Springer (2016)

[170] Nicolis C., Solar variability and stochastic effects on climate, Solar Physics, 74:473478 (1981)

[171] Benzi R., Sutera A., Vulpiani A., The mechanism of stochastic resonance, J. Phys. A, 14:L453 (1981)

[172] Yang J. H., Sanjuan M. A. F. , Liu H.G. , Litak G. , Li X., Stochastic P-bifurcation and stochastic resonance in a noisy bistable fractional-order system, Commun. Nonlinear Sci. Numer. Simul., 41:10417 (2017)

[173] Mokem Fokou I. S., Nono D.B. C., Siewe Siewe M., C. Tchawoua, Nonlinear analysis and analog simulation of a piezoelectric buckled beam with fractional derivative.Eur. Phys. J. Plus, 132:344 (2017)

[174] Mokem Fokou I. S., Nono D.B. C., Siewe Siewe M., C. Tchawoua, Circuit implementation of a piezoelectric buckled beam and its response under fractional components considerations, Meccanica, 53:2029-2052 (2018)

[175] Knight C., Davidson J., & Behrens, S., Energy options for wireless sensor nodes. Sensors, 8(12), 8037-8066 (2008)

[176] Miki D., Honzumi M., Suzuki Y., & Kasagi, N., Large-amplitude mems electret generator with nonlinear spring, 2010 In Proceedings of IEEE Conference on Microelectromechanical Systems (MEMS)

[177] Yanxia Z., Yanfei J., Pengfei X., Shaomin X., Stochastic bifurcations in a nonlinear tri-stable energy harvester under coloured noise, Nonlinear Dynamics 99:879-897 (2020)

[178] Constantinou P., Roy S., A 3D printed electromagnetic nonlinear vibration energy harvester, Smart Materials and Structures, 25:095053 (2016)

[179] Junlei W., Linfeng G., Shengxi Z., Zhien Z., Zhihui L., Daniil Y., Design, modelling and experiments of broadband tristable galloping piezoelectric energy harvester, Acta Mechanica Sinica, 36:592-605(2020)

[180] Toyabur R.M., Salauddin M., Hyunok C., Jae Y. P., A multimodal hybrid energy harvester based on piezoelectric-electromagnetic mechanisms for low-frequency ambient vibrations, Energy Conversion and Management, 168:454-466 (2018)

[181] Fan K. Q., Chang J. W., Pedrycz W., Liu Z. H. and Zhu Y. M., A nonlinear piezoelectric energy harvester for various mechanical motions, Appl. Phys. Lett., 106:223902 (2015)

[182] Tang L. H., Yang Y. W. and Soh C. K., improving functionality of vibration energy harvesters using magnets, J. Intell. Mater. Syst. Struct., 23:1433-49 (2012)

[183] Fan K. Q., Chang J. W., Chao F. B., and Pedrycz W., Design and development of a multi-purpose piezoelectric energy harvester Energ. Convers. Manage., 96:430-39 (2015)

[184] Salar C., Hasan U., Ali M., Berkay C., Haluk K., Power-Efficient Hybrid Energy Harvesting System for Harnessing Ambient Vibrations, IEEE Transactions on Circuits and Systems I: Regular Papers, 66:2784-2793 (2019)

[185] Kangqi F., Qinxue T., Haiyan L., Daxing Z., Yingmin Z., Weidong W., Hybrid piezoelectric-electromagnetic energy harvester for scavenging energy from low-frequency excitations, Smart Mater. Struct., 27:085001 (2018)

[186] Mahmoudi S., Kacem N. and Bouhaddi N., Enhancement of the performance of a hybrid nonlinear vibration energy harvester based on piezoelectric and electromagnetic transductions, Smart Mater. Struct., 23:075024 (2014)

[187] Xia H., Chen R. and Ren L., Analysis of piezoelectric - electromagnetic hybrid vibration energy harvester under different electrical boundary conditions, Sens. Actuators A, 234:87-98 (2015)

[188] Aylin T., Noise Reduction Techniques for Medical Equipment Manufacturers, Advancements in Noise Reduction Techniques for Medical Equipment Manufacturers, Parker Hannifin Corporation, (2018)

[189] Angel M. Dzhambov, Donka D. Dimitrova, Heart disease attributed to occupational noise, vibration and other co-exposure: Self-reported population-based survey among Bulgarian workers, Medycyna Pracy 67:435-445 (2016)

[190] Ilona C., Michael G. S., Kerstin P. W., Effects of train noise and vibration on human heart rate during sleep: an experimental study, BMJ Open 3, 2013, e002655(1-10).; Patricia Tassi, Mahnaz Saremi, Sarah Schimchowitsch, Arnaud Eschenlauer, Odile Rohmer, Alain Muzet, Eur J Appl Physiol 108:671-680 (2010)

[191] Sandra P., Elke De V., Raymond C., Nocturnal road traffic noise: A review on its assessment and consequences on sleep and health, Environment International 36:492-498 (2010)

[192] Joseph G., Gallop rhythm of the heart: I. Atrial gallop, ventricular gallop and systolic sounds, The American Journal of Medicine, 28:578-592 (2010)

[193] Schmidt S.E., Graebe M., Toft E., Struijk J.J., No evidence of nonlinear or chaotic behaviour of cardiovascular murmurs, Biomedical Signal Processing and Control 6:157-163 (2011)

[194] Thomas SL, Makaryus AN. Physiology, Cardiovascular Murmurs. [Updated 2019 Jun 3]. In: Stat Pearls [Internet]. Treasure Island (FL): Stat Pearls Publishing; 2020 January. Available from: https://www.ncbi.nlm.nih.gov/ books/ NBK525958.

[195] Mantegna R.N., Spagnolo B., Testa L., Trapanese M., Stochastic resonance in magnetic systems described by preisach hysteresis model. J Appl Phys 97:223-87 (2005)

[196] Arathi S., Rajasekar S., Kurths J., Characteristics of stochastic resonance in asymmetric dufing oscillator, Int J Bifurcation Chaos, 21:2729 (2011)

[197] Gammaitoni L., Hanggi P., Jung P., Marchesoni F., Stochastic resonance, Rev. Mod. Phys., 70:223-87 (1998)

[198] Zheng R., Nakano K., Hu H., Su D., Cartmell M.P., An application of stochastic resonance for energy harvesting in a bistable vibrating system, J. Sound Vib. 333:2568-87 (2014)

[199] Hu H., Nakano K., Cartmell M., Zheng R., Ohori M., An experimental study of stochastic resonance in a bistable mechanical system, J Phys 382:012024 (2012)

[200] Buldu J.M., Chialvo D.R., Mirasso C.R., Torrent M.C., Garcia-Ojalvo J., Ghost Resonance in a Semiconductor Laser with Optical Feedback, Europhys. Lett., 64:178 (2003)

[201] Buldu J.M., Gonzalez C.M., Trull J., Torrent M.C., Garcia-Ojalvo J., Coupling-mediated ghost resonance in mutually injected lasers, Chaos 15:013103 (2005)

[202] Van der S. G., Verschaffelt G., Danckaert J., Mirrasso C.R., Ghost stochastic resonance in vertical-cavity surface-emitting lasers: Experiment and theory, Phys. Rev. E, 72:016113 (2005)

[203] Lopera A., Buldu J.M., Torrent M.C., Chialvo D.R., Garcia-Ojalvo J., Ghost stochastic resonance with distributed inputs in pulse-coupled electronic neurons, Phys. Rev. E, 73:021101 (2006)

Meccanica
https://doi.org/10.1007/s11012-020-01204-3

Probabilistic analysis and ghost-stochastic resonance of a hybrid energy harvester under Gaussian White noise

G. J. Fezeu · I. S. Mokem Fokou · C. Nono Dueyou Buckjohn · M. Siewe Siewe · C. Tchawoua

Received: 29 December 2019 / Accepted: 26 June 2020

Abstract In this present work, a hybrid energy scavenger using two mechanisms of transduction namely piezoelectric and electromagnetic and subjected to the Gaussian white noise is investigated. The stochastic averaging method is used here in other to construct the Fokker–Plank–Kolmogorov equation of the system whose the statistic response in the stationary state is the probability density. The mean square voltage and current are obtained for different value of white noise intensities as the output power generated by piezoelectric circuit and electromagnetic circuit. In addition, combining the Gaussian white noise and coherence excitation, the Ghost-Stochastic resonance is observed through the mean residence time and improve the amount of energy harvested by the scavenger. The agreement between the analytical method and those obtained numerically validates the effectiveness of analytical investigations. The results obtained in this manuscript reveal that, while the natural frequency is absent in the external coherent force, the amount of energy harvested by the energy scavenging device can be improved for certain value of noise intensity.

Keywords Probability · Mean residence time · Ghost-stochastic resonance

G. J. Fezeu · I. S. M. Fokou (✉) · C. N. D. Buckjohn · M. S. Siewe · C. Tchawoua
Faculty of science, Department of Physics, Laboratory of Mechanics, Materials and Structures, University of Yaounde I, PO. Box: 812, Yaoundé, Cameroon
e-mail: igormokem@yahoo.fr

I. S. M. Fokou
The African Center of Excellence in Information and Communication Technologies (CETIC), Yaoundé, Cameroon

1 Introduction

Energy harvesting, known also as energy scavenging, covers a great body of technologies and devices that transform low grade energy sources such as solar energy, environmental vibrations, thermal energy, and human motion into usable electrical energy. Thanks to the recent technology progress recorded in the electronic domain, the electrical energy consumption by the electronics components has dramatically decreased, incited the proliferation of the wireless devices. Thus, the energy harvesting technology has become a very attractive solution for a wide variety of applications such as consumer electronics, outpatient medical electronics (hearing aids, pacemakers, smart implants) or imaging (camera inside the human body).

It is know in the literature that, there are three mechanisms allow to transduce vibration energy to electricity namely electrostatic [1], electromagnetic [2] and piezoelectric [3]. Many authors namely Elvin et al.[4], Inman [5], reviewing the state of the art on the energy harvesting. Most works on energy harvesting

Published online: 16 July 2020

took the deterministic approach by considering the nonlinearity what can exhibit transduction materials and study its impact on the system performance. Mann [6] designed a nonlinear electromagnetic energy harvester that uses magnetic interactions to create a bistable potential well and validated the potential well escape phenomenon can be used to broaden the frequency response by theory and experiments. Spector et al.[7] proposed a theoretical model by using a beam element and performed experiment to harvest power from PZT material. They showed that a simple beam bending can provide the self-power source of the strain energy sensor. Kim et al.[8] reported that piezoelectric energy harvesting showed a promising results under pre-stress cyclic conditions and validated the experimental results with finite element analysis.

Let us notice that, the main objective in this research field is to enhance harvested energy by the devices. For this, build the hybrid system combining two mechanisms of transduction is essential. Bin et al. [9] built a hybrid energy harvester combined piezoelectric with electromagnetic mechanism to scavenge energy from external vibration. They studied the effect of the relative position of the coils and magnets on the PZT cantilever end and the poling direction of magnets on the output voltage of the harvested energy. Wang et al. [10] built a hybrid device for powering wireless sensor nodes in smart grid. It emerges from the results obtained that, from current-carrying conductor of 2.5 A at 50 Hz , the proposed harvester combining piezoelectric components and electromagnetic elements can generate up to 295.3 μW. Madinei et al. [11] developed a hybrid cantilever beam harvester and by using an applied DC voltage as a control parameter to change the resonant frequency of the harvester to ensure resonance as the excitation frequency varies. These hybrid models mentioned above functioning in the surrounding where the vibration source can be modeled by the coherence excitation. However, in the most situations, the vibrations are random and time-varying. Cottone et al.[12] found numerically and experimentally that the nonlinear oscillators can outperform the linear ones under stochastic excitation. Fokou et al.[13] used a probabilistic approach to analytically predict the system's response, the stability and the estimation of system's reliability. Mokem et al.[14] proposed a hybrid device combining piezoelectric and electromagnetic transduction and subjected to the colored noise. The authors shows that, the system performance can be improve for the small value of the relaxation time. Foupouapouognigni et al.[15] built the hybrid model and studied the stochastic resonance phenomenon, which is characterized by the large amplitude of vibration and increase the system performance. Let us remind that, when the nonlinear system is subjected to the combination of the harmonic excitation and the random force, many phenomena can be observed such as the stochastic resonance and the ghost-stochastic resonance. These two phenomena are characterized by the large amplitude of vibration. Indeed, the stochastic resonance occurs when the frequency of system's vibration is present in the frequency bandwidth of the harmonic excitation. However, when the maximum amplitude of the system is reached for a frequency of vibration absent in the frequency bandwidth of the harmonic force, this phenomenon is called a ghost-stochastic resonance.

While one observes in the literature, a growing interest in the theoretical investigation of the ghost-stochastic resonance phenomenon in the nonlinear systems [16–22], in our knowledge, the study of this phenomenon on the performance of the energy harvesting devices is not made. The main objective of this manuscript is to investigated the performance of the hybrid system when the ghost-stochastic resonance occurs (Fig. 1).

The rest of paper is organized as follows: In Sect. 2, we describe the system with model equation, followed by the assessment of the statistic response of the system. We draw the probability density function in

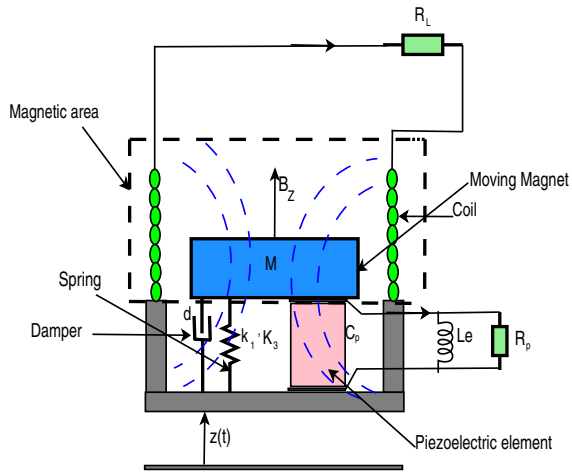

Fig. 1 Schematic of the hybrid energy harvester

order to search for the probable amplitude of the mechanical and electrical response in Sect. 3. In Sect. 4, numerical simulations are made, from which we study the ghost-stochastic resonance. We conclude the Work in Sect. 5

2 Description of the system with the model equation

The design of hybrid energy harvester combining two mechanisms of transduction of ambient energy is composed of two parts namely the mechanical and the electrical part. We used the energy scavenger build by Lefeuvre in Ref.[23] with some modifications, by changing the rigid mass by a permanent magnet rod, and by adding a coil, in oder to enhance the output power and enlarge its application field. It is worth noting that, in the schematic model, the mechanical part is composed of a nonlinear spring with the linear stiffness coefficient k_1 and nonlinear stiffness coefficient k_3 while the electrical part presents two subsystems namely the piezoelectric circuit and the electromagnetic circuit. The piezoelectric circuit is composed of the piezoelectric element and the load resistance R_p. The electromagnetic circuit has a permanent magnet of mass M, that produces a magnetic field B_z, the coil, connected to the rigid housing representing the stator is characterized by an inductance L_e. The load resistance of magnetic circuit is R_L. When the harvester is subjected to the external excitation $Z(t)$, the displacement of the magnetic mass M induces in the piezoelectric circuit, the deformation of piezoelectric element giving rise to the electrical field across the piezoelectric element. However, in the magnetic circuit, the displacement of the magnetic mass M induces a fluctuation of the magnetic flux in the surface of the coil, and consequently, a generation of electromotive force $f_m(i) = B_z i L_{coil}$ in the mechanical part, while in the magnetic circuit, we can note the Lenz electromotive voltage $f_e(\dot{z}) = -B_z L_{coil}\dot{z}$ with z, L_{coil}, and i, the displacement, the length of the coil and the current that flows in the coil respectively, B_z being the magnetic field generated by the permanent magnet. A summary of equations is provided here [23] giving a full derivation of the mechanical and piezoelectric circuit equations. Using the Kirchhoff's law in the electromagnetic circuit by letting $\mathbf{B}_z = B\mathbf{u}_z$, we obtained motion equations given by:

$$\begin{aligned} M\ddot{z} + d\dot{z} + k_1 z + k_3 z^3 + Bil_{coil} - \theta_2 v = Z(t) \\ C_p\dot{v} + \frac{v(t)}{R_p} + \theta_2\dot{z} = 0 \\ L_e\dot{i} + R_l i - Bl_{coil}\dot{z} = 0 \end{aligned} \tag{1}$$

where d is the damping coefficient, C_p, the capacity of the capacitor and θ_2 the electromechanical coupling coefficient. The physical parameters used in this manuscript are given in Table 1.

By using the time-transformation($t = \frac{\tau}{\omega}$), Eq. (1) gives rise to the following non-dimensional system:

$$\begin{aligned} x'' + \mu a\, x' + \omega_0\, x - \beta_2\, y + \sigma\, x^3 + \beta 1\, r = N(\tau)(a) \\ y' + \alpha_2 y - \beta_{22} x' = 0(b) \\ r' + \alpha_3\, r - \beta_{11}\, x' = 0(c) \end{aligned} \tag{2}$$

with $N(\tau) = \sum_{i=1}^{m} f_0 \cos(\omega_i \tau) + \xi(\tau)$ where $\sum_{i=1}^{m} f_0 \cos(\omega_i \tau)$ is a harmonic excitation, with f_0 the amplitude of coherence force, $\omega_i = (k + i - 1)\omega_0$ is the frequency of the coherence force with k a constant took here equal to 2. ω_0 is the fundamental frequency. The variable $\xi(\tau)$, is the Gaussian white noise verifying the statistics properties: $<\xi(\tau)> = 0$,

Table 1 Physical parameters of hybrid model

Parameter	Value	Unit
L_{coil}	0.03	m
M	1	mg
k_1	−100	N/m
k_3	500	N/m
d	0.1	–
θ_2	0.1	–
R_L	1	kΩ
B	0.1	T
L_e	1	mH
C_p	4	F
R_p	500	Ω

$<\xi(\tau)\xi(s)> = 2D\delta(\tau)$. The dimensionless parameters are given as follow:

$$\mu_a = -\frac{\omega\, d}{k_1}; \sigma = -\frac{l^2 k_3}{k_1}; \beta_2 = -\frac{\theta_2 v_o}{l k_1}; \beta_1 = -\frac{BL_{coil} i_o}{l k_1}$$

$$\alpha_2 = \frac{1}{\omega\, C_p R_p}; \beta_{22} = -\frac{\theta_2 l}{v_o C_p}; \beta_{11} = \frac{lBL_{coil}}{Li_o}; \alpha_3 = \frac{R_L}{\omega\, L_e};$$

$$z = lx(t\omega); v = vo\, y(t\omega); i = io\, r(t\omega);$$

$$N(\tau) = -Z\left(\frac{\tau}{\omega}\right) l^{-1} {k_1}^{-1} \tag{3}$$

3 Stochastic averaging method

In this heading, we assume that, $f_0 = 0$. We use the stochastic averaging method to provide the statistic response of the harvester. In the quasi-harmonic regime, the solution of the mechanical system (2) is of the form:

$$x(\tau) = a(\tau)(\tau)\cos(\theta); \quad x'(\tau) = -\omega a(\tau)(\tau)\sin(\theta) \tag{4}$$

where $\theta = \omega\tau + \psi(\tau)$ with ψ, the phase angle and $a(\tau)$ the amplitude. Substituting Eq. (4) into Eq. (2) (b)–(c), the solution of obtained equation can be written as follow:

$$y(\tau) = C_1 \mathrm{e}^{-\alpha 2\,\tau} + \frac{\beta_{22}\, a(\tau)\omega\,(\omega\,\cos(\theta) - \alpha_2\,\sin(\theta))}{\omega^2 + {\alpha_2}^2}$$

$$r(\tau) = C_2 \mathrm{e}^{-\alpha_3\,\tau} + \frac{a(\tau)\beta_{11}\omega\,(\omega\,\cos(\theta) - \alpha_3\sin(\theta))}{\omega^2 + {\alpha_3}^2} \tag{5}$$

In the steady state, Eqs. (5 a)–(b) can be rewritten as:

$$y(\tau) = \frac{\beta_{22}\, a(\tau)\omega\,(\omega\,\cos(\theta) - \alpha_2\,\sin(\theta))}{\omega^2 + {\alpha_2}^2}$$

$$r(\tau) = \frac{a(\tau)\beta_{11}\omega\,(\omega\,\cos(\theta) - \alpha_3\sin(\theta))}{\omega^2 + {\alpha_3}^2} \tag{6}$$

where

$$\omega\,\cos(\theta) - \alpha_2\sin(\theta) = \sqrt{\omega^2 + {\alpha_2}^2}\cos\left(\theta + \arctan\left(\frac{\alpha_2}{\omega}\right)\right)$$

$$\omega\,\cos(\theta) - \alpha_3\sin(\theta) = \sqrt{\omega^2 + {\alpha_3}^2}\cos\left(\theta + \arctan\left(\frac{\alpha_3}{\omega}\right)\right) \tag{7}$$

Thus, the amplitudes of steady-state current and charge are given by:

$$Y = \frac{\beta_{22}\, a\omega}{\sqrt{\omega^2 + {\alpha_2}^2}}; R = \frac{a\beta_{11}\,\omega}{\sqrt{\omega^2 + {\alpha_3}^2}} \tag{8}$$

Substituting Eqs. (4) and (6) into Eq. (2), and applying the determinist averaging method in the determinist part of the obtained system, we have:

$$a' = -\frac{\gamma_{22} N(\tau)\sin(\theta)}{2\omega\,\gamma_{55}} - \frac{\gamma_{11} a}{2\omega\,\gamma_{55}}$$

$$\varphi' = \frac{\gamma_{33} N(\tau)\cos(\theta)}{\gamma_{44} a} + \frac{a^2\gamma_{12}}{\gamma_{44}} + \frac{\gamma_{13}}{\gamma_{44} a} \tag{9}$$

where

$$\gamma_{11} = {\beta_1}^2\omega^3\alpha_3 - {\beta_2}^2\omega^3\alpha_2 + \mu a\,\omega^3{\alpha_3}^2 + \mu a\,\omega^5$$

$$+\mu a\,\omega\,{\alpha_2}^2{\alpha_3}^2 + \mu a\,\omega^3{\alpha_2}^2 - {\beta_2}^2\omega\,\alpha_2\,{\alpha_3}^2 + {\beta_1}^2\omega\,\alpha_3\,{\alpha_2}^2$$

$$\gamma_{22} = 2\,{\alpha_2}^2\omega^2 + 2\,{\alpha_2}^2{\alpha_3}^2 + 2\,\omega^2{\alpha_3}^2 + 2\,\omega^4$$

$$\gamma_{33} = -8\,{\alpha_2}^2{\alpha_3}^2 - 8\,\omega^4 - 8\,\omega^2{\alpha_3}^2 - 8\,{\alpha_2}^2\omega^2$$

$$\gamma_{44} = 8\,\omega^5 + 8\,\omega^3{\alpha_3}^2 + 8\,\omega^3{\alpha_2}^2 + 8\,\omega\,{\alpha_2}^2{\alpha_3}^2$$

$$\gamma_{55} = \omega^4 + \omega^2{\alpha_3}^2 + {\alpha_2}^2\omega^2 + {\alpha_2}^2{\alpha_3}^2$$

$$\gamma_{12} = 3\,\sigma\,\omega^2{\alpha_3}^2 + 3\,\sigma\,{\alpha_2}^2\omega^2 + 3\,\sigma\,\omega^4 + 3\,\sigma\,{\alpha_2}^2{\alpha_3}^2$$

$$\gamma_{13} = -4\,\omega^2{\alpha_2}^2{\alpha_3}^2 + 4\,{\beta_1}^2\omega^4 - 4\,\omega^4{\alpha_2}^2 - 4\,\omega^6 - 4\,{\beta_2}^2\omega^4$$

$$-4\,\omega^4{\alpha_3}^2 + 4\,{\beta_1}^2\omega^2{\alpha_2}^2 - 4\,{\beta_2}^2\omega^2{\alpha_3}^2$$

$$+4\,\omega_0{\alpha_2}^2{\alpha_3}^2 + 4\,\omega_0{\alpha_2}^2\omega^2 + 4\,\omega_0\omega^2{\alpha_3}^2 + 4\,\omega_0\omega^4 \tag{10}$$

Finally, applying the stochastic averaging method, in Eq. (9) , we obtain the *Ito* equation defined as:

$$da = \left(-\frac{2\gamma_{11}a}{\omega\,\gamma_{55}} + \frac{D}{2a\omega^2}\right)dt + \sqrt{\frac{D}{\omega^2}}dB_1$$
$$d\theta = \frac{(\gamma_{12}a^2 + \gamma_{13})dt}{\gamma_{44}} + \sqrt{\frac{D}{\omega^2 a^2}}dB_2 \tag{11}$$

where B_1 and B_2 are the normalized wiener process. We observe in Eq. (11) that a and θ are independent. Thus, we can provided the probability density for the amplitudes(a), rather than a joint probability density for θ. The probability density $P(a,\tau)$ of the instantaneous amplitude a satisfies the Fokker–Planck–Kolmogorov equation:

$$\frac{\partial}{\partial\tau}p(a,\tau) = -\left(-\frac{\gamma_{11}}{2\omega\,\gamma_{55}} - \frac{D}{\omega^2 2a^2}\right)p(a,\tau)$$
$$-\left(-\frac{\gamma_{11}a}{2\omega\,\gamma_{55}} + \frac{D}{2a\omega^2}\right)\frac{\partial}{\partial a}p(a,\tau) + \frac{(D)\frac{\partial^2}{\partial a^2}p(a,\tau)}{2\omega^2} \tag{12}$$

In the stationary state, the solutions of Eq. (12) is given by:

$$p(a) = Nae^{-\frac{\gamma_{11}a^2\omega}{(2D)(\omega^2+\alpha_3{}^2)(\omega^2+\alpha_2{}^2)}} \tag{13}$$

where N is the normalization constant which can be assessed numerically using Simpson's method. Through a transformation from variable (a,θ), to the original variables (x,x'), an expression for the stationary densities function of x and x' can be derived as:

$$P_n(x,x') = \frac{P(a,\theta)}{2\pi\,a} \tag{14}$$

$$p(a) = \frac{N}{2\pi}\exp\left(-\frac{\gamma_{11}\omega\left(x^2 + \frac{x'^2}{\omega^2}\right)}{2D\left(\omega^2+\alpha_3^2\right)\left(\omega^2+\alpha_2^2\right)}\right) \tag{15}$$

Thus, the expected value of the mean square electric current and charge can be calculated following this formula (Fig. 3):

$$\langle y^2(\tau)\rangle = \langle Y^2\rangle = \left(\frac{\beta_{22}\omega}{\sqrt{\omega^2+\alpha_2^2}}\right)^2 \times \langle a^2\rangle$$
$$= \left(\frac{\beta_{22}\omega}{\sqrt{\omega^2+\alpha_2^2}}\right)^2 \int_0^{+\infty} a^2 p(a)da$$
$$\langle Y^2\rangle = \frac{2\beta_{22}^2\omega D\left(\omega^4 + \omega^2\left(\alpha_3^2+\alpha_2^2\right) + \alpha_2^2\alpha_3^2\right)}{\gamma_{11}\left(\omega^2+\alpha_2^2\right)} \tag{16}$$

and

$$\langle r^2(\tau)\rangle = \langle R^2\rangle = \left(\frac{\beta_{11}\omega}{\sqrt{\omega^2+\alpha_2^2}}\right)^2 \times \langle a^2\rangle$$
$$= \left(\frac{\beta_{11}\omega}{\sqrt{\omega^2+\alpha_3^2}}\right)^2 \int_0^{+\infty} a^2 p(a)da$$
$$\langle R^2\rangle = \frac{2\beta_{11}^2\omega D\left(\omega^4 + \omega^2\left(\alpha_3^2+\alpha_2^2\right) + \alpha_2^2\alpha_3^2\right)}{\gamma_{11}\left(\omega^2+\alpha_3^2\right)} \tag{17}$$

4 Numerical simulation

4.1 Algorithm of numerical simulation

The numerical scheme used in this manuscript is based on the Euler version algorithm. By letting $\dot{x} = u$, Eq. (2) can be rewritten as follow:

$$\begin{aligned} x' &= u \\ u' &= -\mu_a u - \omega_0 x + \beta_2 y - \sigma x^3 - \beta_1 r + N(\tau) \\ y' &= -\alpha_2 y + \beta_{22} u \\ r' &= -\alpha_3 y + \beta_{11} u \end{aligned} \tag{18}$$

The discrete equations can be written as:

$$\begin{aligned} x_{i+1} &= x_i + u_i h \\ u_{i+1} &= u_i + \left[-\mu_a u_i - \omega_0 x_i + \beta_2 y_i - \sigma x_i^3 - \beta_1 r_i\right]h + \zeta_k(\tau) \\ y_{i+1} &= y_i + \left[-\alpha_2 y_i + \beta_{22} u_i\right]h \\ r_{i+1} &= r_i + \left[-\alpha_3 y_i + \beta_{11} u_i\right]h \end{aligned} \tag{19}$$

In the purpose to compare the analytical results obtained via the stochastic averaging method, the numerical simulation is made for the harvester.

Figure 4 , shows the good agreement between the numerical results and those obtained analytically. We also draw in Fig. 2, the $3D$ representation of probability density of harvester. It emerges from these results that, the probability distribution is unimodal.

4.2 Mean residence time and ghost-stochastic resonance phenomenon

In this heading, we assume that, $f_0 \neq 0$. Thus, the harvester is subjected to the combination of the coherence excitation $\sum_{i=1}^{m} f_0 \cos(\omega_i \tau)$ and the random force $\zeta_k(\tau)$. In the purpose to get a deep understanding of the observed dynamics and the influence of noise, we can assess the mean residence time and mean amplitude response.

Let us remind that equation(Eq.(2)) is nonlinear and should exhibit many frequency components. For the large value of time($\tau \to \infty$), the asymptotic solution of Eq.(2) can be given as follows:

$$< x(\tau) >_{as} = \sum_{j} x_m(j\omega_i) \cos[j\omega_i \tau - \psi_m(j\omega_i)] \tag{20}$$

where j is a non-negative constant which may be in integer or fractional form, $x_m(j\omega_i)$ and $\psi_m(j\omega_i)$ are the

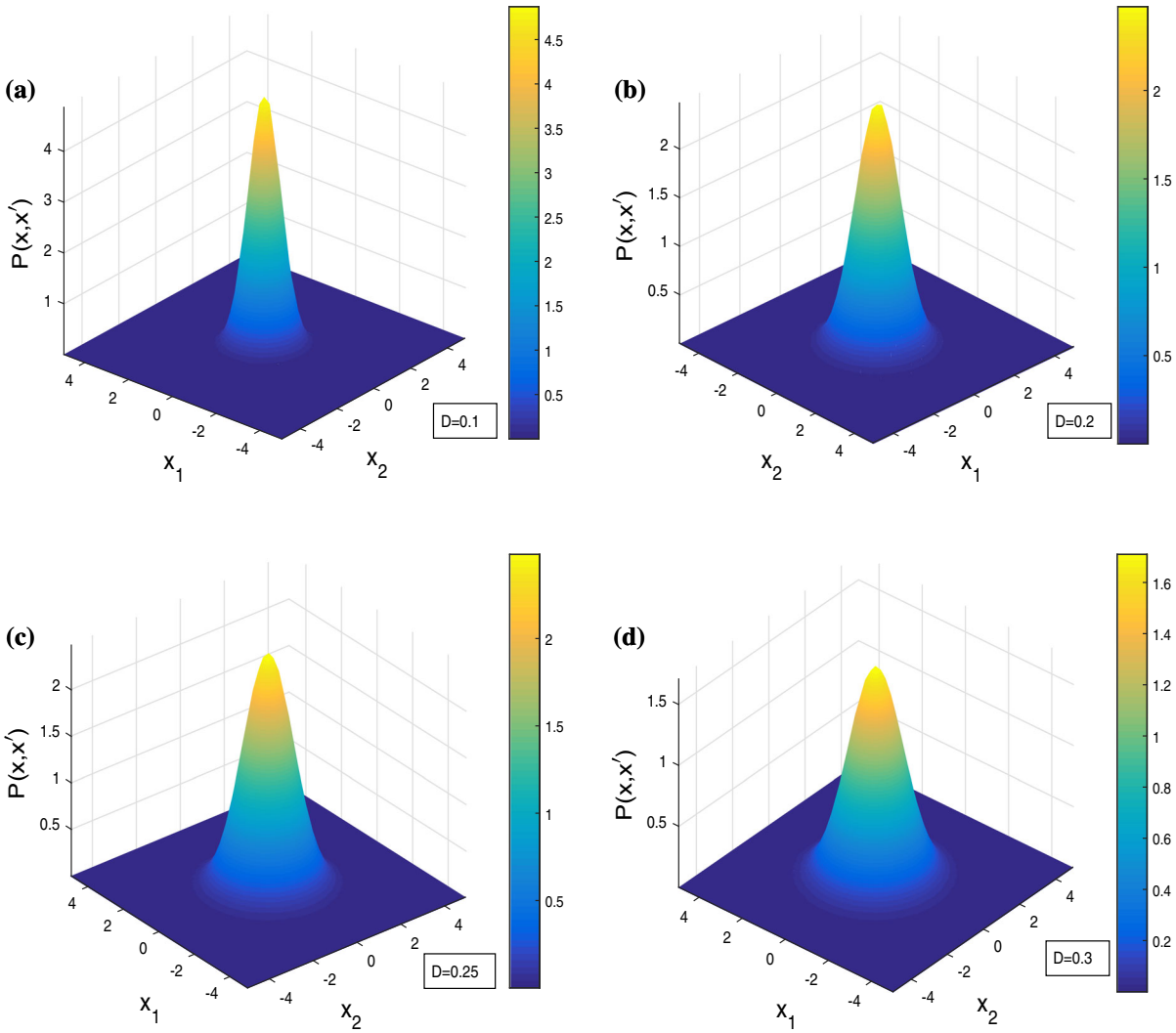

Fig. 2 Stationary probability density of the system in 3D representation for: for $\mu_a = 0.3$, $\beta_2 = 0.005$, $\beta_1 = 0.003$, $\alpha_2 = 0.000001$, $\beta_{22} = -0.005$, $\beta_{11} = 0.003$, $\alpha_3 = 0.0003$, $\sigma = 0.05$, $\omega_0 = 1$

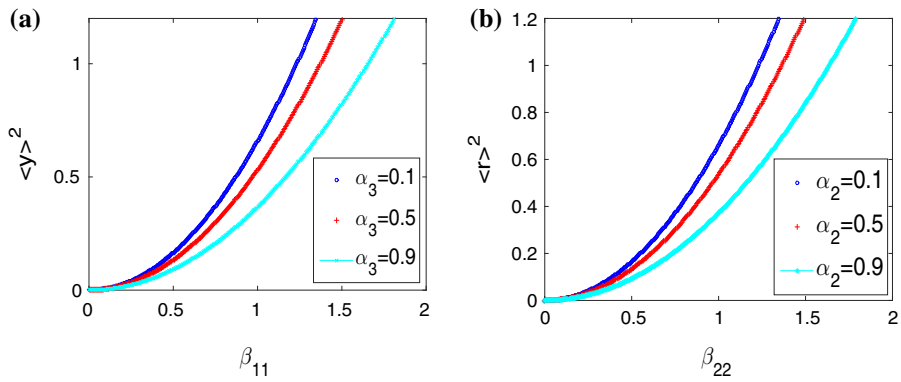

Fig. 3 **a** Evolution of mean square voltage of piezoelectric circuit versus coefficient β_{11},**b** Evolution of mean square current of magnetic circuit versus coefficient β_{22} for $\mu_a = 0.3$, $\beta_2 = 0.005$, $\beta_1 = 0.003$, $\alpha_2 = 0.000001$, $\beta_{22} = -0.005$, $\beta_{11} = 0.003$, $\alpha_3 = 0.0003$, $\sigma = 0.05$, $D = 0.1$, $\omega_0 = 1$

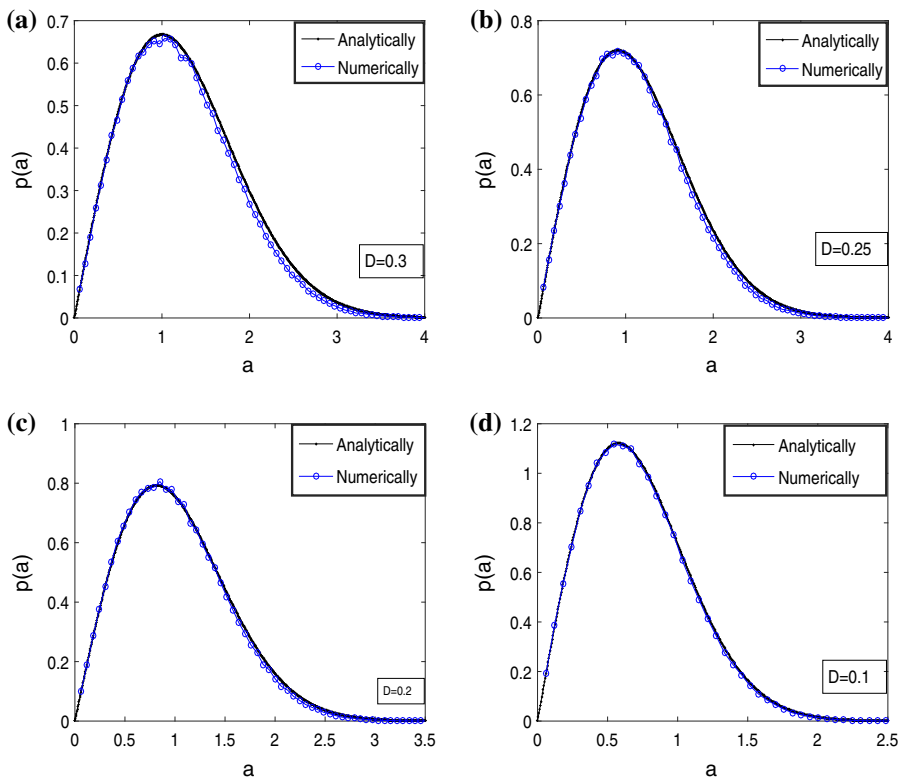

Fig. 4 Stationary probability density for different values of noise intensity for $\mu_a = 0.3$, $\beta_2 = 0.005$, $\beta_1 = 0.003$, $\alpha_2 = 0.000001$, $\beta_{22} = -0.005$, $\beta_{11} = 0.003$, $\alpha_3 = 0.0003$, $\sigma = 0.05$, $\omega_0 = 1$

mean response amplitude and phase lag respectively at the frequency $j\omega_i$. The mean amplitude response is defined as in Ref. [13]:

$$x_m = \sqrt{A_s^2 + A_c^2} \tag{21}$$

where A_s and A_c are the *ith* sine and cosine components of the Fourier coefficients defined as follows:

$$\begin{aligned} A_S &= \frac{2}{nT}\int_0^{nT} x(\tau)\sin(\omega_i\tau)d\tau \\ A_c &= \frac{2}{nT}\int_0^{nT} x(\tau)\cos(\omega_i\tau)d\tau \end{aligned} \tag{22}$$

where $n = 500$, while $T = \frac{2\pi}{\omega_i}$ is the period harmonic excitation.

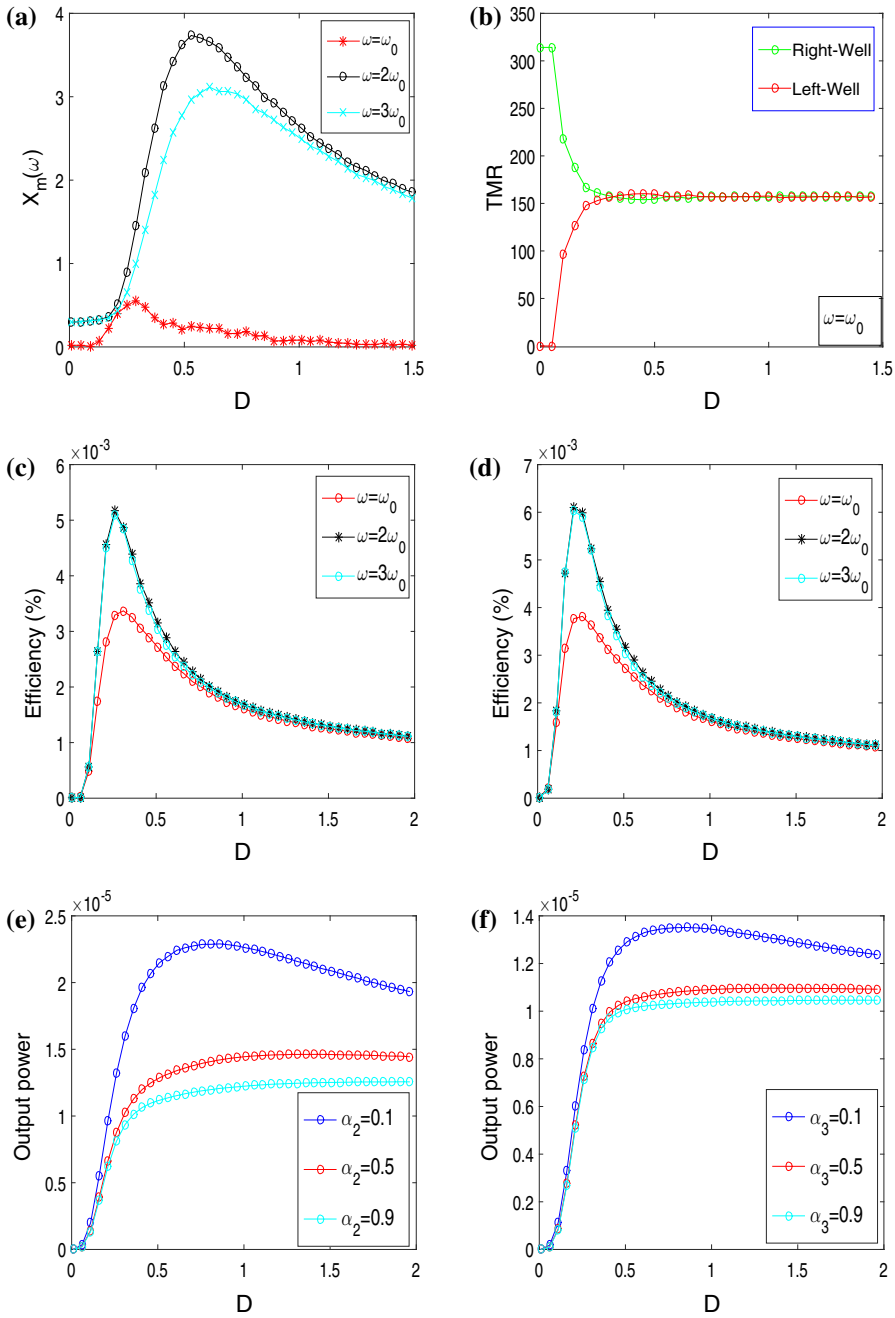

Fig. 5 **a** Mean amplitude response $x_m(\omega)$ versus noise intensity D , **b** Mean residence time versus noise intensity D, **c–d** Efficiency versus noise intensity D for $\alpha_3 = 0.0003, \alpha_2 = 0.000001$, **e–f** Output voltage versus noise intensity for $\mu_a = 0.3$, $\beta_2 = 0.005$, $\beta_1 = 0.003$, $\beta_{22} = -0.005$, $\beta_{11} = 0.003$, $\sigma = 0.05$, $f_0 = 0.39$, $\omega_0 = 1$

Figure 5a shows the evolution of the numerically computed $x_m(\omega)$ for $\omega = \omega_0$, $\omega = \omega_1 = 2\omega_0$ and $\omega = \omega_2 = 3\omega_0$ as a function of the noise intensity D. A typical noise-induced resonance is realized with theses frequencies. ω_1 and ω_2 are present in the input signal. The resonance observed with these frequencies is the usual stochastic resonance [24, 25]. The resonance associated with the missing frequency ω_0 is ghost-stochastic resonance. The ghost-stochastic resonance occurs at $D = D_{max} = 0.3$. This can be corroborated in

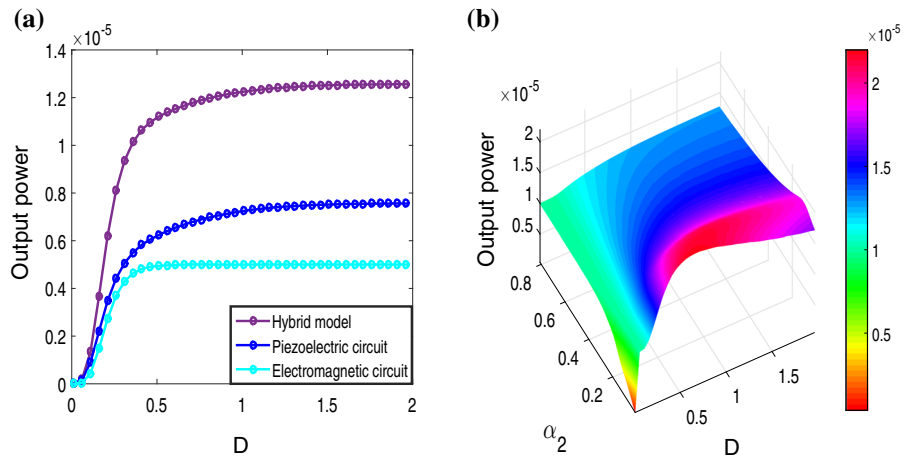

Fig. 6 **a** Output power versus noise intensity D, **b** 3D-representation of the Output power of hybrid model versus noise intensity D and piezoelectric coupling coefficient for $\alpha_3 = 0.0003, \alpha_2 = 0.000001$, $\mu_a = 0.3$, $\beta_2 = 0.005$, $\beta_1 = 0.003$, $\beta_{22} = -0.005$, $\beta_{11} = 0.003$, $\sigma = 0.05$, $f_0 = 0.39$, $\omega_0 = 1$

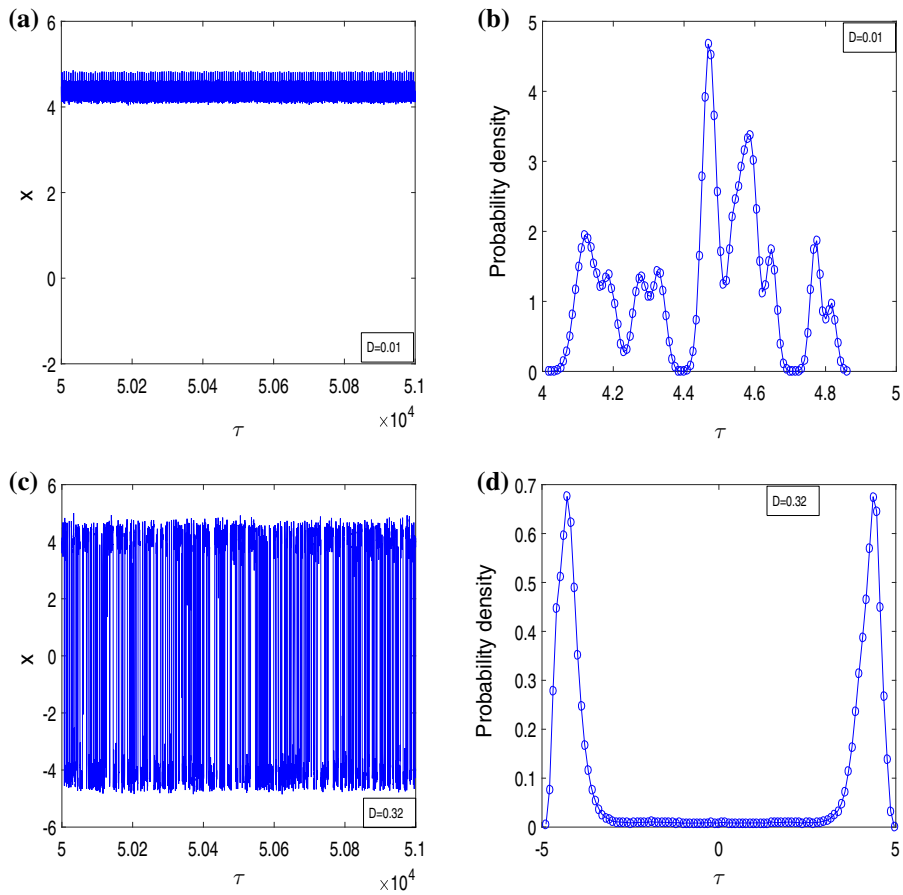

Fig. 7 **a**, **c**, Time series of the mechanical subsystem, **b**, **d**, Probability distribution of the mechanical subsystem for for $\mu_a = 0.3$, $\beta_2 = 0.005$, $\beta_1 = 0.003$, $\alpha_2 = 0.000001$, $\beta_{22} = -0.005$, $\beta_{11} = 0.003$, $\alpha_3 = 0.0003$, $\sigma = 0.05$, $f_0 = 0.39$, $\omega_0 = 1$

Fig. 5b by plotting the mean residence time. Indeed, in Fig. 5b, when the noise intensity D is equal to $D = 0.05$, the size of the orbit increases when the value of D increases. However, the orbit remains in the

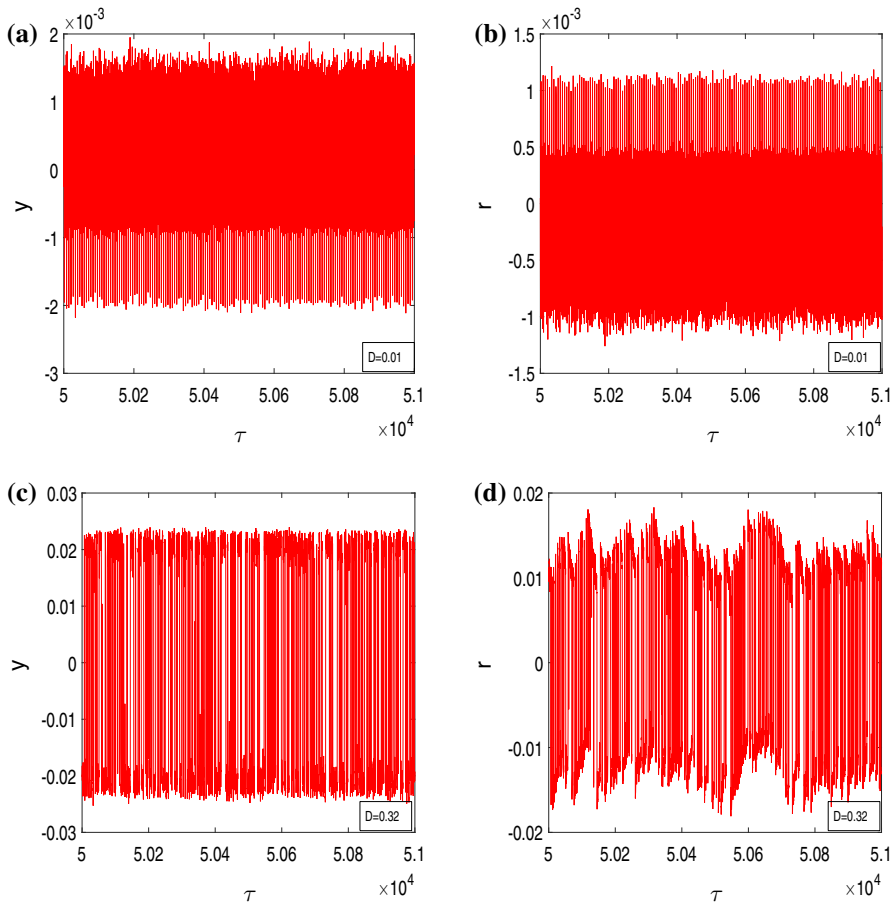

Fig. 8 Time series of the piezoelectric voltage and magnetic current, **a** Voltage of piezoelectric circuit before the ghost-stochastic resonance, **b** Magnetic current of the magnetic circuit before the ghost-stochastic resonance,**c** Voltage of piezoelectric circuit when the ghost-stochastic resonance occurs, **d** Magnetic current of the magnetic circuit when the ghost-stochastic resonance, for for $\mu_a = 0.3$, $\beta_2 = 0.005$, $\beta_1 = 0.003$, $\alpha_2 = 0.000001$, $\beta_{22} = -0.005$, $\beta_{11} = 0.003$, $\alpha_3 = 0.0003$, $\sigma = 0.05$, $f_0 = 0.39$, $\omega_0 = 1$

right well. For $D \geq 0.05$, the orbit visits the left well and gives rise to the ghost-stochastic resonance phenomenon when the noise intensity takes the value $D = D_{max} = 0.3$.

In Fig. 6a, we compare the output power generated by the hybrid model and those obtained by the piezoelectric and electromagnetic model respectively. We notice that the energy harvested by the hybrid model is higher than the one harvested by the piezoelectric or electromagnetic circuit. We provide in Fig. 6b, the 3D-representation of the output power of the hybrid model versus noise intensity and electrical impedance of piezoelectric circuit α_2. We observe that, for a fixed value of noise intensity D, the maximum of output power decreases when α_2 increases.

4.3 Efficiency in power conversion of the harvester

The efficiency conversion of energies dispersed in the environment by the electricity's generator is the one of the fundamental elements for evaluating the system's performance. Thus, the efficiency of the hybrid model is assessed by using this formula:

$$\eta = \frac{P_e}{P_m} \times 100 \tag{23}$$

with P_e and P_m, are respectively, the electrical and the mechanical power effective value. It is well known in the literature that the power effective value is defined as:

$$p_t = \sqrt{\frac{1}{\tau}\int_0^{\tau} \left(p_t^{ins}\right)^2 d\tau} \tag{24}$$

where p_t^{ins} is the instantaneous power and τ is the time.

In Fig. 5c, d, we drawn the efficiency conversion of the piezoelectric and electromagnetic subsystem versus noise intensity D. It emerges from these figures that, when $\omega = \omega_0$, the efficiency increases for $D < D_{max}$, reaches a maximum for $D = D_max = 0.3$ when the ghost-stochastic resonance occurs, and decreases for $D > D_{max}$. We also provided in Fig. 5e, f, the output power for $\omega = \omega_0$, for different values of electrical impedance of the piezoelectric α_2 and magnetic circuit α_3. We observe in these figures that, while the fundamental frequency is absent in the input signal, the harvester can generated a significative energy. In addition, we also notice in these figures Fig. 5e, f that, an enhancing the α_2 and α_3 lead to decrease the output power.

We plotted in Fig. 7, the time series of the harvester, with the corresponding probability distribution. In Fig. 7a, b, we observe that the system vibrates in the right-well and presents a lot of maximum and minimum. No any transition is observed in this condition. However, in Fig. 7c, the transition phenomenon is observed. The system vibrates around the position X = 0 between the positions X = −4.29 and X = 4.359. This is corroborated by Fig. 7d. We plot in Fig. 8a–d, the voltage of the piezoelectric subsystem and the magnetic current of the magnetic circuit versus the time, corresponding to the probability density function plotted in Fig. 7b, d. We notice in Fig. 8, the amplitude of the voltage of the piezoelectric circuit and magnetic current of the magnetic circuit is higher when the ghost-stochastic resonance occurs. Thus, when the ghost-stochastic resonance occurs, the piezoelectric output power and the magnetic output power will be maximized, and consequently, improves the amount of energy harvested by the scavenger. This shows the correlation between the peaks location in the probability density function and the output power.

5 Discussion

In a broad sense and as we show in this work, kinetic energy harvesters can convert any mechanical motion (like fluid flows, pressure variations and ambient vibrations) into electrical energy to power systems located in its environs [26]. In this purpose, it is necessary to take account of the presence of nonlinearity, both desired and undesired. Nonlinearities appear through nonlinearity in the spring force [27] and others component's nonlinearities. A number of recent contributions seek to use nonlinearity in a novel way to improve the harvesters performances (see [28–30]), thus justifying the consideration of nonlinearity in this work.

This work shows that for our device, the maximum power of the hybrid model is greater than that of the piezoelectric and electromagnetic models independently (Fig.6). As pointed in [31], hybridization of two conversion mechanisms in a single system improved the functionality of the harvester in the low frequency range (such as vehicle motion, human motion, and wave heave motion, which usually occur at low frequencies ($< 20Hz$) [32–34]). It is seen that the results are qualitatively in rather good agreement with those from [35], that noticed that the total synergistically extracted power from the hybrid harvester is more than the power obtained from each independently. Many authors [36–38] have pointed that, hybridization could be deliberately exploited within a mechanical system for optimized energy harvesting. Experimental results from [35] confirms that the extracted power at various loading conditions for available ambient excitations is greater.

In this manuscript, the harmonic excitation is combined with Gaussian white noise. As we mentioned in the preceding sections, the type of energy harvester system under study, could be subjected to noise, coming from many sources (such as physical structure-generated noise [39], environmental and transportation noise [40–43] and pneumatic noise [44–46].

The results obtained in this work, shows an improvement of the system performance when the noise intensity is around $D \approx 0.3$ (See Fig. 5c, d) for a frequency of vibration absent in the frequency bandwidth of the harmonic force. It is known in the literature that, when the nonlinear system is subjected to the combination of the harmonic excitation and the random force, many phenomena can be observed such as the stochastic resonance and the ghost-stochastic resonance. These two phenomena are characterized by the large amplitude of vibration [47–49]. Zheng at al. [50, 51] in their work, have indicated that the available power generated under stochastic resonance is noticeably higher than the power that can be collected under

other harvesting conditions. As in this study this resonance occurs and the maximum amplitude of the system is reached for a frequency of vibration absent in the frequency bandwidth of the harmonic force, this phenomenon is called a ghost-stochastic resonance [52–55].

6 Conclusion

In summary, the hybrid energy scavenging device subjected to the Gaussian White noise is investigated. Using the stochastic averaging method, we constructed the $Fokker - Plank - Kolmogorov$ equation whose the solution in the stationary state is the probability density. From this statistic response, we assessed the output power of the piezoelectric and electromagnetic circuit under the form of mean square voltage and current. The impact of electrical impedance of piezoelectric and electromagnetic subsystem is presented with detail. It emerges from these results that, the output power of the two electrical circuit enhance when the coupling parameters increase while a enhancing of the electrical impedances lead to the reduction of the output power. In addition, combining the coherence force with random excitation, the ghost-stochastic resonance occur and improved the system performance. The agreement between the analytical and numerical results validated the efficiency of the analytical method proposed. The results obtained in this manuscript reveal that, while the natural frequency is absent in the coherent excitation, the system performance can be improved for certain value of the noise intensity.

Compliance with ethical standards

Conflict of interest The authors declare that they have no conflict of interest.

References

1. Mitcheson PD, Miao P, Stark BH, Yeatman EM, Holmes AS, Green TC (2004) MEMS electrostatic micropower generator for low frequency operation. Sens Actuators, A 115:523
2. Sari I, Balkan T, Kulah H (2008) An electromagnetic micro power generator for wideband environmental vibrations. Sens Actuators, A 145:405
3. Buckjohn CND, Martin SS, Mokem Fokou IS, Tchawoua C, Kofane TC (2013) Investigating bifurcations and chaos in magnetopiezoelastic vibrating energy harvesters using Melnikov theory. Phys Scr 88:015006
4. Elvin N, Erturk A (2013) Advances in energy harvesting methods. Springer, New York
5. Daqaq MF, Masana R, Erturk A, Quinn DD (2014) On the role of nonlinearities in vibratory energy harvesting: a critical review and discussion. Appl Mech Rev 66:040801
6. Mann BP, Owens BA (2010) Investigations of a nonlinear energy harvester with a bistable potential well. J Sound Vib 329:1215–1226
7. Elvin NG, Elvin AA, Spector M (2001) A self-powered mechanical strain energy sensor. Smart Mater Struct 10(2):293–299
8. Kim HW, Priya S, Uchino K, Newnham RE (2005) Piezoelectric energy harvesting under high pre-stressed cyclic vibrations. J Electroceramics 15(1):27–34
9. Lee B, Wei L (2010) Hybrid energy harvester based on piezoelectric and electromagnetic mechanisms. J Micro/Nanolith MEMS MOEMS 9(Apr–Jun (2)):023002
10. Wang C, Yanlong C, Jin X (2015) Piezoelectric and electromagnetic hybrid energy harvester for powering wireless sensor nodes in smart grid. J Mech Sci Technol 29:4313
11. Madinei H, Haddad KH, Adhikari S, Friswell MI (2016) A hybrid piezoelectric and electrostatic vibration energy, harvester. In: Brandt A, Singhal R, (eds), Shock, vibration, aircraft/aerospace, energy harvesting acoustics optics, vol 9 pp 189–95
12. Cottone F, Vocca H, Gammaitoni L (2009) Nonlinear energy harvesting. Phys Rev Lett 102:08060
13. Mokem Fokou IS, Nono Dueyou Buckjohn C, Siewe Siewe M, Tchawoua C (2016) Probabilistic behavior analysis of a sandwiched buckled beam under Gaussian white noise with energy harvesting perspectives. Chaos, Solitons Fractals 92:101–114
14. Fokou ISM, Buckjohn CND, Siewe MS, Tchawoua C (2018) Probabilistic distribution and stochastic P-bifurcation of a hybrid energy harvester under colored noise Commun. Nonlinear Sci Numer Simulat 56:177–197
15. Foupouapouognigni O, Nono Dueyou Buckjohn C, Siewe Siewe M, Tchawoua C (2018) Hybrid electromagnetic and piezoelectric vibration energy harvester with Gaussian white noise excitation. Physica A Stat Mech Appl 509:346–360
16. Berthet R, Petrosyan A, Roman B (2002) Am J Phys 70:744
17. Rowland DR (2004) Am J Phys 72:758
18. Chialvo DR, Calvo O, Gonzalez DL, Piro O, Savino GV (2002) Phys Rev E 65:050902(R)
19. Chialvo DR (2003) Chaos 13:1226
20. Buldu JM, Chialvo DR, Mirasso CR, Torrent MC, Garcia-Ojalvo J (2003) Europhys Lett 64:178
21. Buldu JM, Gonzalez CM, Trull J, Torrent MC, Garcia-Ojalvo J (2005) Chaos 15:013103
22. Van der Sande G, Verschaffelt G, Danckaert J, Mirrasso CR (2005) Phys Rev E 72:016113
23. Lefeuvre E, Badel A, Richard C, Petit L, Guyomar D (2006) A comparison between several vibration-powered piezoelectric generators for standalone systems. Sens Actuators A 126(2):405–416

24. Mokem Fokou IS, Nono Dueyou Buckjohn C, Siewe Siewe M, Tchawoua C (2017) Nonlinear analysis and analog simulation of a piezoelectric buckled beam with fractional derivative. Eur Phys J Plus 132:344
25. Mokem Fokou IS, Nono Dueyou Buckjohn C, Siewe Siewe M, Tchawoua C (2018) Circuit implementation of a piezoelectric buckled beam and its response under fractional components considerations. Meccanica 53(8):2029–2052
26. Knight C, Davidson J, Behrens S (2008) Energy options for wireless sensor nodes. Sensors 8(12):8037–8066
27. Miki D, Honzumi M, Suzuki Y, Kasagi N (2010). Large-amplitude mems electret generator with nonlinear spring. In: Proceedings of IEEE conference on microelectromechanical systems (MEMS) 2010, 24–28 January 2010, Wanchai, Hong Kong, (pp. 176–179)
28. Yanxia Z, Yanfei J, Pengfei X, Shaomin X (2020) Stochastic bifurcations in a nonlinear tri-stable energy harvester under coloured noise. Nonlinear Dyn 99:879–897
29. Constantinou P, Roy S (2016) A 3D printed electromagnetic nonlinear vibration energy harvester. Smart Mater Struct 25(9):095053 (1-14)
30. Junlei W, Linfeng G, Shengxi Z, Zhien Z, Zhihui L, Daniil Y (2020) Design, modelling and experiments of broadband tristable galloping piezoelectric energy harvester. Acta Mechanica Sinica. https://doi.org/10.1007/s10409-020-00928-5
31. Toyabur RM, Salauddin M, Hyunok C, Park Jae Y (2018) A multimodal hybrid energy harvester based on piezoelectric-electromagnetic mechanisms for low-frequency ambient vibrations. Energy Convers Manage 168:454–466
32. Fan KQ, Chang JW, Pedrycz W, Liu ZH, Zhu YM (2015) A nonlinear piezoelectric energy harvester for various mechanical motions. Appl Phys Lett 106:223902
33. Tang LH, Yang YW, Soh CK (2012) Improving functionality of vibration energy harvesters using magnets. J Intell Mater Syst Struct 23:1433–49
34. Fan KQ, Chang JW, Chao FB, Pedrycz W (2015) Design and development of a multipurpose piezoelectric energy harvester. Energ Convers Manage 96:430–39
35. Salar C, Hasan U, Ali M, Berkay C, Haluk K (2015) Power-efficient hybrid energy harvesting system for harnessing ambient vibrations. IEEE Trans Circuits Syst I Regul Pap 66(7):2784–2793 2019
36. Kangqi F, Qinxue T, Haiyan L, Daxing Z, Yingmin Z, Weidong W (2018) Hybrid piezoelectric-electromagnetic energy harvester for scavenging energy from low-frequency excitations. Smart Mater Struct 27(8):085001
37. Mahmoudi S, Kacem N, Bouhaddi N (2014) Enhancement of the performance of a hybrid nonlinear vibration energy harvester based on piezoelectric and electromagnetic transductions. Smart Mater Struct 23:075024
38. Xia H, Chen R, Ren L (2015) Analysis of piezoelectric—electromagnetic hybrid vibration energy harvester under different electrical boundary conditions. Sens Actuators A 234:87–98
39. Aylin T (2018) Noise Reduction Techniques for Medical Equipment Manufacturers, Advancements in Noise Reduction Techniques for Medical Equipment Manufacturers, Parker Hannifin Corporation
40. Dzhambov Angel M, Dimitrova Donka D (2016) Heart disease attributed to occupational noise, vibration and other co-exposure: self-reported population-based survey among Bulgarian workers. Med Pr 67(4):435–445
41. Ilona C, Michael GS, Kerstin PW (2013) Effects of train noise and vibration on human heart rate during sleep: an experimental study. BMJ Open 3(5):e002655
42. Tassi P, Saremi M, Schimchowitsch S, Eschenlauer A, Rohmer O, Muzet A (2010) Eur J Appl Physiol 108:671–680
43. Sandra P, De Elke V, Raymond C (2010) Nocturnal road traffic noise: a review on its assessment and consequences on sleep and health. Environ Int 36:492–498
44. Joseph G (1960) Gallop rhythm of the heart: I atrial gallop, ventricular gallop and systolic sounds. Am J Med 28(4):578–592
45. Schmidt SE, Graebe M, Toft E, Struijk JJ (2011) No evidence of nonlinear or chaotic behaviour of cardiovascular murmurs. Biomed Signal Process Control 6(2):157–163
46. Thomas SL, Makaryus AN (2020) Physiology, cardiovascular murmurs. [Updated 2019 Jun 3]. In: Stat Pearls [Internet]. Treasure Island (FL): Stat Pearls Publishing. Available from: https://www.ncbi.nlm.nih.gov/books/NBK525958
47. Mantegna RN, Spagnolo B, Testa L, Trapanese M (2005) Stochastic resonance in magnetic systems described by Preisach hysteresis model. J Appl Phys 97:223–87
48. Arathi S, Rajasekar S, Kurths J (2011) Characteristics of stochastic resonance in asymmetric dufing oscillator. Int J Bifurcation Chaos 21:2729
49. Gammaitoni L, Hanggi P, Jung P, Marchesoni F (1998) Stochastic resonance. Rev Mod Phys 70:223–87. https://doi.org/10.1103/RevModPhys.70.223
50. Zheng R, Nakano K, Hu H, Su D, Cartmell MP (2014) An application of stochastic resonance for energy harvesting in a bistable vibrating system. J Sound Vib 333:2568–87
51. Hu H, Nakano K, Cartmell M, Zheng R, Ohori M (2012) An experimental study of stochastic resonance in a bistable mechanical system. J Phys 382:012024 (1-6)
52. Buldu JM, Chialvo DR, Mirasso CR, Torrent MC, Garcia-Ojalvo J (2003) Ghost resonance in a semiconductor laser with optical feedback. Europhys Lett 64:178
53. Buldu JM, Gonzalez CM, Trull J, Torrent MC, Garcia-Ojalvo J (2005) Coupling-mediated ghost resonance in mutually injected lasers. Chaos 15:013103
54. Van der Sande G, Verschaffelt G, Danckaert J, Mirrasso CR (2005) Ghost stochastic resonance in vertical-cavity surface-emitting lasers: experiment and theory. Phys Rev E 72:016113
55. Lopera A, Buldu JM, Torrent MC, Chialvo DR, Garcia-Ojalvo J (2006) Ghost stochastic resonance with distributed inputs in pulse-coupled electronic neurons. Phys Rev E 73:021101

Physica A 557 (2020) 124857

Contents lists available at ScienceDirect

Physica A

journal homepage: www.elsevier.com/locate/physa

Resistance induced P-bifurcation and Ghost-Stochastic resonance of a hybrid energy harvester under colored noise

G.J. Fezeu [a], I.S. Mokem Fokou [a,b,*], C. Nono Dueyou Buckjohn [a], M. Siewe Siewe [a], C. Tchawoua [a]

[a] University of Yaounde I, Faculty of Science, Department of Physics, Laboratory of Mechanics, Materials and Structures, PO. Box: 812, Yaounde, Cameroon

[b] The African Center of Excellence in Information and Communication Technologies (CETIC) Yaounde, Cameroon

ARTICLE INFO

Article history:
Received 24 June 2019
Received in revised form 1 March 2020
Available online 26 June 2020

Keywords:
Ghost-stochastic resonance
Stochastic P-bifurcation
Nonlinear resistance

ABSTRACT

In this paper, a hybrid energy harvester using two mechanisms of transduction namely piezoelectric and electromagnetic and subjected to the colored noise is investigated. Using the stochastic averaging method, the *Fokker − Planck − Kolmogorov* equation of the system is constructed whose the statistic response in the stationary state is the probability density. The mean square voltage and current are obtained for different values of the linear and nonlinear resistance as the output power generated by piezoelectric circuit and electromagnetic circuit. The stability of the harvester is investigated by using probability approach. In addition, combining the colored noise and coherence excitation, the Ghost-Stochastic resonance is observed through the mean residence time and improve the amount of energy harvested by the scavenger. The agreements between the analytical method and those obtained numerically validate the effectiveness of analytical investigations. The results obtained in this manuscript shows the interest to use the load resistance exhibiting the nonlinearity in this research field and also, these results reveal that, while the natural frequency is absent in the coherent excitation, the system performance can be improved for a certain value of noise intensity.

1. Introduction

The concept of harvesting electrical energy from ambient vibration sources has been a popular topic of research in recent years [1–3]. The overall goal of energy harvesting sometimes referred to as energy scavenging is to create electrical energy from an energy source which is already present in the environment. Possible ambient sources include light, thermal energy, and mechanical energy. It is well known in the literature that, three transduction principles are commonly used to convert vibration energy into electricity: electrostatics, electromagnetic and piezoelectric [4–6]. The motivation behind this research is largely due to recent advancements in micro-electromechanical systems (MEMS) technology, specifically the construction of small low powered sensors which are low power, low weight, cheap to produce and, because of their small size, can be applied to a large variety of scenarios and capable of being placed in inaccessible or hostile environments [7,8]. Using an assortment of different sensing techniques, MEMS technology can be used to develop sensors of millimeter-order. It is shown that MEMS sensors can also be used in the biomedical domain, in modern constructions such as

* Corresponding author at: University of Yaounde I, Faculty of Science, Department of Physics, Laboratory of Mechanics, Materials and Structures, PO. Box: 812, Yaounde, Cameroon.

E-mail addresses: fezeuj@yahoo.fr (G.J. Fezeu), igormokem@yahoo.fr (I.S.M. Fokou), bucknono@yahoo.fr (C.N.D. Buckjohn), martinsiewesiewe@yahoo.fr (M. Siewe Siewe), ctchawa@yahoo.fr (C. Tchawoua).

https://doi.org/10.1016/j.physa.2020.124857
0378-4371/

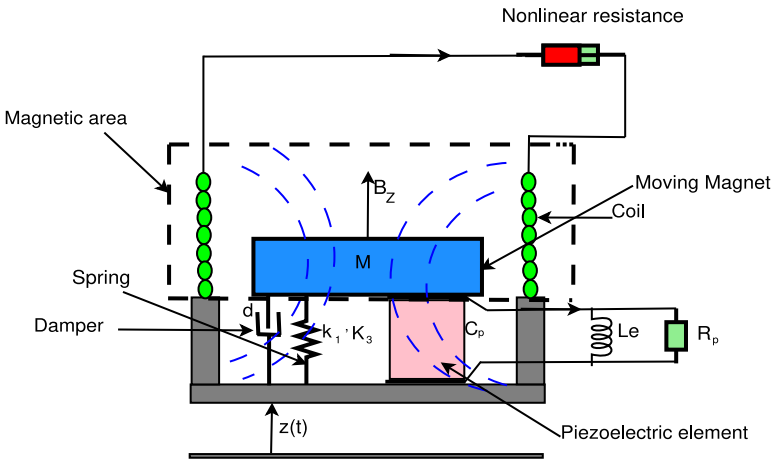

Fig. 1. Schematic of the hybrid energy harvester.

pacemakers and electrical stimulation pain management devices, or being part of a wearable network of autonomous sensor systems which can monitor the health and/or comfort of an individual [9–12].

Although one observes in the literature an exponential increase of the number of publications concerning the energy harvesting field, let us notice that, the most of these models suffer of the optimization problem because of their linear configuration. Indeed, the linear scavengers or resonance scavengers work efficiently with limited bandwidth near their resonant frequency [13,14]. If the natural vibration frequency slightly shifts from the designed frequency, the performance of harvester can dramatically decrease. Thus resonance harvesters are therefore suited only for fixed narrow-band excitations. However, realistic vibration environments are likely composed of multi-frequency harmonics as well as broadband stochastic excitation [15], such linear vibration theory is inefficient for application. Thus, widening the bandwidth of the energy harvesting devices in the order to improve the harvested energy by the harvester is the main challenge of this research field.

Many optimization technique have been proposed by researchers in the literature. Nonlinear systems have proven to be capable of responding over a broad range of frequency [6]. Jin et al. [16] found a Semi-analytical solution of random response for nonlinear vibration energy harvesters; the energy-dependent frequency have been obtained through an averaging process. Zhao et al. [17] studied the deterministic and band-limited stochastic energy harvesting from uniaxial excitation of a multilayer piezoelectric stack; they found that a quadratic relation between maximum power and pressure is observed for bandlimited stochastic excitation. Always in order to optimize the amount of energy harvested by the harvesters, the hybrid model is proposed. Di et al. [18] proposed a probabilistic response analysis of nonlinear vibration energy harvesting system driven by Gaussian colored noise [19]. Tao et al. [20] proposed a dynamics and energy generation of a hybrid energy harvester under colored noise excitations. They authors remarked that, noise-enhanced stability is very beneficial for energy harvesting. Vinicius et al. [21] investigated the nonlinear dynamics of a bistable energy harvesting system with colored noise disturbances. They authors studied the effects of the standard deviation on the system response. Yanxia et al. [22] studied the dynamics of a coupled nonlinear energy harvester under colored noise and periodic excitations. They showed that tri-stable vibration energy harvester can achieve better stochastic resonance effect and higher power conversion efficiency compared with bi-stable vibration energy harvester. Friswell et al. [23] proposed a hybrid cantilever beam harvester with piezoelectric and electrostatic transducers for narrow band base excitation; using an applied DC voltage as a control parameter to change the resonant frequency of the harvester to ensure resonance as the excitation frequency varies. Mokem et al. [24] proposed a hybrid device combining piezoelectric and electromagnetic transduction and subjected to the colored noise. The authors shows that, the system performance can be improve for the small value of the relaxation time. Foupouapouognigni et al. [25] built the hybrid model and studied the stochastic resonance phenomenon, which is characterized by the large amplitude of vibration and increase the system performance. Zhenlong et al. [26] presented a novel tunable multi-frequency hybrid energy harvester. It comes from their study that the magnitude and direction of magnetic force have significant effects on the performance of the system. In the literature, the models of energy harvesting using one mechanism of transduction and the hybrid models present the nonlinearity for the most, in the mechanical subsystem to warden the bandwidth of harvesters. However, the electrical part is composed of a lot of elements which can exhibit the nonlinearity such as: the coil, capacitor and resistor. Oumbé et al. [27] analyzed an electromechanical energy harvester system with geometric and ferroresonant nonlinearities. Form the model provided by Lefeuvre et al. [28], we build the hybrid model combining piezoelectric and electromagnetic mechanisms where the magnetic circuit is composed of the nonlinear resistor. In fact, the nonlinear resistor can be realized using a block consisting of transistors [29,30]. This resistor exhibiting the nonlinearity with a negative slope was used in Ref. [30] for the dynamics of self-sustained electromechanical transducer. In addition, while one observes in the literature,

Table 1
Physical parameters of hybrid model.

Parameter	Value	Unit
L_{coil}	0.03	m
M	1	mg
k_1	-100	N/m
k_3	500	N/m
d	0.1	–
θ	0.001	N/V
R_0	-316	Ω
B	0.1	T
i_0	1	mA
L_e	1	H
L_m	1	H
C_p	10	μF
R_p	5	kΩ

a growing interest in the theoretical investigation of the ghost-stochastic resonance phenomenon in the nonlinear systems [31], in our knowledge, the study of this phenomenon on the performance of the energy harvesting devices is still in its infancy. This manuscript investigate the stochastic P-bifurcation phenomenon induced by the resistor and the impact of the nonlinear resistor via the ghost-stochastic resonance under the system performance.

The rest of paper is organized as follows: In Section 2, we give a brief description of the system with model equation; followed by the investigation of the stochastic bifurcation phenomenon which allow us to determine the maximal amplitude of voltage in Section 3. The stability analysis is also done in this section. Section 4 is consecrated to the numerical simulation. Here, the ghost-stochastic resonance is investigated followed by a conclusion in Section 5.

2. Description of the system with the model equation

The conception of energy scavenging device combining two mechanisms of transduction of ambient energy presents two main parts namely the mechanical and the electrical part (see Fig. 1). In order to improve the amount of energy harvested by Lefeuvre et al. [28], we construct the present model by changing on the model proposed in Ref. [28], the rigid mass by permanent magnet, which allow us to build the hybrid model enhancing thus the application field of the harvester build by Lefeuvre (Ref. [28]). It is worth noting that, the mechanical part is composed of a nonlinear spring with the linear stiffness coefficient k_1 and nonlinear stiffness coefficient k_3 while the electrical part presents two subsystems namely the piezoelectric circuit and the electromagnetic circuit. The piezoelectric circuit is composed of a self with inductance L_e, the load resistance R_p and the piezoelectric element which gives rise to the capacitor of capacity C_p when it is undergone to an external force. However, the electromagnetic circuit has a permanent magnet of mass M, which produces a magnetic field B_z. The coil, connected to the rigid housing representing the stator is characterized by an inductance L_m. The length of the space where the magnetic field exists is L_{coil}. The load resistance of magnetic circuit is considered here as nonlinear where the Ohm's law is given by $U_R = -R_0 i_0 \left[\left(\frac{i}{i_0}\right) - \frac{1}{3}\left(\frac{i}{i_0}\right)^3 + \frac{1}{5}\left(\frac{i}{i_0}\right)^5 \right]$ [29], with R_0 and i_0, the normalized resistance and current respectively while i be the value of the current corresponding to the limit resistor voltage. Let us notice that, the nonlinear resistor can be realized using a block consisting of two transistor [29,30]. When the harvester is subjected to the external excitation $Z(t)$, the displacement of the magnetic mass M induce in the piezoelectric circuit, the deformation of piezoelectric element giving rise to the electrical field across the piezoelectric element, consequently the voltage v. However, in the magnetic circuit, the displacement of the magnetic mass M induces a fluctuation of the magnetic flux in the surface of the coil, and consequently, a generation of electromotive force $f_m(i) = B_z i L_{coil}$ in the mechanical part, while in the magnetic circuit, we can note according to the Lenz's law, the electromotive voltage $f_e(\dot{z}) = -B_z L_{coil}\dot{z}$ with z, L_{coil}, and i, the displacement, the length of the coil and the current that flows in the coil respectively, B_z being the magnetic field generated by the permanent magnet. A summary of equations is provided here [28] giving a full derivation of the mechanical and piezoelectric circuit equations. Using the Kirchhoff's law in the electromagnetic circuit by letting $\vec{B}_z = B\vec{u}_z$, we obtained motion equations given by:

$$\begin{aligned} &M\ddot{z} + d\dot{z} + k_1 z + k_3 z^3 + BiL_{coil} - \theta\, v = Z\,(t) \\ &C_p\ddot{v} + \frac{\dot{v}}{R_p} + \frac{v}{L_e} + \theta\ddot{z} = 0 \\ &L_m\ddot{i} - R_0 i_0\left[\frac{\dot{i}}{i_0} - \frac{i^2\dot{i}}{i_0^3} + \frac{i^4\dot{i}}{i_0^5}\right] - BL_{coil}\ddot{z} = 0 \end{aligned} \tag{1}$$

where d is the damping coefficient and C_p, the capacity of the capacitor. The physical parameters used in this manuscript are given in Table 1.

By using the time-transformation ($t = \frac{\tau}{\omega}$), Eq. (1) gives rise to the following non-dimensional system:

$$\begin{aligned}
&\ddot{x} + \mu_a \dot{x} + \omega_0 x - \beta_2 y + \sigma x^3 + \chi r = N(\tau) \\
&\ddot{y} + \alpha_2 \dot{y} + \mu_{33} y - \beta_{22} \ddot{x} = 0 \\
&\ddot{r} + \mu_1 \dot{r} + \mu_2 r^2 \dot{r} + \mu_3 r^4 \dot{r} - \beta_{11} \ddot{x} = 0 = 0
\end{aligned} \tag{2}$$

with $N(\tau) = \sum_{i=1}^{m} f_0 \cos(\omega_i \tau) + \xi(\tau)$ where $\sum_{i=1}^{m} f_0 \cos(\omega_i \tau)$ is a harmonic excitation, with f_0 the amplitude of coherence force, $\omega_i = (k + i - 1)\omega_0$ is the frequency of the coherence force with k a constant took here equal to 2. ω_0 is the fundamental frequency . The variable $\xi(\tau)$, is the colored noise verifying the statistics properties: $< \xi(\tau)\xi(s) >= \frac{D}{\tau_1} e^{-\frac{|\tau - s|}{\tau_1}}$ with D and τ_1, the parameters characterizing the colored noise and denote the intensity and the correlation times of the noise. The variables x, y and r denote respectively the displacement of the mechanical subsystem, the voltage and current of piezoelectric and electromagnetic circuits. The dimensionless parameters are giving as follow:

$$\begin{aligned}
&\mu_a = -\frac{\omega d}{k_1}; \sigma = -\frac{l^2 k_3}{k_1}; \beta_2 = -\frac{\theta\, vo}{l k_1} \\
&\chi = -\frac{BL_{coil} io}{l k_1}; f(\tau) = -\tfrac{1}{l k_1} u\left(\frac{\tau}{\omega}\right); \alpha_2 = \frac{1}{\omega C_p R_p} \\
&\beta_{22} = -\frac{\theta\, l}{vo\, C_p}; \beta_{11} = \frac{BL_{coil} l}{io\, L_m}; \mu_1 = -\frac{Ro}{\omega L_m}; \mu_2 = \frac{io^2 Ro}{\omega L_m io^2}; \\
&\mu_3 = -\frac{io^4 Ro}{\omega L_m io^4}; \mu_{33} = \frac{1}{\omega^2 C_p Le}; M = -\frac{k_1}{\omega^2} \\
&z = lx(t\omega); v = vo\, y(t\omega); i = io\, r(t\omega)
\end{aligned} \tag{3}$$

3. Stochastic averaging method

3.1. Ito's equation and probability density

In this heading, we use the stochastic averaging method to provide the statistic response of the harvester. In the quasi-harmonic regime, the solution of the harvesting energy divice (2) is of the form [3]:

$$\begin{aligned}
x(\tau) &= a_1(\tau)(\tau)\cos(\theta_1); \quad x'(\tau) = -\omega a_1(\tau)(\tau)\sin(\theta_1) \\
y(\tau) &= a_2(\tau)(\tau)\cos(\theta_2); \quad y'(\tau) = -\omega a_2(\tau)(\tau)\sin(\theta_2) \\
r(\tau) &= a_3(\tau)(\tau)\cos(\theta_3); \quad r'(\tau) = -\omega a_3(\tau)(\tau)\sin(\theta_3)
\end{aligned} \tag{4}$$

where $\theta_j = \omega\tau + \psi_j(\tau)$ with ψ_i, the phase angle and $a_i(\tau)$ the amplitude with the integer number varying between 1...3. Substituting Eq. (4) into Eq. (2), and applying the stochastic averaging method in the obtained system, we obtained the following equations so called Ito's equations:

$$\begin{aligned}
da_1 &= \left(-\frac{\mu_a}{2} a_1 + \frac{D}{2\omega_1^2 a_1 (\tau_1^2 + 1)} a_1\right) d\tau + \sqrt{\frac{D}{\omega_1^2 (\tau_1^2 + 1)}} dw_1(a) \\
da_2 &= \left(-\frac{\alpha_2}{2} a_2 + \frac{\beta_{22}^2 D}{2\omega_2^2 a_2 (\tau_1^2 + 1)}\right) d\tau + \sqrt{\frac{\beta_{22}^2 D}{\omega_2^2 (\tau_1^2 + 1)}} dw_2(b) \\
da_3 &= \left(\Omega_{11} + \frac{\beta_{11}^2 D}{2\omega_3^2 a_3 (\tau_1^2 + 1)}\right) d\tau + \sqrt{\frac{\beta_{11}^2 D}{\omega_3^2 (\tau_1^2 + 1)}} dw_3(c) \\
d\varphi_1 &= \left(\frac{3a_1^2 \sigma}{8\omega_1} - \frac{\omega_1}{2} + \frac{\omega_0}{2\omega_1}\right) d\tau + \sqrt{\frac{D}{\omega_1^2 a_1^2 (\tau_1^2 + 1)}} dw_4(d) \\
d\varphi_2 &= \left(-\frac{\beta_{22}\beta_2}{2\omega_2} - \frac{\omega_2}{2}\right) d\tau + \sqrt{\frac{\beta_{22}^2 D}{\omega_2^2 a_2^2 (\tau_1^2 + 1)}} dw_5(e) \\
d\varphi_3 &= \left(\frac{\beta_{11}\beta_1}{2\omega_3} - \frac{\omega_3}{2}\right) d\tau + \sqrt{\frac{\beta_{11}^2 D}{\omega_3^2 a_3^2 (\tau_1^2 + 1)}} dw_6(f)
\end{aligned} \tag{5}$$

where $\Omega_{11} = -\frac{\mu_3}{16}a_3^5 - \frac{\mu_2}{8}a_3^3 - \frac{\mu_1}{2}a_3$ while w_1, w_2, w_3, w_4, w_5 and w_6 are the normalized wiener process. Is is worth noting that, in Eq. (5), $a_1, a_2, a_3, \varphi_1, \varphi_2$ and φ_3 are independent. Thus, we can provided the probability density for the amplitudes(a_1, a_2, a_3), rather than a joint probability density for φ_1, φ_2 and φ_3. The probability density $P(a_1, \varphi_1)$, $P(a_2, \varphi_2)$ and $P(a_3, \varphi_3)$ of the instantaneous amplitude a_1, a_2 and a_3 satisfies the Fokker-Planck-Kolmogorov equations:

For the mechanical subsystem:

$$\frac{\partial p(a_1,\tau)}{\partial \tau} = \frac{\partial}{\partial a_1}\left[\left(-\frac{\mu_a a_1}{2} + \frac{D}{2\omega_1^2 a_1\left(\tau_1^2+1\right)}\right)p(a_1,\tau)\right] + \frac{\partial^2}{2\partial a_1^2}\left[p(a_1,\tau)\left(\frac{D}{\omega_1^2\left(\tau_1^2+1\right)}\right)\right] \tag{6}$$

For the electrical subsystems:

-Piezoelectric circuit

$$\frac{\partial p(a_2,\tau)}{\partial \tau} = \frac{\partial}{\partial a_2}\left[\left(-\frac{\alpha_2 a_2}{2} + \frac{\beta_{22}^2 D}{2\omega_2^2\left(\tau_1^2+1\right)}\right)p(a_2,\tau)\right] + \frac{\partial^2}{2\partial a_2^2}\left[p(a_2,\tau)\left(\frac{\beta_{22}^2 D}{\omega_2^2\left(\tau_1^2+1\right)}\right)\right] \tag{7}$$

- Electromagnetic circuit

$$\frac{\partial p(a_3,\tau)}{\partial \tau} = \frac{\partial}{\partial a_3}\left[\left(\Omega_{11} + \frac{\beta_{11}^2 D}{2\omega_3^2 a_3\left(\tau_1^2+1\right)}\right)p(a_3,\tau)\right] + \frac{\partial^2}{2\partial a_3^2}\left[p(a_3,\tau)\left(\frac{\beta_{11}^2 D}{\omega_3^2\left(\tau_1^2+1\right)}\right)\right] \tag{8}$$

In the context of energy harvesting systems, we are primarily interested in the long-term system behavior, we then have to obtain stationary probability density function. Hence, the stationary solutions of Eqs. (6)–(8) of electrical and mechanical part respectively are obtained as:

$$p(a_1,\tau) = C_1 a_1 \exp\left(-\frac{\mu_a a_1^2\omega_1^2\left(\tau_1^2+1\right)}{2D}\right) \tag{9}$$

$$p(a_2,\tau) = C_2 a_2 \exp\left(-\frac{\alpha_2 a_2^2\omega_2^2\left(\tau_1^2+1\right)}{2\beta_{22}^2}\right) \tag{10}$$

$$p(a_3,\tau) = C_3 a_3 \exp\left(-\frac{a_3^2\omega_3^2\left(\tau_1^2+1\right)\left(\mu_3 a_3^4 + 3\mu_2 a_3^2 + 24\mu_1\right)}{48D\beta_{11}^2}\right) \tag{11}$$

where C_1, C_2 and C_3 are the constant of normalization assessed numerically.

Through a transformation from variable (a_1, θ_1), (a_2, θ_2) and (a_3, θ_3) to the original variables $\left(x, \dot{x}\right)$, $\left(y, \dot{y}\right)$ and $\left(r, \dot{r}\right)$, an expression for the stationary densities function of x and $\dot{x}$, y and $\dot{y}$ and r and $\dot{r}$ can be derived as

$$p_{1n}\left(x,\dot{x}\right) = \frac{1}{2\pi\omega_1 a_1} p_1(a_1) \tag{12}$$

$$p_{1n}\left(x,\dot{x}\right) = \frac{C_1}{2\pi\omega_1}\exp\left[-\frac{\mu_a\omega_1^2\left(\tau_1^2+1\right)\left(x^2+\frac{\dot{x}^2}{\omega_1^2}\right)}{2D}\right] \tag{13}$$

$$p_{2n}\left(y,\dot{y}\right) = \frac{1}{2\pi\omega_2 a_2} p_2(a_2) \tag{14}$$

$$p_{2n}\left(y,\dot{y}\right) = \frac{C_2}{2\pi\omega_2}\exp\left[-\frac{\alpha_2\omega_2^2\left(\tau_1^2+1\right)\left(y^2+\frac{\dot{y}^2}{\omega_2^2}\right)}{2\beta_{22}^2}\right] \tag{15}$$

$$p_{3n}\left(r,\dot{r}\right) = \frac{1}{2\pi\omega_3 a_3} p_3(a_3) \tag{16}$$

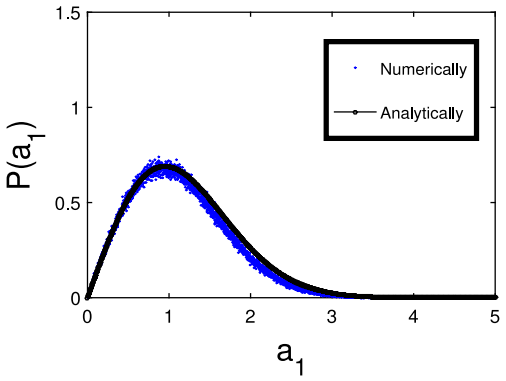

Fig. 2. Stationary probability density of the mechanical subsystem (Eq. (9)) for: $\mu_a = 0.11$, $\alpha_2 = 0.06$, $\beta_2 = 0.1$, $\mu_{33} = 1$, $\beta_{22} = -0.01$, $\mu_1 = 0.11$, $\mu_2 = -1$, $\mu_3 = 1$, $\chi = 0.003$, $\sigma = 0.05$, $\omega_0 = 1$, $\beta_{11} = 0.00003$, $\tau_1 = 0.01$.

$$p_{3n}\left(r,\dot{r}\right) = \frac{C_3}{2\pi\omega_3}\exp\left[\frac{\Lambda_{12}\left(r^2+\frac{\dot{r}^2}{\omega_3^2}\right)\left(\Lambda_{11}+24\mu_1\right)}{48D\beta_{11}^2}\right] \tag{17}$$

where $\Lambda_{12} = \omega_3^2\left(\tau_1^2+1\right)$ and $\Lambda_{11} = \mu_3\left(r^2+\frac{\dot{r}^2}{\omega_3^2}\right)^2 + 3\mu_2\left(r^2+\frac{\dot{r}^2}{\omega_3^2}\right)$, while $a_1 = \sqrt{x^2+\frac{\dot{x}^2}{\omega_1^2}}$; $a_2 = \sqrt{y^2+\frac{\dot{y}^2}{\omega_2^2}}$ and $a_3 = \sqrt{r^2+\frac{\dot{r}^2}{\omega_3^2}}$

3.2. Stability analysis of the harvester

In the order to investigated the stability of the system, a rewriting of Eq. (5)(a)–(c) is required.

$$\begin{aligned} da_1 &= \frac{dV\left(a_1\right)}{da_1} + \sqrt{\frac{D}{\omega_1^2\left(\tau_1^2+1\right)}}dw_1 \\ da_2 &= \frac{dV\left(a_2\right)}{da_1} + \sqrt{\frac{\beta_{22}^2 D}{\omega_2^2\left(\tau_1^2+1\right)}}dw_2 \\ da_3 &= \frac{dV\left(a_3\right)}{da_1} + \sqrt{\frac{\beta_{11}^2 D}{\omega_3^2\left(\tau_1^2+1\right)}}dw_3 \end{aligned} \tag{18}$$

with $V\left(a_1\right)$, $V\left(a_2\right)$ and $V\left(a_3\right)$, the effective potentials of mechanical and two electrical (piezoelectric and electromagnetic circuit) subsystem respectively. The expression of these potentials are given as follow:

$$\begin{aligned} V\left(a_1\right) &= \frac{\mu_a a_1^2}{4} - \frac{D\ln\left(a_1\right)}{2\omega_1^2\left(\tau_1^2+1\right)}(a) \\ V\left(a_2\right) &= \frac{\alpha_2 a_2^2}{4} - \frac{\beta_{22}^2 D\ln\left(a_2\right)}{2\omega_2^2\left(\tau_1^2+1\right)}(b) \\ V\left(a_3\right) &= \frac{\mu_3 a_3^6}{96} + \frac{\mu_2 a_3^4}{32} + \frac{\mu_1 a_3^6}{4} - \frac{\beta_{11}^2 D\ln\left(a_3\right)}{2\omega_3^2\left(\tau_1^2+1\right)}(c) \end{aligned} \tag{19}$$

In order to validate the efficiency of the analytical method used in this manuscript, numerical simulation is made. Fig. 2 show the probability density function obtained from Eq. (9). The agreement between these tow results is observed.

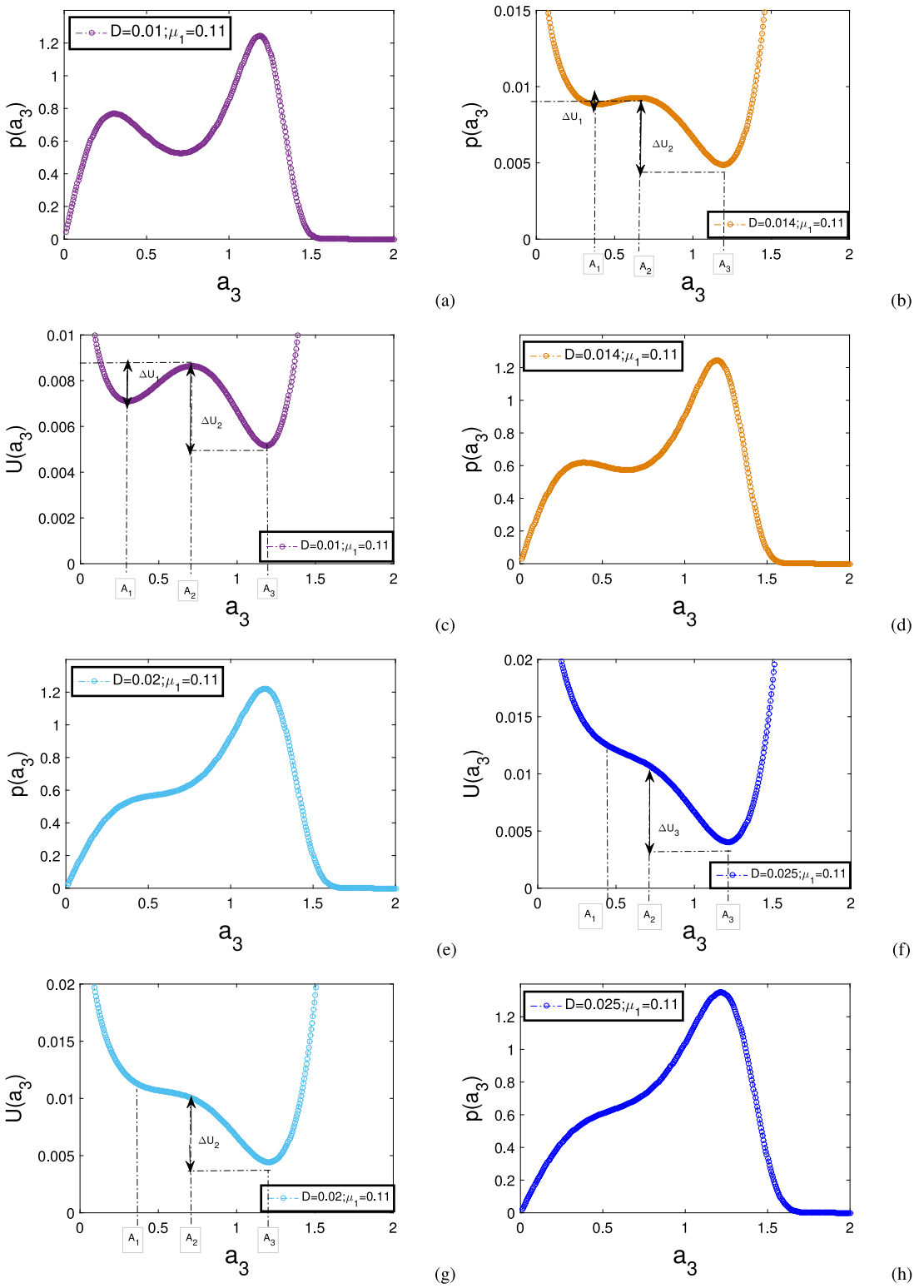

Fig. 3. Stationary probability density of the magnetic circuit (Eq. (11)) with its corresponding effective potential of the system: for $\mu_a = 0.11$, $\mu_2 = 0.06$, $\beta_2 = 0.1$, $\mu_3 = 1$, $\alpha_2 = 0.06$, $\beta_{22} = -0.01$, $\mu_1 = 0.11$, $\mu_1 = 0.11$, $\mu_2 = -1$, $\mu_3 = 1$, $\chi = 0.003$, $\sigma = 0.05$, $\omega_3 = 1$, $\beta_{11} = 0.00003$.

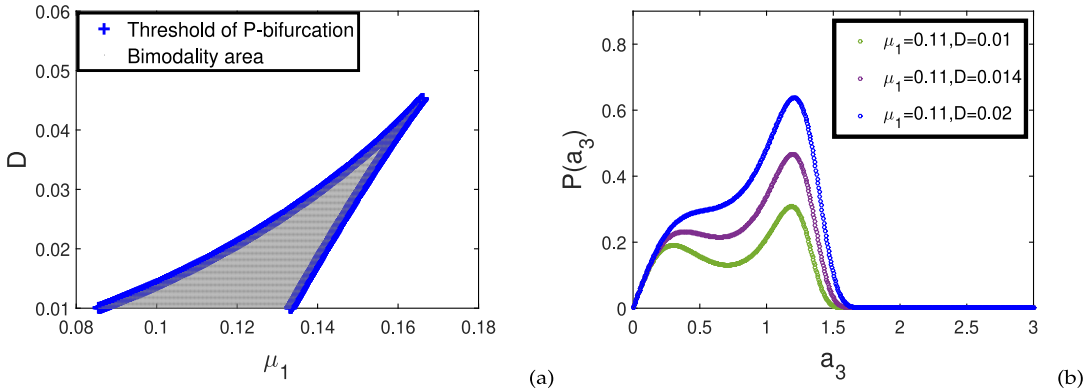

Fig. 4. (a) Bifurcation diagram, (b) Stationary probability density for different values of noise intensity for $\mu_a = 0.11$, $\alpha_2 = 0.06$, $\beta_2 = 0.1$, $\mu_{33} = 1$, $\beta_{22} = -0.01$, $\mu_1 = 0.11$, $\mu_2 = -1$, $\mu_3 = 1$, $\chi = 0.003$, $\sigma = 0.05$, $\omega_0 = 1$, $\beta_{11} = 0.00003$.

Fig. 3(a)–(h) show the probability density function of the electromagnetic circuit (Eq. (11)) with its corresponding effective potential (Eq. (19)(c)) configurations when we modify the intensity of the colored noise. We observe in these figures, two-well effective potential for certain values of D with two stable points A_1 and A_3 while A_2 represents the unstable equilibrium point(Fig. 3 (b,c,g,f)). A disappearance of equilibrium point (A_1) is observed when we increase the intensity of colored noise. In addition, by enhancing the noise intensity, an asymmetric effective potential is destructed at detriment of the monostable effective potential (see Fig. 3(f)). Let us notice that, when the effective potential presents two stable equilibrium points, the probability density function $p(a_3)$ as a function of amplitude of current a_3 exhibits two peaks (Fig. 3(a), (d) and (g)) at different equilibrium points A_1 and A_3. It is worth reminding that, in the stochastic models, the peaks of the probability density function correspond to attractors, and troughs correspond to repellers. Moreover, an equilibrium point is more stable (high resilience) if the probability density function peak is large in comparison with another equilibrium point which is less stable (low resilience) as the probability density function peak is small.

3.3. Stochastic P-bifurcation induced by load resistance

This heading is consecrated to the investigation of the P-bifurcation phenomenon in the harvester most particulary in the magnetic circuit constituted of the nonlinear resistor. First and foremost, it is worth reminding that, stochastic P-bifurcation takes place when the mode of the stationary probability density function changes in nature [3]. It indicates the jump of the distribution of the random variable in probability sense. We provide in this subsection of the manuscript, the condition for which this phenomena can be observed in the system most particularly in the electromagnetic circuit. For reaching our objective, we let, $\frac{dp\,(a_3)}{da_3} = 0$. The extrema of distribution Eq. (11) are the roots of equations:

$$\omega_3^2\left(1+\tau_1^2\right)\left(-\frac{\mu_3 a_3^6}{8}-\frac{\mu_2 a_3^4}{4}-\mu_1 a_3^2\right)+D\beta_{11}^2=0 \tag{20}$$

Fig. 4(a) show the bifurcation diagram drawn in the parameter plan (μ_1, D). It emerges from this result that, the probability distribution is unimodal in the white area and bimodal in the colored domain while the blue line corresponds to the threshold of the bimodality. Let's notice that, the bimodality area allow us to know the interval of the variation of the linear resistance for which the amount of harvested energy can be improved. This result is corroborated by plotting in Fig. 4(b), the corresponding probability density.

We provided in Fig. 5(a)–(f), and Fig. 6(g)–(l), the joint stationary probability density (normalized $p_{n3}(r_1, r_2)$, and unnormalized $p(r_1, r_2)$) of the magnetic circuit (Eq. (11)) for divers values of dimensionless linear resistance μ_1 and noise intensity D. Fig. 5(a)–(c) show the bimodality distribution. In this condition, the amplitude of the electrical current flowing in the load resistance of the magnetic circuit presents two limit circles whose the first has an amplitude close to ≈ 0.05 and the second near to ≈ 1.05. However, from Figs. 5(d)–(f) to 6(g)–(l), we observe a disappearance of the first limit circle and a high probability of the appearance of the second limit circle. The distribution is unimodal.

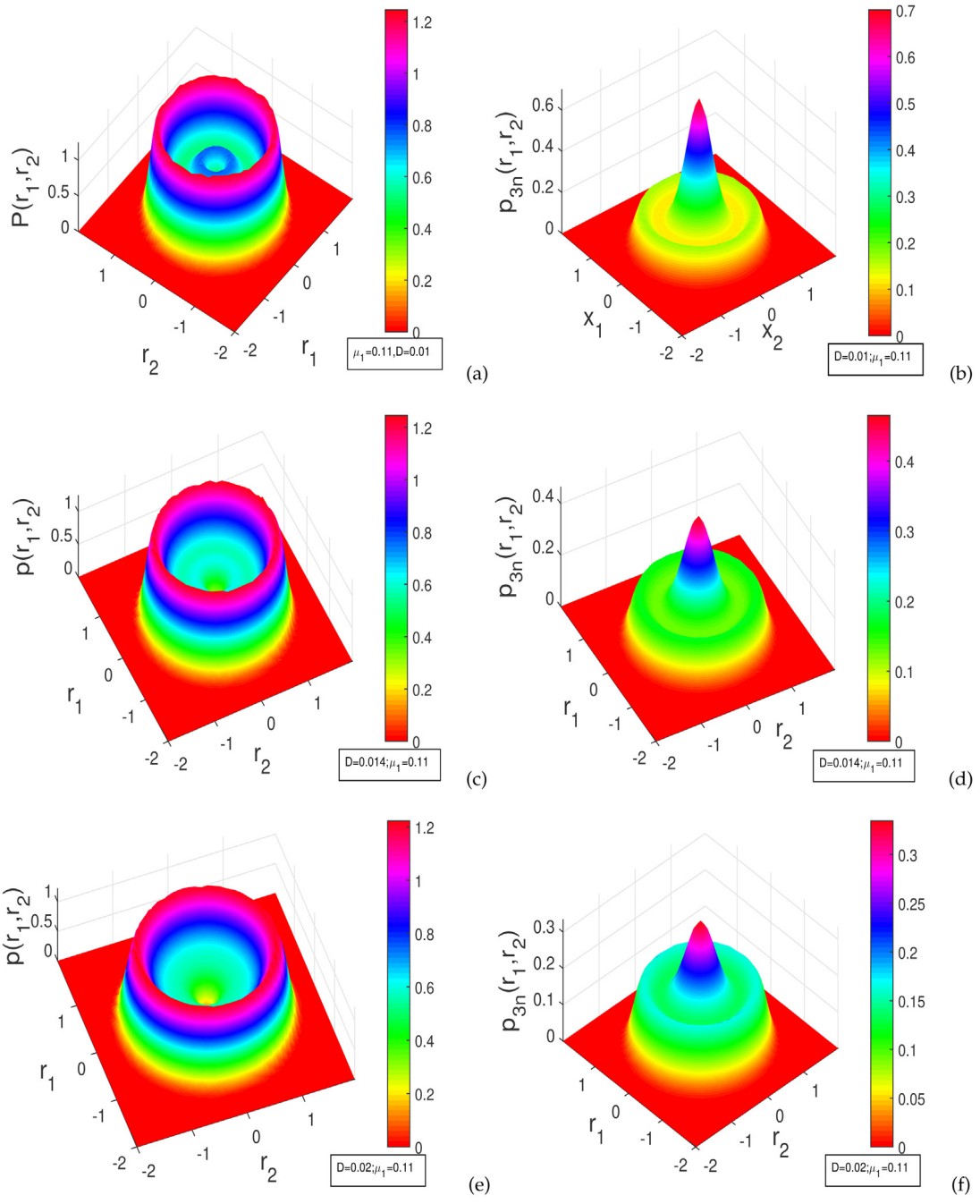

Fig. 5. 3-D representation of the stationary probability density of Eq. (11) for different values of noise intensity for $\mu_a = 0.11$, $\alpha_2 = 0.06$, $\beta_2 = 0.9$, $\mu_{33} = 1$, $\beta_{22} = -0.01$, $\mu_1 = 0.11$, $\mu_2 = -1$, $\mu_3 = 1$, $\chi = 0.003$, $\sigma = 0.05$, $\omega_0 = 1$, $\beta_{11} = 0.00003$, $\tau_1 = 0.01$.

We also plotted in Fig. 7, the amplitude of the dimensionless current for different value of noise intensity. By varying the dimensionless linear resistance μ_1, Fig. 7 presents the domain of bimodality of the electromagnetic circuit. The two modes observed for certain values of linear resistance (see Fig. 7), correspond to the two maximal values of the probability density (see Fig. 3(a), (d) and (g)), corresponding to two stable limits cycle.

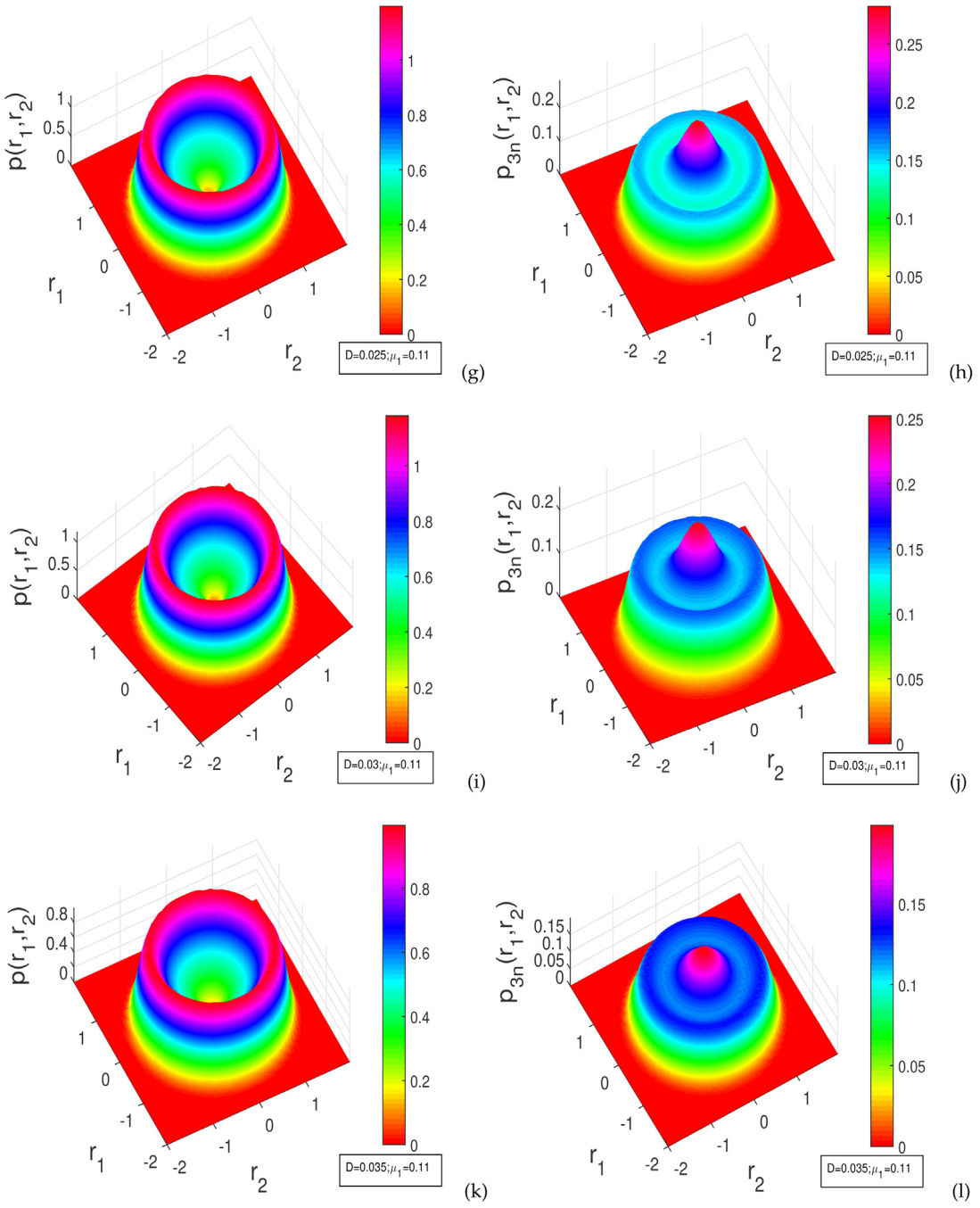

Fig. 6. 3-D representation of the stationary probability density of Eq. (11) for different values of noise intensity for $\mu_a = 0.11$, $\alpha_2 = 0.06$, $\beta_2 = 0.9$, $\mu_{33} = 1$, $\beta_{22} = -0.01$, $\mu_1 = 0.11$, $\mu_2 = -1$, $\mu_3 = 1$, $\chi = 0.003$, $\sigma = 0.05$, $\omega_0 = 1$, $\beta_{11} = 0.00003$, $\tau_1 = 0.01$.

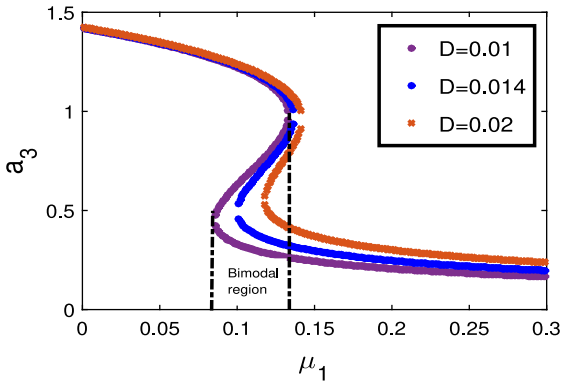

Fig. 7. Amplitude of voltage of the magnetic (Eq. (20)) and piezoelectric (Eq. (20)) circuit for different values of noise intensity with $\mu_a = 0.11$, $\alpha_2 = 0.06$, $\beta_2 = 0.1$, $\mu_{33} = 1$, $\beta_{22} = -0.01$, $\mu_1 = 0.11$, $\mu_2 = -1$, $\mu_3 = 1$, $\chi = 0.003$, $\sigma = 0.05$, $\omega_0 = 1$, $\beta_{11} = 0.9$, $\tau_1 = 0.01$.

4. Numerical simulation

4.1. Algorithm of numerical simulation

The numerical scheme used in this paper is based on the Euler version algorithm. By letting $\dot{x} = u$, $\dot{y} = w$ and $\dot{r} = z$, Eq. (2) can be rewritten in the following form:

$$\begin{aligned} \dot{x} &= u \\ \dot{u} &= -(\mu_a u + \omega_0 x - \beta_2 y + \chi r + \sigma x^3) + N(\tau) \\ \dot{y} &= w \\ \dot{w} &= -(\alpha_2 w + \mu_{33} y + \beta_{22}\dot{u}) \\ \dot{r} &= z \\ \dot{z} &= -\left(\left(\mu_1 + \mu_2 r^2 + \mu_3 r^4\right) z - \beta_{11}\dot{u}\right) \end{aligned} \tag{21}$$

The discrete equations can be written as:

$$\begin{aligned} x_{k+1} &= x_k + h u_k \\ u_{k+1} &= u_k + \left[-(\mu_a u_k + \omega_0 x_k - \beta_2 y_k + \chi r_k + \sigma x_k^3)\right] h \\ &\quad - \left[\sigma\, x_k^3 + \eta_1 y_k\right] h + \xi_k(\tau) \\ y_{k+1} &= y_k + h w_k \\ w_{k+1} &= w_k + \left[-(\alpha_2 w_k + \mu_{33} y_k + \beta_{32} u_{k+1})\right] h \\ r_{k+1} &= r_k + h z_k \\ z_{k+1} &= z_k + \left[-\left(\mu_1 + \mu_2 r_k^2 + \mu_3 r_k^4\right) z_k - \beta_{11} u_{k+1}\right] h \end{aligned} \tag{22}$$

4.2. Mean residence time and ghost-stochastic resonance

In this subsection, the ghost-stochastic resonance is investigated in order to know the amount of energy harvested by the hybrid system. For reaching our objective, we consider that, the harvester is subjected to the combination of the harmonic and the random excitation defined as follow:

$$F(\tau) = \sum_{i=1}^{m} f_0 \cos\left(\omega_i \tau\right) + \xi\left(\tau\right) \tag{23}$$

with $\sum_{i=1}^{m} f_0 \cos\left(\omega_i \tau\right)$ is a harmonic excitation, with f_0 the amplitude of coherence force, $\omega_i = (k + i - 1)\,\omega_0$ is the frequency of the coherence force with k a constant took here equal to 2. ω_0 is the fundamental frequency. $\xi\left(\tau\right)$ is the additive colored noise. It is worth noting that, equation(Eq. (3)) is nonlinear and should exhibit many frequency components. For the large value of time($\tau \to \infty$), the asymptotic solution of Eq. (3) can be given as follows:

$$\langle x(\tau)\rangle_{as} = \textstyle\sum_j x_m(j\omega_i)\cos\left[j\omega_i\tau - \psi_m(j\omega_i)\right] \tag{24}$$

where j is a non-negative constant which may be in integer or fractional form, $X_m(j\omega_i)$ and $\psi_m(j\omega_i)$ are the mean response amplitude and phase lag respectively at the frequency $j\omega_i$. The mean amplitude response is defined as in Refs. [3,32]:

$$X_m = \sqrt{A_s^2 + A_c^2} \tag{25}$$

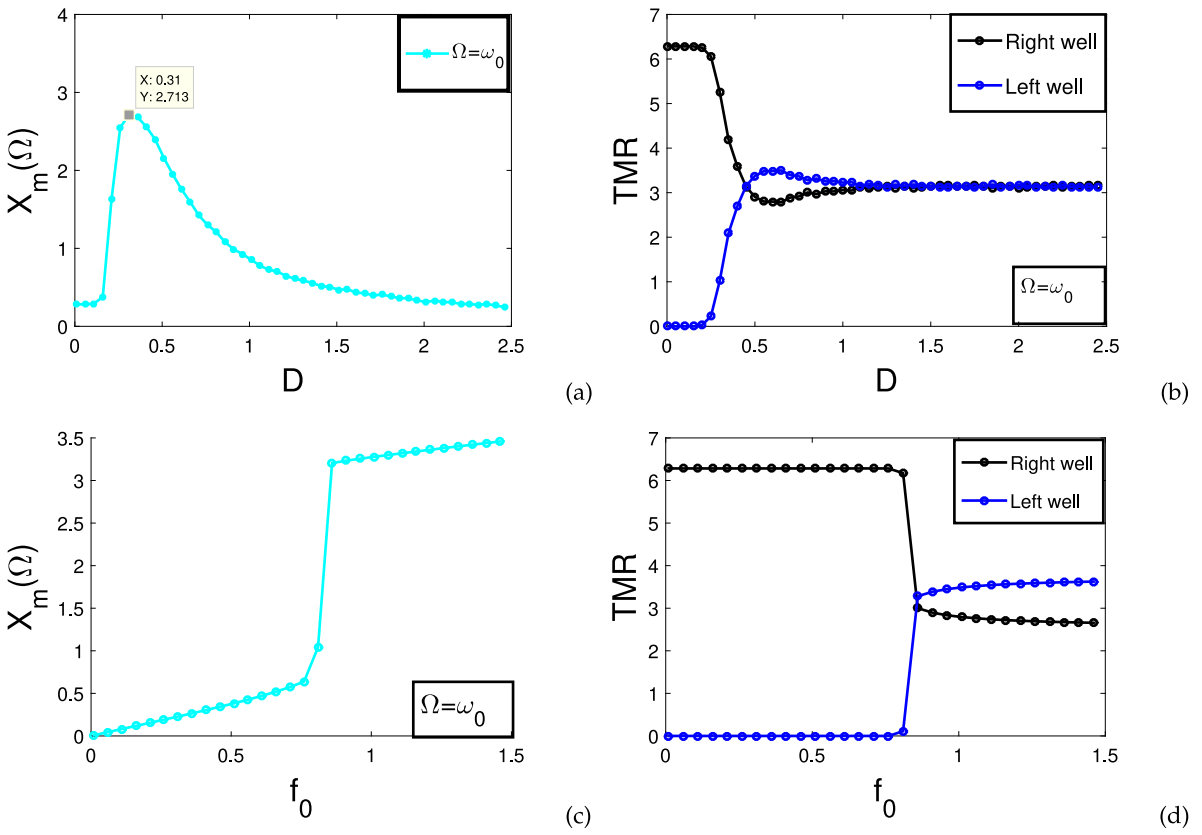

Fig. 8. (a)–(b) Mean amplitude response $X_m(\omega)$ and Mean residence time versus noise intensity D for $f_0 = 0.38$, (c)-(d) Mean amplitude response $X_m(\omega)$ and Mean residence time versus noise intensity f_0 for $D = 0.01$, The other system parameters are given as follow: for $\mu_a = 0.11$, $\alpha_2 = 0.06$, $\beta_2 = 1$, $\mu_{33} = 1$, $\beta_{22} = -0.001$, $\mu_1 = 0.11$, $\mu_2 = -1$, $\mu_3 = 1$, $\chi = 0.003$, $\sigma = 0.05$, $\omega_0 = 1$, $\beta_{11} = 0.003$, $\tau_1 = 0.01$, $m = 2$.

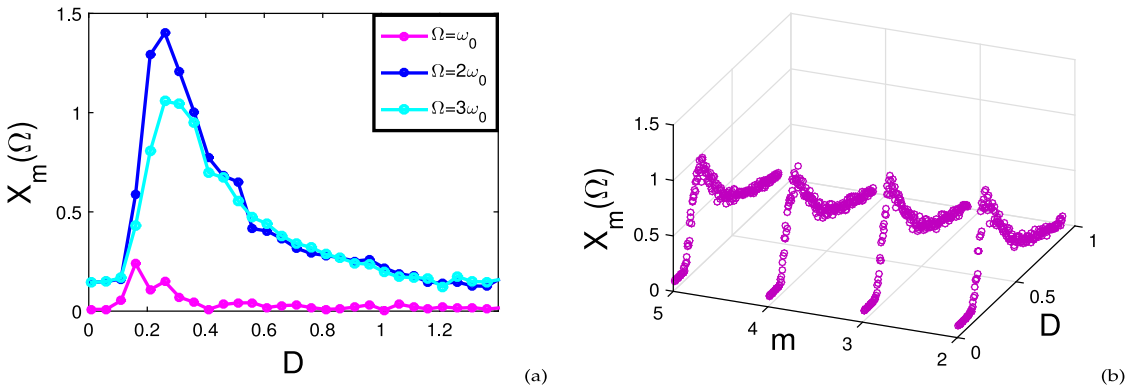

Fig. 9. (a) Mean amplitude response $X_m(\omega_i)$ versus noise intensity D for different value of $\Omega = \omega_i$, (b) 3D-representation of Mean amplitude response $X_m(\omega_i)$ versus m and noise intensity D with: $\mu_a = 0.11$, $\alpha_2 = 0.06$, $\beta_2 = 1$, $\mu_{33} = 1$, $\beta_{22} = -0.001$, $\mu_1 = 0.11$, $\mu_2 = -1$, $\mu_3 = 1$, $\chi = 0.003$, $\sigma = 0.05$, $\omega_0 = 1$, $\beta_{11} = 0.003$, $\tau_1 = 0.01$, $m = 5$.

where A_s and A_c are the *jth* sine and cosine components of the Fourier coefficients defined as follows:

$$\begin{aligned} A_S &= \frac{2}{nT}\int_0^{nT} x(\tau)\sin(\omega_i\tau)d\tau \\ A_c &= \frac{2}{nT}\int_0^{nT} x(\tau)\cos(\omega_i\tau)d\tau \end{aligned} \tag{26}$$

where $n = 500$, while $T = \dfrac{2\pi}{\omega_i}$ is the period harmonic excitation.

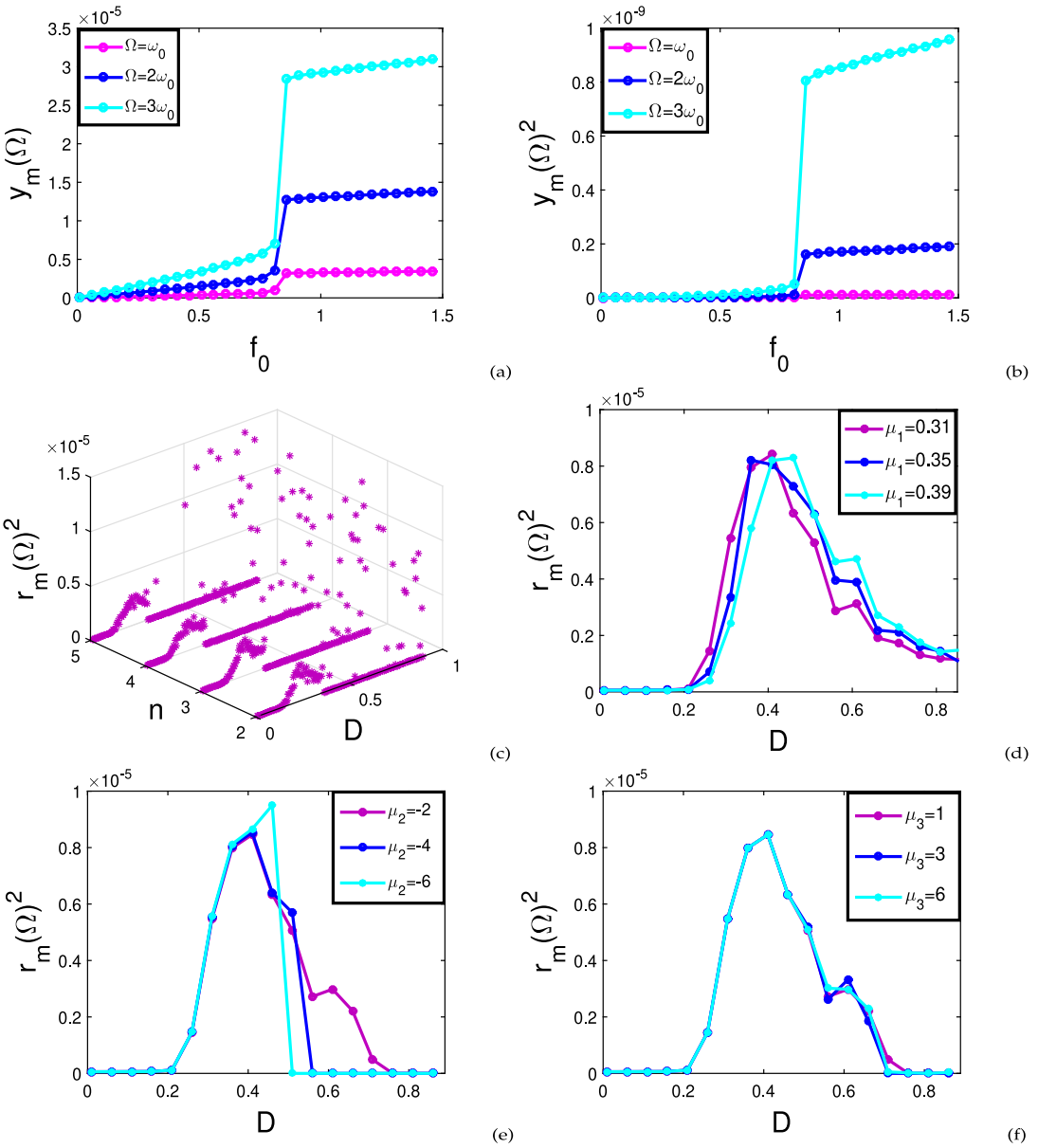

Fig. 10. (a)–(b) Mean amplitude response $y_m(\Omega)$ and mean square voltage $y_m(\Omega)^2$ of the piezoelectric circuit for diverse values of Ω with $D = 0.01$, $\mu_1 = 0.31$, (c)-(d) 3D-representation of mean square current $y_m(\Omega)^2$ of the magnetic circuit versus D and m, and mean square current $y_m(\Omega)^2$ of the magnetic circuit versus D for $\Omega = 2\omega_0$, $\mu_2 = 1$ $\mu_3 = -1$, (e)–(f) Mean square current $y_m(\Omega)^2$ of the magnetic circuit versus D for diverse value of μ_2 for $\mu_1 = 0.31$, $\mu_3 = -1$, mean square current $y_m(\Omega)^2$ of the magnetic circuit versus D for diverse values of μ_3 for $\Omega = 2\omega_0$, $\mu_1 = 0.31$, $\mu_2 = 1$ with $\mu_a = 0.11$, $\alpha_2 = 0.06$, $\beta_2 = 0.1$, $\mu_{33} = 1$, $\beta_{22} = -0.01$, $\chi = 0.003$, $\sigma = 0.05$, $\omega_0 = 1$, $\beta_{11} = 0.00003$, $\tau_1 = 0.01$.

Fig. 8(a) and (c) show the mean amplitude response $X_m(\omega_i)$ versus the intensity of the colored noise D and the amplitude of the coherence force f_0 for $\omega_i = \Omega = \omega_0$. We observe in Fig. 8 that, while the fundamental frequency (ω_0) is absent in the frequency's spectrum of the harmonic excitation force $\omega_i = \Omega$, it exists one value of the noise intensity D for which the system response is optimum. The appearance of the maximum in Fig. 8(a) at $D = Dmax = 0.31$ and its corresponding amplitude of mechanical subsystem $X_m = 2.713$ in absence of ω_0 within the frequency's spectrum of harmonic excitation corresponds to the ghost stochastic resonance. This can be corroborate by plotting in Fig. 8(b), the mean residence time (TMR). The same phenomenon is observed when f_0 vary (see Fig. 8(c)). Let us notice that, when the ghost-stochastic resonance occurs, the output power of the harvester is maximal (see Fig. 10(b)–(f)).

We provided in Fig. 9(a), the amplitude response $X_m(\omega_i)$ for $\Omega = \omega_0$, $\Omega = \omega_1 = 2\omega_0$, $\Omega = \omega_2 = 3\omega_0$ versus noise intensity D. A typical noise-induced resonance is realized with these frequencies. $\Omega = \omega_1$ and $\Omega = \omega_2$ are present in the input signal. The resonance observed with these frequencies is the usual stochastic resonance which is largely study

in this research field [3]. The resonance associated with the missing frequency $\Omega = \omega_0$ is ghost-stochastic resonance. Fig. 9(b) shows the 3D-representation of the mean amplitude response $X_m(\omega_i)$ versus noise intensity D and m. We note in this figure that, when m and D increase, the variation of the maximum amplitude of $X_m(\Omega)$ is not perceptible.

We plotted in Fig. 10(a)–(b), the mean amplitude voltage $y_m(\Omega)$ and the mean square voltage $y_m(\Omega)^2$ of the piezoelectric circuit when f_0 varies with $\Omega = \omega_0$, $\Omega = \omega_1 = 2\omega_0$, $\Omega = \omega_2 = 3\omega_0$. We observe in these figures that, for a given value of $\Omega = \omega_i$, it exists one value of f_0 for which the mean amplitude voltage $y_m(\Omega)$ and the mean square voltage $y_m(\Omega)^2$ rapidly increase. Fig. 10(c) shows the 3D-representation of the mean square current $r_m(\Omega)^2$ versus D and m. It emerges from this result that, regardless of the value of m, the resonance, characterized by a peak is observed.

We also provided in Fig. 10(d)–(f), the mean square current of the magnetic circuit versus D for divers values of the coefficient of linear μ_1 and nonlinear (μ_2, μ_3) resistance. Fig. 10(d) shows the impact of linear resistance on the amount of energy collected by the system. It emerges from this result that, when the coefficient of the dimensionless resistance μ_1 increases, the peak of the output power of the magnetic circuit which is proportional to the peak of the mean square current increases by shifting towards the large value of noise intensity D. However, in Fig. 10(c)–(d), when the value of the dimensionless nonlinear coefficient of resistance enhances (μ_2 and μ_3), the change on the amount of the harvested energy is not perceptible.

5. Conclusion

In this present work, we investigate the ghost-stochastic resonance resulting of the combination coherence and random force and the stochastic P-bifurcation induced by the resistor in a hybrid energy harvester under colored noise. By using the stochastic averaging method, the *Fokker-Planck-Kolmogorov (FPK)* equations of the mechanical and the two electrical circuits are constructed. We discuss the stability of the harvester by plotting the probability density function. The system is more stable if the peak of the probability density is large and less stable in the contrary case. We also discuss the effective potential of the electromagnetic subsystem and it interaction with noise intensity D, in order to predict the activation energy necessary for switching between two probable stationary states or limit cycle that was recorded as greatly increasing the efficacy of electromagnetic transduction. In addition, We studied the mode of the stationary probability density function. It emerges from this result that the electrical subsystem undergoes qualitative changes called stochastic P-bifurcation. By combining the harmonic excitation and random force, the ghost-stochastic resonance is observed characterized by the large amplitude of vibration allowing thus to harvest more energy while fundamental frequency be absent in the harmonic signal. The impact of linear and nonlinear resistance is studied in this manuscript showing the important of the nonlinear resistor in this research field.

CRediT authorship contribution statement

G.J. Fezeu: Conceptualization, Methodology. **I.S. Mokem Fokou:** Software, Writing - original draft. **C. Nono Dueyou Buckjohn:** Visualization, Investigation. **M. Siewe Siewe:** Supervision. **C. Tchawoua:** Supervision.

Declaration of competing interest

The authors declare that they have no known competing financial interests or personal relationships that could have appeared to influence the work reported in this paper.

References

[1] B. Nana, P. Woafo, Physica A 387 (2008) 3305.
[2] I. Iliuk, I. Balthazar, J.M. Angelo, M.T. Jose, R.C.P. Bento, R. de Pontes, L.P.F. Jorge, M. Atila Bueno, Application of passive control to energy harvester efficiency using a nonideal portal frame structural support system, J. Intell. Mater. Syst. Struct. 25 (4) (2014) 417–429.
[3] I.S. Mokem Fokou, C. Nono Dueyou Buckjohn, M. Siewe Siewe, C. Tchawoua, Probabilistic behavior analysis of a sandwiched buckled beam under Gaussian white noise with energy harvesting perspectives, Chaos Solitons Fractals 10 (2016) 1–114.
[4] P.D. Mitcheson, P. Miao, B.H. Stark, E.M. Yeatman, A.S. Holmes, T.C. Green, MEMS Electrostatic micropower generator for low frequency operation, Sensors Actuators A 115 (2004) 523–529.
[5] I. Sari, T. Balkan, H. Kulah, An electromagnetic micro power generator for wideband environmental vibrations, Sensors Actuators A 145–146 (2008) 405–413.
[6] C. Nono Dueyou Buckjohn, M. Siewe Siewe, I.S. Mokem Fokou, C. Tchawoua, Investigating bifurcations and chaos in magnetopiezoelastic vibrating energy harvesters using Melnikov theory, Phys. Scr. 88 (2013) 015006, 9pp.
[7] W.H. Ko, Piezoelectric energy converter for electronic implants, US Patent 3456134, Jul 15, 1969. 4, 6.
[8] E.A. Schroeppel, Pacing lead with piezoelectric power generating means, US Patent 4690143, 4, 6, 1987.
[9] H. Goto, T. Sugiura, Y. Harada, et al., Feasibility of using the automatic generating system for quartz watches as a leadless pacemaker power source, Med. Biol. Eng. Comput. 37 (1999) 377380.
[10] A. Hansen, S. van Leeuwen, A. Stevels, Design of a fuel cell powered radio, a feasibility study in alternative power sources for portable products, in: IEEE Intl. Symp. on Electronics and the Environment, 2000.
[11] D. Iskos, K. Lurie, S. Sakaguchi, Benditt, Termination of implantable pacemeker ther- apy: Experience in five patients, Ann. Intern. Med. 126 (1997) 787–790.
[12] T. Starner, Human-powered wearable computing, IBM Syst. J. 35 (3–4) (1996).
[13] C.B. Williams, R.B. Yates, Analysis of a micro-electric generator for microsystems, Sensors Actuators A 52 (1996) 811.

[14] S.P. Beeby, M.J. Tudor, W.N.M, Energy harvesting vibration sources for microsystems applications, Meas. Sci. Technol. 17 (12) (2006) R175R195.
[15] A.K. Cedrik, G. Litak, C. Nataraj, Nonlinear analysis of energy harvesting systems with fractional order physical properties, Nonlinear Dynam. 80 (2015) 491–501.
[16] X. Jin, Y. Wang, M. Xu, Semi-analytical solution of random response for nonlinear vibration energy harvesters, J. Sound. Vib. 340 (2015) 267–282, http://dx.doi.org/10.1016/j.jsv.2014.11.043.
[17] S. Zhao, A. Erturk, Deterministic and band-limited stochastic energy harvesting from uniaxial excitation of a multilayer piezoelectric stack, Sensors Actuators A 214 (2014) 58–65, http://dx.doi.org/10.1016/j.sna.2014.04.019.
[18] L. Di, X. Yong, L. Junlin, Probabilistic response analysis of nonlinear vibration energy harvesting system driven by Gaussian colored noise, Chaos Solitons Fractals 104 (2017) 806–812.
[19] Shrabani, D. Joydip, C.B. Bidhan, M. Fabio, Autonomous stochastic resonance driven by colored noise, Phys. Rev. E 98 (2018) 012120.
[20] Y. Tao, C. Qingjie, Dynamics and energy generation of a hybrid energy harvester under colored noise excitations, Mech. Syst. Signal Process. 121 (2019) 745–766.
[21] L. Vinicius, P. João, C.J. Americo, The nonlinear dynamics of a bistable energy harvesting system with colored noise disturbances, in: Conference of Computational Interdisciplinary Science 2019, 2019, Atlanta, United States, 2019, (hal-02010224).
[22] Z. Yanxia, J. Yanfei, X. Pengfei, Dynamics of a coupled nonlinear energy harvester under colored noise and periodic excitations, Int. J. Mech. Sci. 172 (2020) 105418.
[23] H. Madinei, K.H. Haddad, S. Adhikari, M.I. Friswell, A hybrid piezoelectric and electrostatic vibration energy, harvester, in: Singhal R. Brandt A (Ed.), Shock, Vibration, Aircraft/Aerospace, Energy Harvesting, in: Acoustics Optics, vol. 9, Springer, 2016, pp. 189–195.
[24] I.S.M. Fokou, C.N.D. Buckjohn, M.S. Siewe, C. Tchawoua, Probabilistic distribution and stochastic p-bifurcation of a hybrid energy harvester under colored noise, Commun. Nonlinear Sci. Numer. Simul. 56 (2018) 177–197.
[25] O. Foupouapouognigni, C. Nono Dueyou Buckjohn, M. Siewe Siewe, C. Tchawoua, Hybrid electromagnetic and piezoelectric vibration energy harvester with Gaussian white noise excitation, Physica A (2018).
[26] X. Zhenlong, S. Xiaobiao, C. Danpeng, X. Tao, A novel tunable multi-frequency hybrid vibration energy harvester using piezoelectric and electromag- netic conversion mechanisms, 6, 2016, p. 10.
[27] G.T. Oumbé Tékam, E.B. Tchawou Tchuisseu, C.A. Kitio Kwuimy, P. Woafo, Analysis of an electromechanical energy harvester system with geometric and ferroresonant nonlinearities, Nonlinear Dynam. (2014).
[28] E. Lefeuvre, A. Badel, C. Richard, L. Petit, A comparison between several vibration-powered piezoelectric generators for standalone systems, Sensors Actuators A 126 (2) (2006) 405–416.
[29] J.C. Chedjou, P. Woafo, S. Damngang, J. Vib. Accoust. 123 (170) (2001).
[30] R. Yamapi, Dynamics and sychronization of electromechanical devices with duffing linearity, 2003, Physics [Physics]. Université de Abomey-Calavy, English.
[31] D.R. Rowl, Am. J. Phys. 72 (2004) 758.
[32] J.H. Yang, M.A.F. Sanjuan, H.G. Liu, G. Litak, X. Li, Stochastic p-bifurcation and stochastic resonance in a noisy bistable fractional-order system, Commun. Nonlinear Sci. Numer. Simul. 41 (2016) (2017) 104–117.